To the Graduate Council:

I am submitting herewith a thesis written by Jitender Batra entitled "In-line Monitoring of Filler Content in Polyethylene Terephthalate Extrusion Using Near Infrared Spectroscopy". I have examined the final copy of this thesis for form and content and recommend that it be accepted in partial fulfillment of the requirements for the degree of Master of Science, with a major in Chemical Engineering.

Marion G. Hansen

Dr. Marion G. Hansen, Major Professor

We have read this thesis
and recommend its acceptance:

Edward A. Clark

Accepted for Council:

Associate Vice Chancellor
and Dean of The Graduate School

STATEMENT OF PERMISSION TO USE

In presenting this thesis in partial fulfillment of the requirements for a Master's degree at The University of Tennessee, Knoxville, I agree that the library shall make it available to borrowers under rules of the Library. Brief quotations from this thesis are allowable without special permission, provided that accurate acknowledgement of the source is made.

Requests for permission for extensive quotation from or reproduction of this thesis in whole or in parts may be granted by the copyright holder.

Signature 

Date 08/19/93

IN-LINE MONITORING OF FILLER CONTENT IN POLYETHYLENE TEREPHTHALATE EXTRUSION USING NEAR INFRARED SPECTROSCOPY

A Thesis

Presented for the

Master of Science

Degree

The University of Tennessee, Knoxville

Jitender Batra

December 1993

Copyright @ Jitender Batra, 1993

All rights reserved

DEDICATION

This thesis is dedicated to my parents

Mr. Lal Chand Batra

and

Mrs. Nirmala Batra

who have inspired me at all times of life.

ACKNOWLEDGEMENTS

I would like to thank my major professor Dr. Marion G. Hansen, for his guidance and patience. I would like to thank Dr. Tse-Wei Wang for her comments and assistance, especially with regards to multivariate data analysis. I would also like to thank Dr. Edward S. Clark for agreeing to be on my thesis committee. A special note of thanks to my colleagues, Mr. Atul Khettry and Mr. David A. Stewart, for their help and encouragement. Finally, and yet the most important, I would like to thank my parents whose love, care, and encouragement, has been a source of inspiration for me.

ABSTRACT

Viability of using NIR spectroscopy for in-line composition monitoring of polymeric system was demonstrated. Spectroscopic measurements were made in-line, at the exit port of a single screw extruder and a gear pump. System of polyethylene terephathalate (PET) filled with an inorganic filler, titanium dioxide (TiO_2), was the subject of study. Various mixtures of filled and unfilled PET resins, in increments of 10%, were run through the extrusion system. The spectral data, in the wavelength range of 1200 nm to 2400 nm, was collected on the flowing polymer stream. Presence of inorganic filler caused the scattering of light. The scattering of light resulted in a systematic baseline shift.

Changes in the baseline were correlated to the TiO_2 concentration data. Multivariate techniques involving the use of singular value decomposition (SVD) to perform principal component regression (PCR) and partial least squares regression (PLS) were applied to quantitatively determine TiO_2 content in the PET melt stream. The results for both PLS and PCR were almost similar. Qualitative interpretation of loadings and scores for various factors showed meaningful contribution from the first two factors only. Different types of cross validation also suggested two factors as optimal. The standard error of prediction (SEP) values of about 1% were obtained for calibration model using two factors.

TABLE OF CONTENTS

CHAPTER.	PAGE
1. INTRODUCTION	1
1.1 Motivation	1
1.2 Problem Statement	6
2. BACKGROUND	9
2.1 Near Infrared Spectroscopy	9
2.1.1 Introduction to Near Infrared Region	9
2.1.2 Theory	12
2.1.3 Sampling Methods	15
2.1.4 Advantages of NIR	18
2.2 Multivariate Techniques	21
2.2.1 Classical Least Squares	23
2.2.2 Principal Component Regression	25
2.2.3 Partial Least Squares	31
2.2.4 Calibration Procedure	33
3. LITERATURE REVIEW	36
3.1 Agricultural Products	36
3.2 Petrochemical Substances	40
3.3 Polymers	44
3.3.1 Pure Polymers	45
3.3.2 Blend Composition	49

CHAPTER PAGE

3.3.3 Copolymer Composition 51
3.3.4 Additive Content 55
3.3.5 Hydroxyl Number 57
3.3.6 Molecular Weight 60
3.3.7 Components of Packaging Laminates 61
3.3.8 Progress of Reaction 62
3.3.9 Miscellaneous 64
4. EXPERIMENTATION AND ANALYSIS 67
4.1 Equipment 67
4.1.1 Extruder Assembly 67
4.1.2 Flow Cell 69
4.1.3 Analyzer 71
4.2 Experimental 72
4.2.1 Samples 72
4.2.2 Experimental Runs 73
4.3 Data Analysis 74
5. RESULTS AND DISCUSSION 77
5.1 Spectral Features of Filled and Unfilled PET 77
5.2 Analysis of In-Line Data 80
5.2.1 Qualitative understanding of Calibrations 83
5.2.2 Cross Validation 90
5.2.3 Proposed Calibration Model 101
5.2.4 Summary of Results for Data Analysis 106

CHAPTER PAGE

6. CONCLUSIONS 107

7. FUTURE WORK 110

LIST OF REFERENCES 112

APPENDICES 120

A. Program Codes for PLS and PCR 121

A.1 Code for PLS 121

A.2 Code for PCR 125

B. Complete Spectral Data 128

C. Program Output 138

VITA 143

LIST OF TABLES

Table		Page
5.1	Position and assignments for peak maxima in NIR spectra of filled and unfilled PET	79
5.2	Results of percent variance captured by PLS and PCR models	84
5.3	The results for leave-one-group-out cross validation using PLS	93
5.4	The results for leave-one-group-out cross validation using PCR	94
5.5	The improved results for leave-one-group-out cross validation using PLS	99
5.6	The improved results for leave-one-group-out cross validation using PCR	100

LIST OF FIGURES

Figure		Page
1.1	Options for process analysis	3
2.1	Location of near infrared region in the electromagnetic radiation spectrum	10
2.2	Potential energy diagram for harmonic and anharmonic oscillator	14
2.3	Geometric interpretation of Singular Value Decomposition for the case of two variables	27
3.1	Overlaid spectra of wheat and its components	38
3.2	Spectrum of pure polystyrene showing the four characteristic absorbance bands	47
4.1	System for in-line monitoring	68
4.2	Schematic of the flow cell	70
5.1	Overlaid spectra of filled and unfilled PET	78
5.2	Chemical structure of PET	79
5.3	Overlaid spectra of PET with varying filler content	81
5.4	Plot of variance in absorbance versus wavelength	82
5.5	Plot of scores for first five factors v/s sample number	85
5.6	Loadings spectra for first five factors	87
5.7	Mean-centered and normalized spectra of different concentration level	88
5.8	Plot of SEP_{CV} versus the number of factors for cross validation using PLS	92
5.9	Plot of the second factor scores versus the first factor scores	96

Figure Page

5.10 Comparison of three bad spectra to one good spectrum of 10% concentration level 97

5.11 Scatter plot for predictions in the leave-one-group-out cross validation 102

5.12 Plot of SEP and SEC versus the number of factors for cross validation using PLS, with user selected groups in the validation set 103

5.13 Scatter plot for the predictions on the calibration samples in the proposed calibration model using two factor PLS 104

5.14 Overlaid spectra of PET with varying filler content, regenerated using two factor PLS model 105

B.1 Overlaid spectra of all the samples of 10% concentration level 129

B.2 Overlaid spectra of all the samples of 20% concentration level 130

B.3 Overlaid spectra of all the samples of 30% concentration level 131

B.4 Overlaid spectra of all the samples of 40% concentration level 132

B.5 Overlaid spectra of all the samples of 50% concentration level 133

B.6 Overlaid spectra of all the samples of 60% concentration level 134

B.7 Overlaid spectra of all the samples of 70% concentration level 135

B.8 Overlaid spectra of all the samples of 80% concentration level 136

B.9 Overlaid spectra of all the samples of 90% concentration level 137

NOMENCLATURE

SYMBOL/ ABBREVIATION	DESCRIPTION
A	: absorbance
CLS	: classical least squares
E	: matrix of residuals in **X**
E_q	: quantum energy levels (Joules)
F	: matrix of residuals in **Y**
FT-IR	: Fourier Transformed Infrared
I	: intensity of light (watts/m^2)
I_0	: reference intensity of light (watts/m^2)
IR	: infrared
k	: force constant (N/m)
m	: number of samples in **X** or **Y**
mid-IR	: mid-infrared
MLR	: multilinear regression
MLSR	: multiple least squares regression
n	: number of variables in **X**
nc	: number of calibration samples
np	: number of prediction samples
NIPALS	: non-linear iterative partial least squares
NIR	: near infrared
P	: matrix of loadings for **X**
p	: number of variables in **Y**
PET	: polyethylene terephthalate
PCR	: principal component regression
PLS	: partial least squares
Q	: matrix of loadings for **Y**
R	: correlation coefficient
S	: matrix of spectra of pure analytes
$\hat{\mathbf{S}}$	: estimate of **S**

SYMBOL/ ABBREVIATION	DESCRIPTION
SEC	: standard errors of calibration
SEP	: standard errors of prediction
SEP_{cv}	: SEP for leave-one-out cross validation
SVD	: singular value decomposition
$\mathbf{T}$	: matrix of scores for $\mathbf{X}$
TiO_2	: titanium dioxide
$\mathbf{U}$	: matrix of eigenvectors of $\mathbf{X}(\mathbf{X}^T)$
U_q	: potential energy (Joules)
$\mathbf{U_r}$	: reduced $\mathbf{U}$
UV	: ultra violet
$\mathbf{V}$	: matrix of eigenvectors of $\mathbf{X}^T\mathbf{X}$
$\mathbf{V_r}$	: reduced $\mathbf{V}$
v	: vibrational quantum number
$\mathbf{X}$	: matrix for spectral data
x	: displacement (m)
x_e	: anharmonicity constant
$\mathbf{X_r}$	: reduced $\mathbf{X}$
$\mathbf{X_r}^+$	: pseudoinverse of $\mathbf{X_r}$
$\mathbf{Y}$	: matrix of properties or concentrations
$\mathbf{Y}^+$	: pseudoinverse of $\mathbf{Y}$
$\mathbf{y_p}$	: predicted value of unknown concentration
$\bar{y}$	: mean of all observations of $\mathbf{Y}$
$\mathbf{Z}$	: matrix of scores for $\mathbf{Y}$
β	: matrix of coefficients of regression
$\hat{\beta}$	: estimate of β
Σ	: singular value matrix
σ	: singular value
Σ_r	: reduced rank Σ
ν_{osc}	: frequency of vibration (sec^{-1})

1. INTRODUCTION

1.1 MOTIVATION

Any manufacturing process is a dynamic system. Incoming raw ingredients are subjected to a series of usually complex intermediate production stages before the manufacture of finished product can be completed. The condition of the product at all critical stages of the process should be known in order to ensure the production of an acceptable product in most efficient manner possible. This is usually accomplished by monitoring the physical and/or chemical characteristics of the product. The information obtained is used to change the process operating parameters within acceptable limits. The waste of costly ingredients and manufacturing costs for an out-of-specification product are both expensive.

Extrusion is a major process for manufacture and fabrication of plastics. The word "extrusion" is derived from the Latin words *ex* and *trudere* meaning respectively, "out" and "to thrust" "or to push" (1). These words literally describe the process of extrusion, where polymer melt is pushed across the die into the desired form. Polymer products like wires, cables, rods, tubes, pipes, films and sheets are manufactured by extrusion. Standard chemical engineering measurements such as temperature, pressure and motor torque are used to monitor and control extruders (2). The need for more uniform polymer based products and for lower waste outside useful specifications has lead the plastics industry to adopt monitoring and control

of chemical quantities when practically and economically feasible (3). The control of extruders via monitoring chemical quantities is more of a challenge due to the presence of extreme process conditions. Highly viscous polymers at high temperatures and pressures pose a major obstacle to sampling. This is an important consideration in development of all suitable analytical method for composition monitoring.

Unfortunately, simply monitoring certain quality parameters by various analytical methods will not result in automatic improvement of process efficiency. It is also required that targeted analytical results obtained, be timely and relatively accurate (4). If the process at the point at which it is monitored is slow relative to the interval between analytical results, corrections to the process can be made with minimal waste of ingredients and only slightly higher manufacturing expenses and minor delays in the production schedule. If on the other hand the process is fast relative to sampling, large quantities of ingredients can be lost, significantly higher costs, resulting from the manufacture of an unacceptable product can be expected, and there may be considerable production delays. Of even greater consequence, perhaps, is the possibility that if an out-of-specification condition exists between analyses, the presence of resulting out-of-specification product may not be detected. Untimely analytical analyses can result in the production of significant quantities of unacceptable product.

There are several options available for process analysis (5) as shown in Fig. 1.1. The traditional off-line analysis is the simplest method. A sample is drawn from the process stream and taken to the laboratory for analysis. This is a cumbersome procedure. Additionally, there is substantial time delay, and

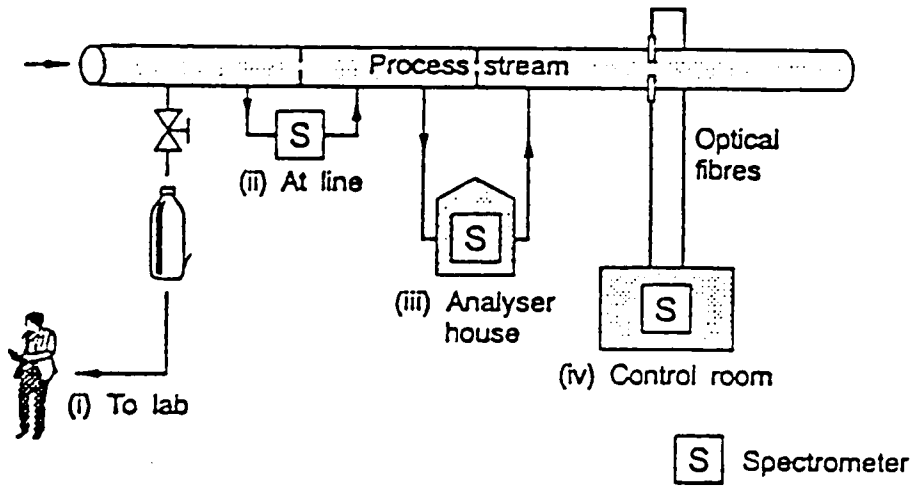


Figure 1.1 Options for process analysis (5).

thus, it is not useful for real time control. A second option, referred to as at-line, needs the analyzer to be placed near the process stream. The analyzer is interfaced to the process by a short length fiber optic cable. A rugged instrument is required due to hazardous process environment. Further, since analyzer needs to be located near the process stream, it can monitor only one process stream.

As a compromise between the two options mentioned above, on-line analysis can be carried. The analyzer is housed in a safe area, such as an analyzer house, sited some distance from the process. Sample is transferred via a "fast sample loop" to the flow cell in the analyzer. There are a number of problems associated with this methodology. Analyzer houses add considerably to the capital costs of the plant. Sample loop may become blocked and hence inoperable. Blocking of the sample loop is especially severe in the case of polymers because of its high viscosity, and high shear rates due to thin lines. Some of the rheological properties which are dependent on the shear history are also different in the sample stream than their counterparts in the main process stream. The material in the sample loop may have been chemically altered since leaving the process stream. In the case of reactive processing, the material continues to react in the loop and consequently a different composition is measured instead of the actual composition at the sampling point. Above all this, there is substantial time delay for this technique to be feasible for real-time process control.

The fourth option and the most promising one is of "remote in-line" process monitoring. The measurements are made directly in the process stream. Optical probes, inserted directly into the process stream, can be

connected to the spectrophotometer, to as far as 1 km, by a pair of optical fibers. Instrument is located in a safe area, remote from the process, thus eliminating the need for a rugged instrument or an analyzer house in the production area. There are no sampling problems associated and the measurements can be made in real time. In a multiplex mode, one instrument can monitor several sample points. Thus in-line monitoring is the most promising option with absolutely negligible time delay, constrained only by instrument response time, and require very low labor and maintenance costs. The only obstacle is the availability of rugged probes which can withstand severe process conditions typical of polymeric processes.

The usefulness of an analytical method does not depend entirely on how rapidly it can provide relevant information; reasonably good agreement between numerical values obtained from the analysis and the physical or chemical parameters that are being monitored is also necessary. The standard error between measured values and the true values is used as the criterion for judging the accuracy of a particular analytical method.

Several analytical methods can accurately determine the physical, chemical and structural properties of polymers for quality and process control. Spectroscopic methods such as infrared, NMR, and Raman can determine compositional and structural properties of polymers (6). Thermal analysis (7) and chromatography (8) can also provide compositional and structural information. All of these methods provide useful information that can be used to assess the quality of a polymeric material. Unfortunately, most of these methods also require substantial sample preparation, are labor

intensive, and are usually destructive. In a situation where rapid quality control is necessary, these methods cannot provide timely results (9).

Only infrared spectroscopy has stood out as a viable option. Fourier Transformed Infrared (FT-IR) instruments in the mid-infrared range have typically been used for process control applications. In the area of polymeric processes these instruments have mainly been restricted to on-line measurements (10-13). The renewed interest in the near infrared (NIR) range has been revolutionary in terms of developing process control for polymeric processes. The low absorbances in the NIR region have facilitated use of higher pathlengths. In the past decade there have been several efforts in development of in-line monitoring system using NIR spectroscopy for extruder control (2,14-17). These efforts have only been limited by the availability of rugged probes. There are probes available to withstand severe process conditions (15) but a design more in agreement with industrial size specifications has just been completed. The evaluation of this probe design is still in progress (17).

1.2 PROBLEM STATEMENT

The general objective of the present work is to demonstrate viability of using NIR spectroscopy for in-line composition monitoring of polymeric systems. The spectroscopic measurements are to be made in-line at the exit port of a single screw extruder. The spectroscopic data would then be correlated to the composition data to build a calibration model. These calibration models can then be used for future predictions of composition.

More specifically, the present thesis will deal with monitoring inorganic filler content of polymers. The system of interest is polyethylene terephthalate (PET) filled with titanium dioxide (TiO_2). PET has the clear, shiny optical properties characteristic of many thermoplastics, providing a bright, sparkle effect desirable for some end uses, such as silk like apparel. Where this effect is not desired, particulate materials like TiO_2 are added to obtain desired optical properties. TiO_2 reduces luster i.e. brightness and shine, and improves whiteness (18). TiO_2 is sometimes introduced during PET melt extrusion. In such a case, in-line monitoring system, located at the port of a single screw extruder and a gear pump, is ideally suited for better monitoring and control of optical properties of PET. The use of a gear pump, which is a positive displacement pump and can be used to control the flow rate, makes this monitoring system adaptable to the fiber spinning process.

Presence of TiO_2 will cause the NIR light to scatter. The spectral changes due to scattering and any other absorbing phenomenon will be correlated to the filler content. A number of different types of calibrations would be done. The calibration would then be tested for predictability. The models would be optimized to produce minimum prediction errors. Finally, a sound calibration model would be presented for future predictions.

This chapter focussed mainly on discussing the merits of in-line monitoring and problem definition for the present work. Next chapter will deal with theory of NIR spectroscopy and principles of multivariate techniques. Various advantages offered by NIR spectroscopy will also be discussed. The third chapter will summarize the applications of NIR in the fields of agriculture, petrochemicals, and polymers. The fourth chapter will

deal with experimentation and data analysis. Finally, the fifth chapter will be a discussion on the results of experiment and data analysis.

2. BACKGROUND

Discovered by Sir William Herschel in 1800, NIR spectral region has long been ignored due to lack of sharp peaks, loss of baseline resolution, abundance of overlapping and shoulder peaks, and dramatically low sensitivity (19). Researchers have come a long way since then, unraveling the abundance of applications of NIR spectroscopy. Two decades back Whestel (20) described NIR as a sleeping technique. Few years back Davies (21) wrote about the diversity of the potential NIR applications in the article " Near Infrared Spectroscopy: Time for Giant to wake up". In a recent article, Goldner (22) writes " Near IR opens a window to rapid analysis". Today NIR has found its way into many laboratories and industries to provide information within seconds that once took hours or even days to obtain by classical analytical methods.

2.1 NEAR INFRARED SPECTROSCOPY

2.1.1 Introduction to Near Infrared Region

The infrared region extends from the red end of the visible spectrum to the radio waves; this region includes radiation at wavelengths between 0.7 μm (700 nm) and 500 μm (500,000 nm) or the wavenumbers between 14000 cm^{-1} and 200 cm^{-1}. This is schematically shown in Fig. 2.1 below, depicting the whole spectrum of electromagnetic radiation (19). The infrared region is further divided into near infrared (0.7 μm to 2.5 μm), mid-infrared (2.5 μm to 50 μm) and far infrared (50 μm to 500 μm). NIR spectral region, as

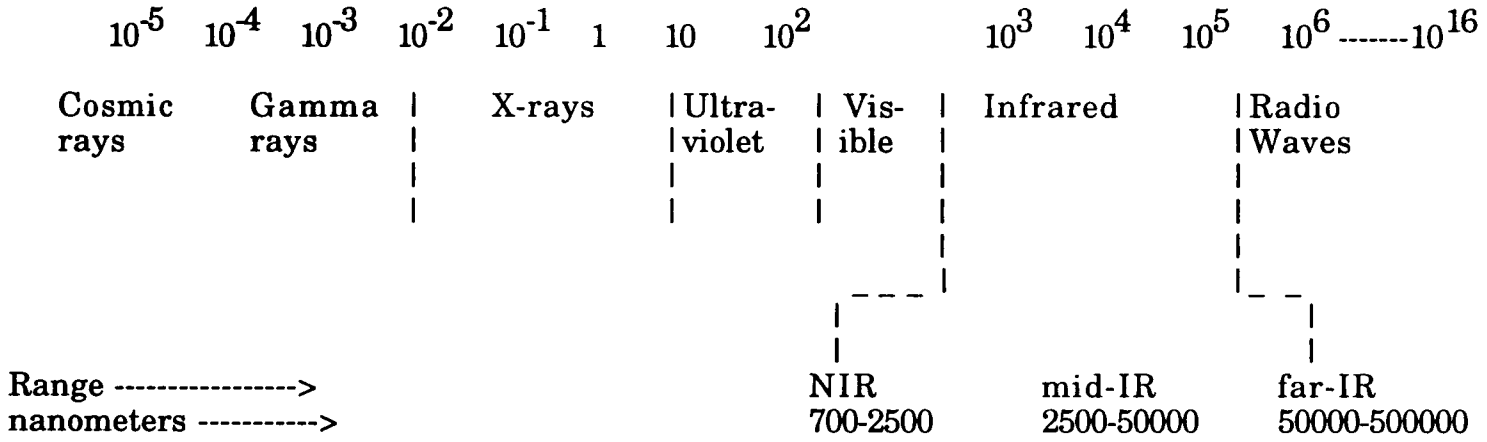


Figure 2.1 Location of near infrared region in the electromagnetic radiation spectrum.

described by ASTM (American Society for Testing and Materials) Working Group, is the range of electromagnetic spectrum from 780 nm to 2500 nm (23).

Traditionally, chemists have exploited the mid-IR region. This region exhibits sharp absorption peaks, characteristic of functional groups. These peaks arise, mainly from fundamental vibrations and very few first overtones. The fundamental vibrations arise from the energy transitions between ground state and first excited state. While, the overtone vibration modes arise from the transitions between ground state and second or higher order excited states.

The absorption bands in the NIR region are due to overtones and combination of the fundamental mid-IR molecular vibrations. Since these transitions are of higher energy (higher frquency) than fundamentals, these are less likely to occur. Correspondingly, the absorption bands in this region are comparatively weaker in intensities. Although all fundamental vibrational modes can have overtones, the most prominent bands observed in the NIR are those related to O-H, C-H, and N-H groups. This is because the first overtone of other types of vibrations, for example the C-O stretch, occur due in the mid-IR region, and have only second or third overtones in the NIR. In addition to the simple overtones, combination bands also occur. These usually involve C-H, O-H, or N-H stretch plus one or more bending or rocking modes. Multiplicity of possible combinations, leads to a complex NIR spectra, with many band assignments unresolved. Inspite of this complexity, there have been several attempts for both qualitative analysis in terms of band assignment and quantitative analysis in terms of determining physical and

chemical properties of materials. Several comprehensive reviews have been published, summarizing band assignments and analytical applications for NIR spectral region (20, 24-28).

2.1.2 Theory

Infrared radiation absorbed by a molecule causes individual bonds to vibrate in a manner similar to that of a simple harmonic oscillator. If a molecule were an ideal harmonic oscillator, its potential energy (Uq) could be described by:

$$Uq = - kx^2 \qquad (2.1)$$

where k = spring force constant

x = displacement

Unlike this classical spring model for molecular vibrations, there is not an infinite number of energy levels. Instead of this continuum of energies, there are discreet energy levels based on quantum mechanical treatment (24). A simplified solution of energy levels for diatomic molecules may be written as

$$E_q = h\nu_{osc}(v + 1/2) \qquad (2.2)$$

where h = Planck's constant

v = vibrational quantum number

ν_{osc} = frequency of vibration

The separation between these discreet levels, which determines absorbance frequency, is given as

$$\Delta E_q = h\nu_{osc} \qquad (2.3)$$

For polyatomic molecules with N atoms, the energy levels become quite numerous. Treating such a molecule as series of diatomic molecules, the generalized equation for energy levels is

$$E_q(v_1, v_2, ...) = \sum_{i=1}^{3N-6} h\nu_{osc,i}(v_i + 1/2) \qquad (2.4)$$

$$(v_1, v_2, ..=0,1,2, ...)$$

In cases where transition of energy is from 0 to 1 in any one of the vibrational states (v_1, v_2, ...) the transition is considered a fundamental. Where the transition is from the ground state to $v_i = 2$ and higher, and all others are zero, it is known as an overtone. Transitions from the ground state to a state for which $v_i = 1$ and $v_j = 1$ simultaneously are known as combinations. For ideal oscillators, quantum mechanical selection rules forbid transitions between more than one energy level. Only the fundamental vibrations would be observed and there would be no NIR spectrum.

However, molecules are not ideal oscillators. In the case of real springs, as masses approach each other, real compression forces are fighting against the bulk of spring (not accounted for in ideal calculations). As the spring stretches, it eventually reaches a point where it loses its shape and fails to return to its original coil. Similarly, the respective electron clouds of two bound atoms limit the approach of nuclei during the compression step, creating an energy barrier. At the extension of stretch, the bond eventually breaks when the vibrational energy level reaches the dissociation energy. The ideal parabola of Eq. (2.1) is therefore distorted, and becomes unsymmetrical or anharmonic. This deviation from ideality is referred as "anharmonicity" and is schematically shown in Fig. 2.2 (28).

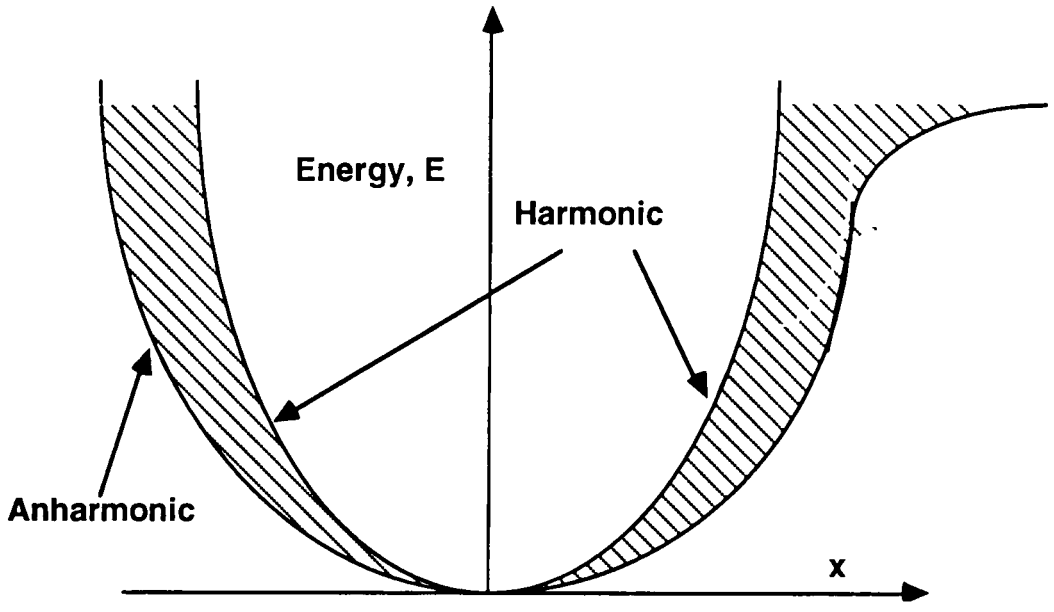


Figure 2.2 Potential energy diagram for harmonic and anharmonic oscillator.

Cubic and higher order terms maybe added to the potential energy equation (2.1) to account for this anharmonic behavior. Consequently, the energy values of the anharmonic oscillator model, obtained from modification of Eq. (2.4), are given as

$$E_q(v_1, v_2, ...) = \sum_{i=1}^{3N-6} h\nu_{osc,i}(v_i + 1/2) - h\nu_{osc,i}x_e(v_i + 1/2)^2 + \text{higher order terms} \quad (2.5)$$

$$(v_1, v_2, ..=0,1,2, ...)$$

where x_e is the anharmonicity constant.

The most important consequence of the anharmonic nature of molecular vibrations is that transitions between more than one energy level are allowed. These transitions give rise to overtone absorption. The separation between energy levels is slightly lower with each successive ascending level and is dependent on the anharmonicity constant x_e. The general formula is given as

$$\Delta E_q = h\nu_{osc,i}(1 - 2v_i x_e) \quad (2.6)$$

2.1.3 Sampling Methods

When incident radiation strikes a sample, it can be transmitted, absorbed or reflected. Concurrent with different modes, there are several sampling techniques in the NIR spectroscopy. Each of these have advantages for a particular application. Overall they cover a wide range of application areas ranging from pure inorganic liquids using transmission spectroscopy to analysis of spectrally complex agricultural products by diffuse reflectance.

Transmission

NIR transmission spectroscopy is perhaps the simplest of all spectroscopic measurement techniques. It is most useful in analyzing liquids but much less so for solids. In the area of polymers it has been used for both bulk polymers and polymer solutions (9). Recently, it has been used for in-line monitoring of polymeric processes (18).

A transmission measurement at a single wavelength involves the measurement of intensity of an incident light beam (I_0) and the intensity of light beam after it traverses through the sample (I). The absorbance (A) can then be calculated:

$$A = -\log(I/I_0) \tag{2.7}$$

If there is only one absorbing component in the sample, the absorbance is proportional to the concentration of that component, according to the Beer-Lambert law:

$$A = abc \tag{2.8}$$

where a is molar absorptivity of the component, b is pathlength, usually the sample thickness and c is the molar concentration in the sample.

For off-line analysis, NIR in the transmission mode has been used on bulk polymers and polymer solutions (9). In case of solutions, pathlength corresponds to the width of the cuvettes. For bulk, the sample thickness is usually the pathlength. Unfortunately, it is difficult to measure the thickness of bulk sample. Some of the data treatment methods, like Multiplicative Scatter Correction (MSC) (29) and Pathlength Correction with Chemical Modeling (PLC-MC) (30), can be used to reduce the variable thickness effects.

Transmission spectroscopy has also been used for analysis of flowing polymeric streams. The low absorbances permit, use of larger sample stream size i.e. larger optical pathlength, and thus facilitate in-line monitoring of polymer composition. In the present case, it is application of NIR transmission spectroscopy to a highly scattering system. As a trend, highly scattering systems have not been analyzed in transmission mode.

Diffuse Reflectance

Diffuse reflectance is perhaps the most widely studied and applied technique for NIR spectroscopy. It has been used to analyze samples from a whole spectrum of application areas. The major work done has been on studying agricultural products. In fact this one technique has kept interest in NIR spectroscopy alive.

In diffuse reflectance spectroscopy, the intensity of light reflected by the sample (R) is used to define a pseudo-absorbance value (A_r):

$$A_r = -\log(R/R_0) \qquad (2.9)$$

where R_0 is a reference intensity value (intensity of incident light or one reflected from a highly scattering non-absorbing surface). The intensity of light reflected from the sample has contributions from both, specular and diffuse reflectance (9). Specular reflectance arises from the incident light that is regularly reflected, but not absorbed, by the sample. Diffuse reflectance arises from the incident light that has been absorbed and incoherently emitted by the sample (26). In NIR spectroscopy, only diffusely reflected light contains the chemical information about the sample. The pseudo absorbance

is related to concentration in a Beer-Lambert law manner:

$$A_r = abc \qquad (2.10)$$

This relation is commonly used, even though it is theoretically incorrect. The above relation holds when specular component is negligible. When this component is significant, a more general correlation based on Kubelka-Munk theory is applicable (31).

Other Methods

Transflectance is a measurement that combines transmission with diffuse reflectance. The incident radiation enters the sample where it is partially absorbed and a large part is diffusely reflected from a reflector plate at the back of the sample. This technique is good for turbid liquids and suspensions such as milk or paints.

Attenuated total reflectance (ATR) is a measurement technique that uses slight penetration of light into sample during specular reflectance to create an absorption signal. This is not such a useful technique in NIR because of long sample required to attenuate light signal significantly (26).

2.1.4 Advantages of NIR

Those complex and overlapping absorbance peaks in the NIR region which had kept its application limited, are now being cited as its main advantages. The low sensitivity in the NIR region, once thought to be less fascinating, is turning out as an advantage in this era of rapid process monitoring. The following discussion highlights these advantages for process monitoring application, in comparison to other spectroscopic techniques.

Comparison with mid-IR

The mid-IR region, extending from 2 μm to 15 μm, has been the first love of spectroscopists. There is an abundance of clear sharp peaks in this region. The sharp peaks characteristic of particular molecular group, known as fundamental bands, make IR spectrum in this region a unique "fingerprint" that can identify each compound (19). In contrast NIR is characterized by abundance of highly complex and overlapping peaks.

Associated with clear peaks in mid-IR is the presence of high sensitivity. This requires that either sample is substantially thin or diluted. In any case sampling method is highly time inefficient. Dilution of sample restricts its application to off-line analysis while limitation in terms of sample thickness can take it at the most to on-line analysis. In both cases there is substantial time delay. If the process is changing fast, the process can go out of control. On the other hand, low sensitivity of NIR permits its application for in-line monitoring. Higher pathlength requirements are achievable with NIR. As discussed in section 1.1, there is negligible time delay for in-line analysis, constrained only by process delays, and thus provides better control.

The overlapping peaks had also been a big deterrent to application of NIR. This has again turned out to be an advantage. The fact that NIR spectrum is rich with bands means it is conceivably possible to find band for almost any property variable of interest (23). With the development of the state-of-the art multivariant methods, this has been transformed into reality. Further, presence of more than one overtone in the NIR, provides the flexibility of selecting the specific overtone, depending upon the sensitivity.

For example one overtone may be causing high absorbance and thus to use a specific pathlength, other overtone could be used.

Availability of bright source for NIR light, is another advantage. Tungsten lamp can provide high throughputs of light. This provides with a better signal to noise ratio. In contrast, the available light sources for mid-IR applications are not capable of such high throughputs.

Comparison with Ultra Violet Region

Absorptions in the ultra violet (UV) region arise due to transitions between atomic or molecular energy levels. Absorption in this region is strong and the absorption bands are typically broad. Consequently selective measurement of one component in presence of the other is difficult. On the other hand, absorption bands in the NIR region are weak, and relatively narrow and characteristic of the functional group causing absorption. The weakness of absorptions is particularly advantageous for polymer applications. Resulting larger pathlengths facilitate in-line monitoring.

Fiber Optic Cables

The development of silica fibers in the telecommunication industry has opened new doors for NIR. These optical fibers are capable of high throughputs. The use of fiber optics enables remote sensing and transmission of spectral information to the spectrophotometer. Distances between the analyzer and the sampling point may vary anywhere from a few meters to thousand meters. This depends on the requirement of the application and the spectral region of interest (5).

Remote sensing enables achievement of safety, cost and performance advantages. Locating instrument in a safe area, remote from process, eliminates the need for purged enclosures or any analyzer house. Thus low costs of equipment maintenance. With design of suitable probes, the sampling problem can be completely eliminated. Availability of rugged probes which can withstand adverse process conditions enables in-situ or in-line process monitoring. Thus fiber optic cables coupled with rugged probes can provide real time measurements.

A single spectrophotometer can be used for measurements at multiple sample points via multiplexer. Ease of multiplexing is another advantage of using fiber optic cables. With such efficient fiber optic cables available for NIR, multiple measurements can be made easily. This in turn results in substantial cost saving per measurement point.

2.2 MULTIVARIATE TECHNIQUES

A NIR spectrum contains absorbance values at various wavelengths. According to Beer-Lambert law, as given by Eq. 2.8, each of these absorbance values is directly proportional to each of the concentrations of species in the mixture. Other properties of interest are related through the proportionality constant. Ideally response at one wavelength could be used for quantification of the desired property in terms of spectral information. As mentioned earlier, the complexity of absorption phenomenon in the NIR range needs more complex analysis. The total number of wavelength responses is very large and is of the order of 1000. With this large amount of complex spectral

information available from NIR spectroscopy, quantitative interpretation has been a major challenge. There is a whole range of multivariate techniques available for such quantification. There are several reviews and books available for basic understanding of these techniques (32-36).

The earliest applications involved the use of multiple least squares regression (MLSR) as a tool for quantitative interpretation of the spectral information. These methods focused more on proper wavelength selection. These methods rely on initial qualitative understanding of the spectral data and subsequent selection, based on this analysis, of particular wavelengths to be used in calibration.

One of the severe disadvantages with this method is the problem of outliers. Outliers are abnormal observations showing some type of deviation from the bulk of the data. The outliers may occur for many different errors. Outliers may arise out of experimental error, instrument error, etc. Inclusion of outliers in calibration is detrimental to the predictability of the model. Presence of small impurity like burned carbon particles can severely alter the quantitative result. In other words, MLSR is very sensitive to extraneous data; yet it is hard to know a priori which constitutes extraneous data.

An alternative approach to the selection of wavelengths, is to use the entire spectral response. The various techniques in this class (36), known as full spectrum techniques, are Partial Least Squares (PLS), Classical Least Squares (CLS) and Principal Component Regression (PCR). Full spectrum techniques, in general, are more accurate and robust. They have better outlier sample detection ability. The use of all wavelength variables also has

signal averaging effect. These also provide qualitative understanding of the relation between the various portions of spectra and the property of interest.

The use of PLS and PCR has not been limited to the area of chemometrics (the use of mathematics and statistics on chemical data), but today they are being used extensively in multivariate process monitoring and controller designs as well (37). Both PLS and PCR are based on the principle reduction of the dimensionality of the original data, removing the dimensions which contribute little to the overall variation. In essence, they are based on extracting a much smaller dimensional model in representing the original data. The reduced data is then regressed in the ordinary least squares sense. PCR and PLS differ in the way they use the information from input variables (**X**) and output variables (**Y**), in the data reduction step. PCR uses information from **X** only, while PLS model incorporates information from both **X** and **Y**.

The following sections briefly review the principles of full spectrum techniques. While PLS and PCR will be used in later data analysis, CLS is also described for the sake of completeness.

2.2.1 Classical Least Squares

Classical least squares (32, 34, 36) is a first order regression method. The m by n matrix **X** containing the spectra of m samples at n wavelengths, is to be correlated to the matrix **Y** of the properties of interest, here concentrations, as

$$\mathbf{X} = \mathbf{YS} + \mathbf{E} \qquad (2.11)$$

where **Y** is a m by p matrix, with $m > p$ usually, containing concentration of p analytes in m samples, **S** is an p by n response matrix containing the spectra of each of the pure p analytes, and **E** is a m by n residual matrix.

The aim of regression is to obtain an estimate of the pure spectral responses matrix **S**. The least squares estimate of the **S** ($\hat{\mathbf{S}}$) is given by the equation

$$\hat{\mathbf{S}} = \mathbf{Y}^{+}\mathbf{X} \qquad (2.12)$$

where $\mathbf{Y}^{+}$ denotes the pseudoinverse matrix of **Y**. The pseudoinverse is used rather than the inverse in anticipation of nonsquare and overdetermined matrices. When the columns of **Y** are linearly independent $\mathbf{Y}^{+} = (\mathbf{Y}^{T}\mathbf{Y})^{-1}\mathbf{Y}^{T}$, that is the ordinary least squares solution is obtained. The columns of Y would be linearly independent, if none of the columns of Y can be obtained as linear combination of other columns of Y.

The estimated pure analyte spectra (in $\hat{\mathbf{S}}$) are the spectra of each analyte as it exits in the calibration samples. These spectra can be used to determine the structure or interactions of analyte molecules in the sample. This estimate, $\hat{\mathbf{S}}$, can be used for prediction of unknown ($\mathbf{y_p}$) from the spectral response of a future sample by

$$\mathbf{y_p} = \mathbf{x_p}\hat{\mathbf{S}}^{+} \qquad (2.13)$$

Again if $\hat{\mathbf{S}}$ has linearly independent columns,

$$\hat{\mathbf{S}}^{+} = (\hat{\mathbf{S}}\hat{\mathbf{S}}^{T})^{-1}\hat{\mathbf{S}} \qquad (2.14)$$

This form of calibration, where the concentrations of all constituents in the calibration samples are known, is called direct or total calibration (32).

An advantage of this method is that the qualitative information from the estimated pure analyte is best of all the calibration methods. Since all the spectral responses are used, a signal-averaging effect can take place. The

main disadvantage is the requirement of knowledge of concentration of all the components giving rise to the signal. This is really difficult, especially in the case of unknown interferent. Indirect or partial calibration methods like principal component regression (PCR) and partial least squares (PLS) overcome this problem.

2.2.2 Principal Component Regression

The relation between spectral response (**X**) and concentration matrix (**Y**), for the indirect calibration, is given as

$$\mathbf{Y} = \mathbf{X}\beta + \mathbf{F} \qquad (2.15)$$

where is β a n by p matrix of coefficients of regression and **F** is a m by p residual matrix of **Y**.

Principal Component Regression (PCR) (32, 34, 36) is a linear multivariate method that can be used to construct a calibration model between the NIR spectral data and a property of interest. This property of interest could be composition, temperature, viscosity, etc. Construction of PCR model involves decomposition of the NIR data for a set of calibration samples (contained in matrix **X**). This decomposition gives a few principal components describing the bulk of the variation in **X**. Traditionally an iterative algorithm has been used to find these principal components (38). In this thesis, a singular value decomposition (SVD) based approach (39) is being described since this is a more robust method and furthermore it is appealing to the engineering community due to its linear algebra based formulation. The SVD approach decomposes **X**, a m by n matrix, as:

$$\mathbf{X} = \mathbf{U}\Sigma\mathbf{V}^{T} \qquad (2.16)$$

where columns of **U** are eigenvectors of $\mathbf{X}(\mathbf{X}^T)$ and columns of **V** are eigenvectors of $\mathbf{X}^T\mathbf{X}$. Σ is a diagonal matrix, with elements being the positive square root of the eigenvalues of $\mathbf{X}(\mathbf{X}^T)$ or $\mathbf{X}^T\mathbf{X}$. The leading columns of **U** and **V** are referred to as the principal components or latent variables, and the elements of Σ are called the singular values. The primary feature of interest is that

$$\mathbf{U}^T\mathbf{U} = \mathbf{I}_{m \times m} \tag{2.17}$$

$$\mathbf{V}^T\mathbf{V} = \mathbf{I}_{n \times n} \tag{2.18}$$

where **I** represents the identity matrix and the subscripts are the dimensions of the identity matrix. The condition described by 2.17 implies that the columns of **U** are orthonormal to each other i.e. they are of unit length and perpendicular to each other. This is also referred to as orthognality of **U**. Equation 2.18 describes orhtognality of **V**.

Geometric interpretation will simplify the above exposition. Lets say **X** is a 5 by 2 matrix; 5 samples and two variables x_1 and x_2. The SVD of **X** will give a 5 by 5 **U**, 2 by 2 **V** and 5 by 2 Σ. Each row of **X** matrix can be interpreted as a point in 2-dimensional space, with coordinates x_1 and x_2. The vectors joining the origin to that point can also be used to represent that point. Consequently, the set of two numbers can be referred as a vector as well as a point. An example **X** matrix represented as 5 points is shown in Fig. 2.3.

Also shown in the same figure are the rows of $\mathbf{V}^T$ i.e. $\mathbf{v_1}$ and $\mathbf{v_2}$. They are represented as vectors. As defined by 2.18, $\mathbf{v_1}$ and $\mathbf{v_2}$ have unit length and they are orthogonal to each other (just as the original axis are perpendicular to each other). Therefore, the two vectors $\mathbf{v_1}$ and $\mathbf{v_2}$ can be

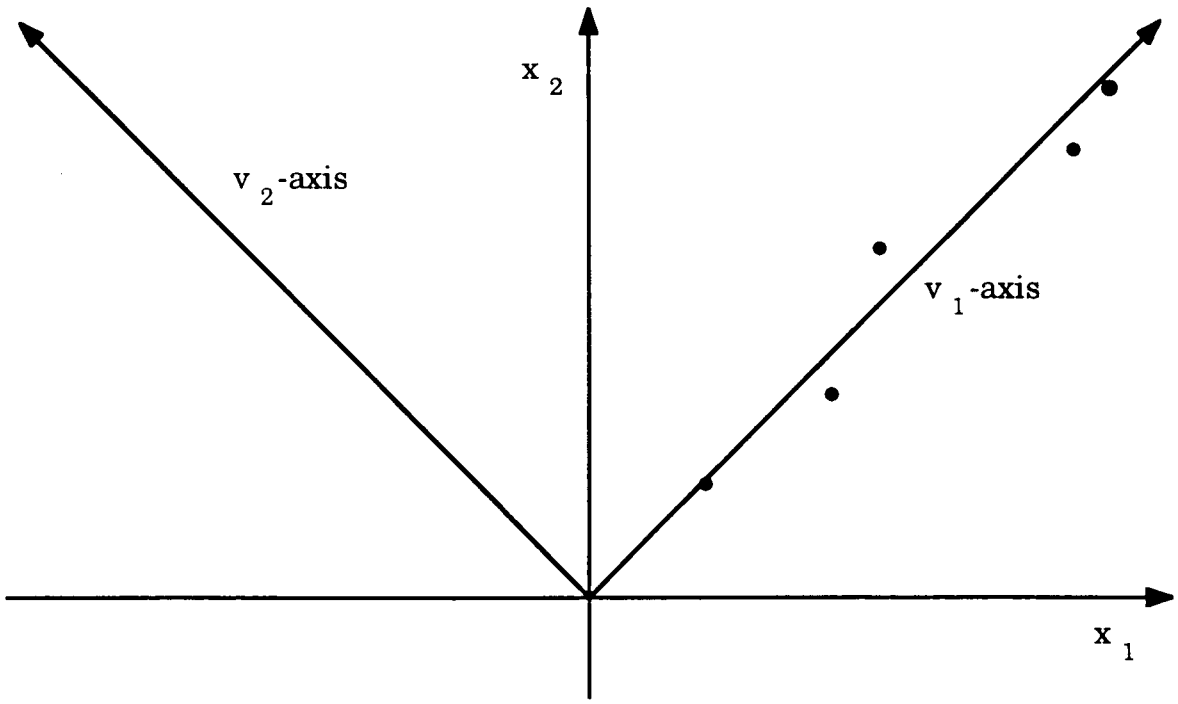


Fig. 2.3 Geometric interpretation of Singular Value Decomposition for the case of two variables.

considered as an alternate set of orthogonal coordinate axis. A coordinate transformation of the original data, for representation in terms of $\mathbf{v}_1$ and $\mathbf{v}_2$, gives the new data points as $\mathbf{u}_1\sigma_1$ and $\mathbf{u}_2\sigma_2$, where $\mathbf{u}_1$ and $\mathbf{u}_2$ are first two columns of U, and σ_1 and σ_2 are elements of Σ. For this particular case, it is evident from the figure, each point has a much more dominant projection on the $\mathbf{v}_1$-axis than on the $\mathbf{v}_2$-axis. In other words, the points represented by the original rows of the **X** matrix fall predominantly along the $\mathbf{v}_1$-axis, and less along the $\mathbf{v}_2$-axis. This is a consequence of the relatively small σ_2. If $\sigma_2 = 0$, the coordinate of each of the five points on the $\mathbf{v}_2$-axis (given by $\mathbf{u}_2\sigma_2$), is zero. All points would lie on the $\mathbf{v}_1$-axis. Thus the purpose accomplished by SVD is to reorient the coordinate frame in such a way as to make them follow more closely the distribution pattern made by the points of the rows of the **X** matrix themselves. SVD provides a coordinate frame for this purpose.

In the above example if $\sigma_2 = 0$, a linear relationship would exist between x_1 and x_2, and information from one variable would not be independent of the other. In general, the condition where one variable can be written as a linear combination of others, is referred to as collinearity. A near zero σ_2 consequently implies an approximate relationship between the two X variables and is called near collinearity. These conditions were easy to visualize on 2-D plots for the case of two variables. The same cannot be done when dealing with a larger number of variables but the concepts developed for two variables using SVD, can be extended to larger number of variables. Reorientation by SVD brings the conditions for collinearity and near collinearity to the forefront.

Presence of collinearity means that the number of independent direction of variations is less than the total number of variables. This is especially true of the spectroscopic data, where absorbance values at number of wavelengths provide overlapping information. Consequently, a least squares solution is not possible. The problem of collinearity is handled by eliminating components with zero singular values. Eliminating these components brings about a reduction in the dimensionality of the data. In the above example if $\sigma_2 = 0$, the data is reduced from 2-D to 1-D.

Near collinearity situations have serious effect on the stability of calibrations. Thus, near collinearity situations are more of concern and require optimization. Near collinearity can arise from random noise, experimental error, presence of an interferent, etc. Using all the singular values for calibration may increase the chance of fitting to noise. The calibration fit would look good, but the predictability may be severly hampered. This phenomenon is called overfitting. On the other hand, using too few singular values amounts to taking too little information into building the model. This phenomenon is known as underfitting. Those singular values representing mostly random errors and presumed to be not correlated with property of interest are cast away.

The overall effect, in eliminating collinearity and near collinearity, is in the reduction of the dimensionality of the principal component space. The reduced $\mathbf{X}$ ($\mathbf{X_r}$) is represented as:

$$\mathbf{X_r} = \mathbf{U_r}\, \Sigma_r\, \mathbf{V_r}^T \qquad (2.19)$$

where $\mathbf{U_r}$, Σ_r and $\mathbf{V_r}$ are the reduced $\mathbf{U}$, Σ and $\mathbf{V}$, respectively and r stands for the number of principal components reatained. Mathematically, $\mathbf{X_r}$ is of a

lower mathematical rank, that containing less error while retaining most of real information caused by non-random sources of variation. The rank of $\mathbf{X_r}$ is the number of principal components retained. The number of principal copmponets is also known as the number of factors (32) .

The estimate of regression coefficient can be obtained by

$$\hat{\beta} = \mathbf{X_r}^{+} \mathbf{Y} \qquad (2.20)$$

where

$$\mathbf{X_r}^{+} = \mathbf{V_r}\, \Sigma_{\mathbf{r}}^{+}\, \mathbf{U_r}^{T} \qquad (2.21)$$

The pseudoinverse $\Sigma_{\mathbf{r}}^{+}$ is obtained by taking the reciprocals of the singular values. The resulting $\hat{\beta}$ can be used for later prediction. The main advantage of using PCR is that it can use the full spectra resulting in the signal averaging effect. It takes care of the collinearity problem by decomposing the spectral response into just a few independent principal components. Further, casting away of the data along the smaller dimensions minimizes the effect of random noise. The casting away procedure is entirely based on the spectral response **X**. This is also an area where the main disadvantage of PCR may surface. There is no consideration given to the property or concentration data or the Y matrix, during the casting away step. If the analyte of interest had a very weak signal, it may contribute little to the first few principal components and may even get discarded as noise.

Partial least squares (PLS) overcomes this problem. PLS uses information from both **X** and **Y** in the process of dimensionality reduction. Consequently, the small information in **X** which is significantly correlated to **Y**, doesn't get discarded.

2.2.3 Partial Least Squares

PLS (32,34-36, 40-44) is by far the most widely used multivariate technique for NIR spectral data treatment. In PLS, the reduced dimension space is optimally correlated to both **X** and **Y**. It takes both **X** and **Y** to be collinear among themselves and corrupted with random noise and thus involves separate models for the spectral response and the concentration of analyte or any other property of interest. Mathematically it is to be decomposed as

$$\mathbf{X} = \mathbf{T}\mathbf{P}^{T} + \mathbf{E} \qquad (2.22)$$

$$\mathbf{Y} = \mathbf{Z}\mathbf{Q}^{T} + \mathbf{F} \qquad (2.23)$$

Here **X** ,**Y**, **E** and **F** are as defined before. Columns of n by r matrix **P** and p by r matrix **Q** are known as the loadings of **X** and **Y**, respectively. Columns of m by r matrices **T** and **Z** are called the scores of **X** and **Y**, respectively. The decomposition as defined by equation 2.22 and 2.23 is based on describing the maximum correlation between **X** and **Y**. The columns of **Z** are regressed against the columns of **T** to obtain regression coefficients.

There are several algorithms for decomposing **X** and **Y** into the above forms. In one case columns of **T** are orthogonal while in another case columns of **P** are orthogonal. In any case, the major deviation from PCR comes from that both **T** and **P** cannot have orthogonal columns simultaneously. This results from describing maximum correlation between **X** and **Y**.

Traditionally, the non-linear iterative partial least squares (NIPALS) algorithm has been used for computation of the principal components in PLS. The NIPALS approach is based on an iterative step for computation of each successive principal component (41). Recently, there have been efforts to

develop SVD-based approach for PLS. Lorber et. al. (44) have tried to give a theoretical understanding of PLS using SVD. In a latest work, Wang et. al. (45) have developed a new approach to PLS. The iterative step in NIPALS approach has been replaced by an SVD based computation. This approach is up to ten times computationally faster than the iterative step in NIPALS-based approach for 500 by 10 X and 500 by 2 Y, matrices. Furthermore, SVD is known to have superior numerical properties as compared to the NIPALS method (46). Thus, the calibration models developed using SVD-based approach are more computationally efficient and robust.

The number of latent variables or the number of principal components r, to be used for calibration are determined by a cross validation procedure, as discussed in section 2.2.4 below. Having chosen the number of latent variables, also commonly referred to as number of factors, a regression is obtained between the reduced forms of **X** and **Y**. The resulting regression coefficients can then be used for prediction.

Since PLS methods are full spectrum methods, important qualitative information can be obtained. The first PLS loading spectrum obtained from the first column of the matrix **P** indicates spectral features that are positively and negatively correlated with the analyte concentration. Instead, if the property of interest is a physical property, a correlation of the property to the specific compositional and structural features can also be obtained. PLS can be used even when unknown spectral interferences or analyte interaction effects are present. The qualitative information obtained by PLS is nevertheless poor compared to that from CLS (36). Direct information about the presence and source of non-linearities is not readily available from PLS

because the method is capable of modeling some type of non-linearities. A system with interactions may be more accurately fit by the PLS, and thus, the molecular interaction information in the residual spectra is lost.

2.2.4 Calibration Procedure

Calibration/Prediction Statistics

Calibration model developed using any regression technique is to be used to predict property of interest, both on calibration and prediction samples. Quantification of errors for these predictions is important in terms of judging the quality of a given calibration model. Quantification of calibration errors is done by measuring the Standard Error of Calibration (SEC), defined as

$$SEC = \sqrt{\frac{\sum_{i=1}^{nc}(y_{i,c} - y_i)^2}{(nc-1)}} \qquad (2.24)$$

where $y_{i,c}$ is the property of calibration sample i that is estimated from the calibration model that uses all the calibration samples. nc is the number of calibration samples. The Standard Error of Prediction (SEP) is a measure of the prediction error, and is given by

$$SEP = \sqrt{\frac{\sum_{i=1}^{np}(y_{i,p} - y_i)^2}{(np)}} \qquad (2.25)$$

where $y_{i,p}$ is the property of prediction sample i predicted from the calibration model, y_i is the known property sample i, and np is the number of prediction samples. SEP value is the best indicator of the ability of NIR spectra to predict the property of interest. Since low errors are desirable, low SEC and SEP value show that the model is good.

As an alternative to quantification of errors, calibration fit to the data can be quantified. Correlation coefficient (R) is used to measure the goodness of fit to the data. It is given as

$$R = \sqrt{1 - \frac{\sum_{i=1}^{nc}(y_{i,p} - y_i)^2}{\sum_{i=1}^{nc}(y_i - \bar{y}_i)^2}} \qquad (2.26)$$

where $\bar{y}_i$ is the mean of all observations for y_i. The value of R varies between 0 and 1. A value of R close to zero indicates that the calibration is a poor approximation of the actual values. As R increases, there is better and better match between predictions and actual values and at R=1 there is perfect match. The correlation coefficient is often mentioned as percentage, too.

Cross Validation

The number of factors to be included in a calibration model using PLS or PCR is determined by the cross validation procedure (47). Use of too few factors may leave out some important information and thus result in underfitting. Use of too many factors may lead to incorporation of noise into

the model. In both cases the predictability would be poorer than an optimum, to be determined by cross validation.

In cross validation procedure, a selected set of samples are used to build calibration models with varying number of factors or latent variables. The constructed calibration models are then used to make predictions of the samples left oout. SEP values are computed as given by Eq. 2.25. SEP values for different number of factors can be plotted against the number of factors. The optimal number of factors is the number at which lowest SEP values are obtained for the first time. Different combinations of the samples left out can be used to get a more confident value for the number of factors. Having selected the number of factors, the calibration model is constructed from the data set.

Leave-one-sample-out cross validation is used when there are not enough samples. Here the cross validation procedure is repeated as many times as the number of samples. Every time a sample is left out and a calibration model is built with the rest of the samples. The standard errors of prediction for this cross validation process is given as

$$SEP_{cv} = \sqrt{\frac{\sum_{i=1}^{n}(y_{i,cv} - y_i)^2}{(n-1)}} \qquad (2.27)$$

Here $y_{i,cv}$ is the property of sample i predicted by the calibration model that excludes sample i, y_i is the known property of sample i and n is the number of samples.

3. LITERATURE REVIEW

Abundance of absorbance bands in the NIR region can be used to find almost any property of organic substances. With the use of the state-of-the-art multivariate techniques, discussed in the previous chapter, this has been transformed into reality. Consequently, there is a whole spectrum of NIR work described in literature. The prominent ones in the area of agricultural products, petrochemical substances and polymers, are summarized below.

3.1 AGRICULTURAL PRODUCTS

This is probably one area which cannot be left unmentioned when discussing the applications of NIR spectroscopy. Much of the technological development in the area of instrumentation for NIR has been done by researchers in the food and agricultural industry. The advantages that NIR offers for reflectance measurements, such as high reflectance to absorbance ratio, high signal-to-noise ratio, have been especially useful for rapid analysis of agricultural products (24) . NIR has been extensively used for analysis of grains, forage and other agricultural products. Much of the quantitative analysis using multivariate techniques for NIR has been developed in these applications. The revival of interest in NIR is in large part due to this work.

Karl Norris and his coworkers were the pioneering researchers in application of NIR spectroscopy to agricultural products (48,49). They had used diffuse reflectance for rapid analysis of grains. The specific absorption

bands in the NIR region suggested possibility of measuring protein and moisture in grains; and protein, oil, and moisture in soybeans. The pioneering work by Norris was followed up by others. Today there are several reviews summarizing the broad spectrum of applications. The few prominent ones are by Williams (50), Watson (51), Osbourne (52), and Polesello and Giancumo (53).

Wheat and flour have been the subject of extensive study using NIR. Norris and Hart (54) were the first ones to determine moisture content in wheat. Later efforts expanded the horizon into determination of oil, starch, sugar and fiber content (55). Fig. 3.1 shows the overlaid spectra of wheat and its components. The significant differences visible, even on a cursory view, were used for analysis. Effects of temperature and granularity on the moisture measurement have also been examined. Today NIR is used for rapid determination of protein and moisture in wheat on site in grain markets (27). The analytical results from NIR are used to segregate grain by protein content and to assure acceptably low moisture levels. Payments and classification are determined on the basis of NIR analysis. Wheat hardness can also be determined by NIR (56).

Major flour-milling companies control product streams by at-line analysis using NIR (27). In addition to protein and moisture determinations, a key requirement for milling control is the measurement of the degree of separation of the bran from the endosperm. This separation is indicated by the bran and ash content. A NIR measurement can estimate bran by its cellulose and oil contents, and predict ash content by its correlation to bran (57). Osborne (58) has discussed the on-line measurement in flour mill using

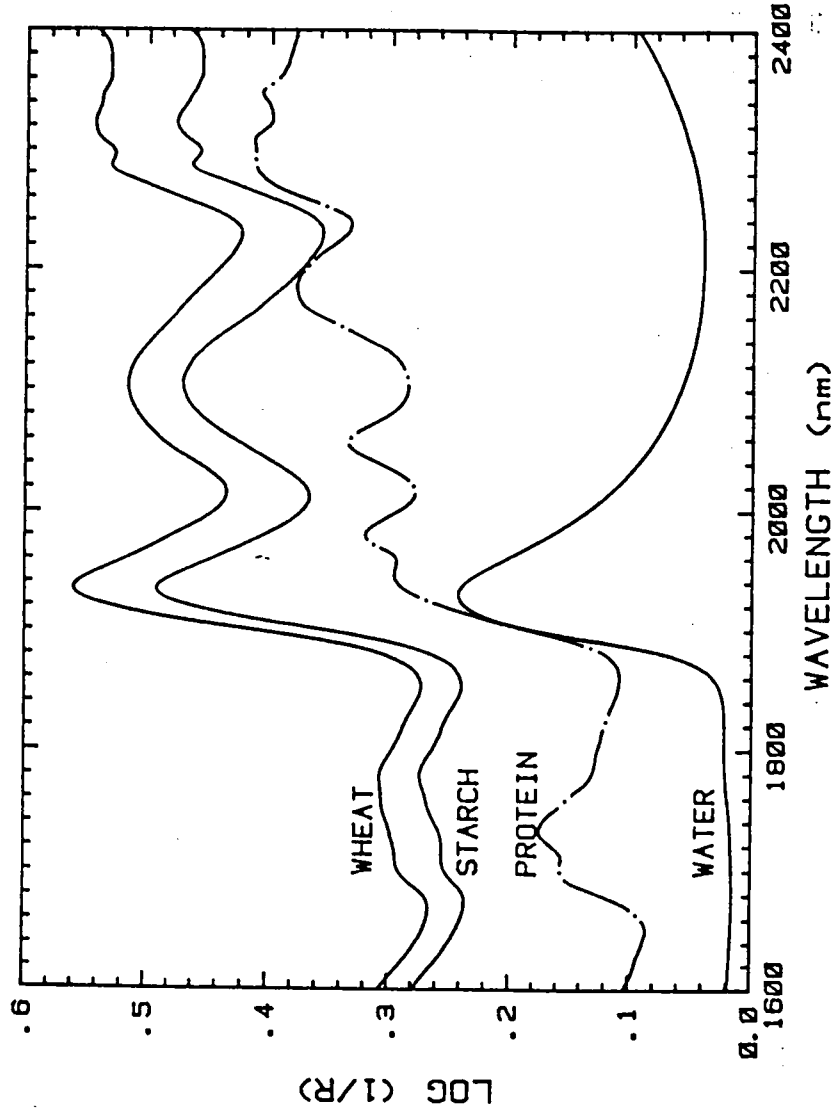


Figure 3.1 Overlaid spectra of wheat and its components (55).

NIR. Rapid measurements accomplished on-site by mill personnel, allow for timely adjustments of the milling process, which increases efficiency and profit.

There are number of applications of NIR in the food processing industry. Process control on incoming flour has already been discussed. Osborne determined the protein, fat and moisture content in intact slices of white bread. Fat and sucrose have been quantified in mixtures of different types of breads (58). Fiber in processed cereals (59), the total sugar content of four different breakfast cereals (60), and fiber and starch content in snack foods (potato and corn chips, popcorn, pretzels, and crackers) (61) have also been determined rapidly using NIR. Fat, protein and carbohydrates have been estimated in cocoa powder (62). Kellogg Company (27) uses NIR for rapid monitoring and control of various process stages.

In the dairy industry, NIR was initially used for fat, moisture, protein and lactose content determination in whole, nonfat and modified milk powders (63). The same contents have been determined in cheese and ice creams (27). Ben-Gera and Norris were the first ones to analyze fat and moisture, of cooked and uncooked beef. Subsequent work incorporated lamb meat for fat, moisture, and protein determination(64). Recent studies have focused more on rapid and noninvasive analysis of meats. Isakasson et. al. (65) have used NIR for nondestructive determination of protein, fat and water in plastic-wrapped, homogenized meat.

3.2 PETROCHEMICAL SUBSTANCES

The analysis of hydrocarbon substances, pure and mixture, has been the area of most extensive study. The earliest analysis date back to 1920's. These were mainly focused on obtaining characteristic spectra and doing band assignments. Later efforts were directed towards cataloging these results into compendiums to be used as reference library. As an example of this Sadtler Laboratory has published a 1000 spectrum compendium of industrially useful compounds (66). The spectra in this collection are in the wavelength range 650-2700 nm. This reference collection can be used for rapid check of wavelength and absorptions characteristics.

For a compact summary of NIR adsorption bands, the correlation chart first published by Goddu in 1960 (25) continues to be very useful. The original charts also include average molar absorptivity data. In a latter work, Weyer (24) has summarized the prominent band assignments for a variety of organic substances. Other reviews have also incorporated various band assignments.

With the advances in computer technology, the visual inspection of spectra for qualitative interpretation is no longer necessary. Recently, Lo and Brown (67) have published an automated library searching method for identification of mixtures using NIR spectroscopy, without any prior chemical information. Spectra for a number of different organic liquids were collected. These were stored on an IBM PC. This spectral information was later used as reference library. The spectra of unknown mixtures were then identified by an automated search using the reference spectral information. The results of

identification were quantified in form of a similarity index. The resulting similarity indices showed around 99% accuracy in identification of 5 unknown mixtures.

The quantitative work, in the area of NIR analysis of petrochemical products, started as early as 1930's. These initial efforts mainly used one wavelength for calibration purpose. Rose (68) reported the use of NIR to calibrate the structural group of 55 hydrocarbons. Absorbance peak at 1600 nm was used to get a correlation for CH_2 functional group. The main problem arose due to deviations in determination of primary, secondary, and tertiary C-H groups. A later study was used to determine number of C-H groups for paraffins and napthenes (69). Use of a correction factor, to account for deviations discussed above, produced good results.

Tosi and Pinto (70) obtained the spectra of 50 individual hydrocarbons. Calibration for carbon-hydrogen groups were then developed at five different wavelengths. A calibration was developed for linear hydrocarbons, branched hydrocarbons, those containing isopropyl functional groups, and branched compounds with isopropyl functional groups. This calibration equation required independent density measurements. An improvement on this would have been to use another wavelength for density correlation and thus solely use NIR for complete quantification (71).

Interferents cause problems when using single wavelength calibrations. Presence of intermolecular or hydrogen bonding can alter the results very much. The advent of faster computers and better multivariate techniques, lead to increase in the number of wavelengths used in calibrations. With this ability, more and more properties of interest could be

measured using NIR. As an example of this, Honigs et. al. (72) determined several physical properties of hydrocarbons. They used NIR to calibrate heats of formation, mean molecular weight (weight average), and number of methyl groups per molecule. Mixtures of benzene, cyclohexane, isooctane and n-heptane were analyzed. Multivariate calibrations yielded satisfactory results with high degree of correlation, 0.993 for heats of formation, 0.986 for molecular weight and 0.997 for methyl groups per molecule. This demonstrated use of single method instead of several labor intensive methods for determining various physical properties. Also the results obtained were much more rapid than the conventional methods.

Callis et. al. (73) have used NIR spectral features, in the wavelength range 600-1215 nm, for prediction of gasoline octane numbers. The quantitative analysis was carried out using MLR and PLS. For MLR, a 3 wavelength calibration gave best results. The SEC value varied between 0.3 - 0.4 octane number while SEP varied between 0.4-0.5 octane number. The results for PLS, using four factors, closely parallel the results of MLR. The entire spectra from 661-1215 nm were used for PLS. The constituent percentage of aromatics, olefins, and saturates was also determined. Extending the scope of this study, Swarin and Drumm (74) analyzed 359 unleaded gasoline samples from 23 cities throughout the United States. This study went beyond determining limited number of properties like octane number and hydrocarbon classes. A wide variety of properties, including oxygenate content, benzene concentration, distillation properties, specific gravity, Reid vapor pressure were determined. Sulfur, ethanol and methyl t-butyl ether (MTBE) were also determined. Calibrations were done using both

the stepwise multilinear regression (SMLR) and PLS, with PLS giving slightly better results. There was high degree of correlation between NIR spectra, and octane numbers ($R > 0.98$), hydrocarbon classes ($R \approx 0.92$), MTBE content (0.991), ethanol content (0.985), oxygen content (0.989) and benzene content (0.952). Most of the calibrations had lower standard errors than the corresponding more laborious ASTM methods. This should not be interpreted as NIR being more accurate because NIR is a secondary technique and any error due to standard method gets multiplied.

Methanol is an additive in gasoline. Methanol is used as a blending agent because it is relatively low cost compared to the gasoline. Quantitative ability of NIR has been demonstrated for, rapid and relatively accurate, determination of methanol content (71). The spectral data was obtained in the range 1500 to 1700 nm. The calibrations were performed using absorbances at 1673 nm, 1619 nm, 1664 nm, and 1702 nm. The calibration using all four wavelengths had the best predictability. The SEC value of 0.2174 and SEP value of 0.6266 were obtained for this calibration.

Determination of above properties is not only critical to engine performance but also has an effect on the toxic emissions. Going a step further, there have been efforts to incorporate NIR for in-line vehicle determination of automotive fuel consumption. Carduner (75) at Ford Motor Company is working on development of NIR absorption sensor for in-line vehicle determination of automotive fuel consumption.

Remote analysis using fiber optic cables is really attractive for volatile hydrocarbons. The explosive nature can pose hazard problems for the instrument. Using the fiber optics, several studies have been done on analysis

of propane and methane (76-78). Extending this concept, several standard mixtures of natural gas have been analyzed. A set of NIR spectra for mixture of methane, ethane and propane, were measured at various pressures in the range 100 to 1000 psi (79). Quantification of the composition was further used for determination of energy content of natural gas. A comparative analysis of predictability of various multivariate techniques was also done. Best results were obtained using a Fourier Transform Quantitative (FTQ) program. The SEP values varied between 31 Btu/ft^3 for measurements at 100 psi to 315 Btu/ft^3 at 1000 psi.

3.3 POLYMERS

Polymeric compounds, a major class of industrially important materials, can be studied advantageously by NIR spectroscopy. The earliest applications go back to as early as 1940. While the early accounts were directed towards band assignments (80), it was soon realized that NIR had the ability to yield much more in terms of quantitative determination of physical and chemical properties of polymers. Information such as molecular weight (81), residual monomer content (82), quantification of components in copolymers and blends (83), rate or degree of cure (84), and crystallinity effects (85) can also be determined.

The main advantage of using NIR for polymers, instead of the fingerprint region of mid-IR, is of weaker absorbances. Weaker absorbances facilitate the use of higher pathlengths. The thin films needed for mid-IR are difficult to prepare and to measure thickness accurately, while NIR work can

be performed on thicker samples. In-line monitoring is facilitated with use of higher pathlengths. Advantages of using in-line monitoring have already been discussed in section 1.1.

A great deal of NIR work has been done in the area of polymers. Pure polymers have been analyzed mainly for band assignments. Compositional analysis of blends and copolymers has also been done. Additive content and hydroxyl numbers, of polymers have also been quantified. Molecular weight determination, analysis of packaging laminates, progress of reaction, viscosity and crystallinity measurements, etc. have also been the subjects of NIR work. The following subsections briefly review some of the prominent work done on polymeric products.

3.3.1 Pure Polymers

NIR studies in this application area have been mainly for qualitative purposes. The characteristic spectra have been interpreted in terms of the polymer structure. There have been efforts on band assignments. These band assignments are of great significance when dealing with copolymers and blends. With the availability of characteristic spectra, one knows what changes to look for with changing composition. At other places, characteristic spectra can be used to follow the chemistry of the reaction. In any case, this is the first step towards doing any study in terms of quantification.

Glatt and Ellis (80) did an extensive study on pure polymers using NIR. They used NIR to study alignment of specimens of polyethylene, nylon, polyvinyl alcohol, polyvinyl chloride and polyvinylidene chloride. Band assignments for various vibration mode of $>CH_2$, >N-H and >C=O were

made. The bands at 1214 nm (8237 cm^{-1}) for polyethylene and 1206 nm (8292 cm^{-1}) for nylon, due to $>CH_2$ third overtone are prominent example of these band assignments. This and several other band assignments along with their intensities have been discussed. This study has also shown presence of hydrogen bonding in nylon. The rupture of N-H --- O bond can be observed in molten and to some extent in hot unmolten polymer.

Crandall and Jagtap (86) have determined the NIR spectra of a series of step reaction and addition polymers for purpose of polymer identification. The polymers analyzed were polystyrene, polyurethane, nylon 66, polyesters and a phenol-formaldehyde resin. Polyethylene and polypropylene glycol prepolymers were also analyzed. Several band assignments were done including aryl N-H, aryl C-H, amide N-H, and carbonyl bands. Band assignments for several polymers have also been made by Foster et. al. (87). These include >N-H, ≡C-H, and >C=O bands in polyethylene, polypropylene, nylon, polyisobutylene, polystyrene, polyvinyl acetate, polyvinyl chloride, and vinylidene chloride-vinyl chloride copolymer.

Danneburg (84) analyzed epoxy resins for epoxide equivalent by NIR. Band assignments were made for terminal epoxy overtone at 1159 nm and the combination at 2208 nm. He used isobestic points (points with same absorbance) in the hydroxyl peak to determine equivalent weight. Isobestic points eliminate the shift in peak due to noise.

Crystalline polystyrene has a distinct NIR spectrum and is often used to check linearity of instruments. Fig. 3.2 shows the characteristic peaks of crystalline polystyrene. There are distinct peaks at 1143.7, 1680.2, 2167.2, and 2306.8 nm to test linearity (88).

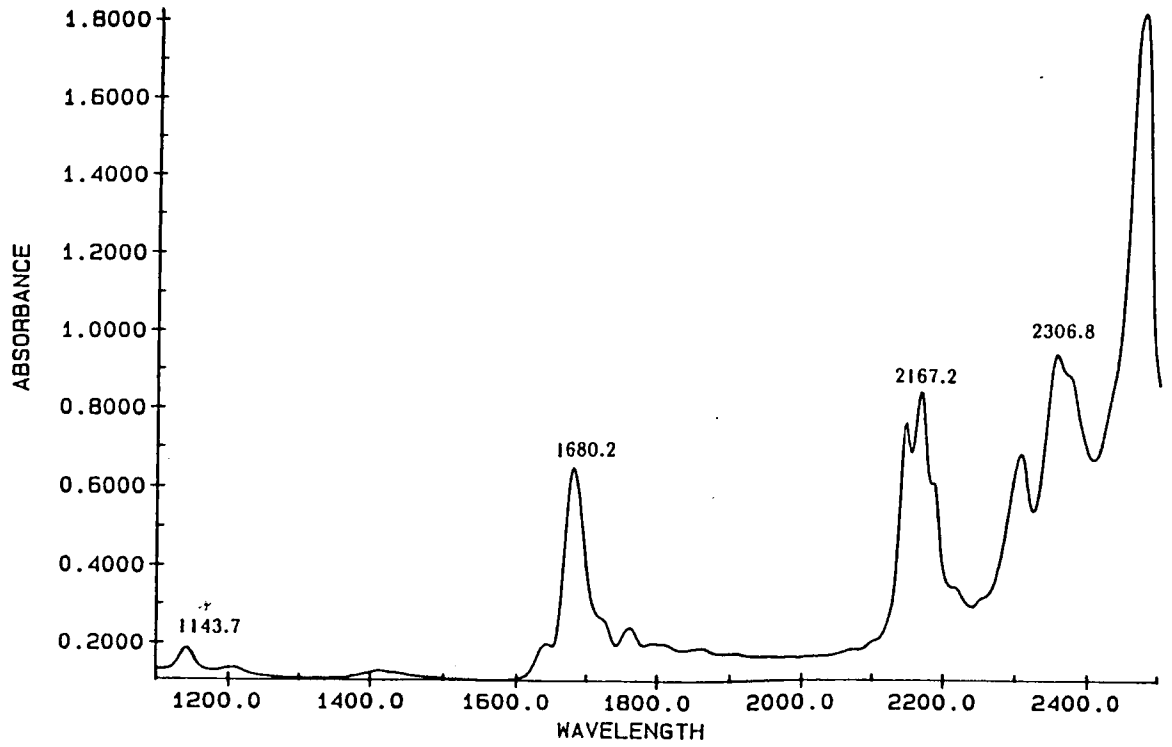


Figure 3.2 Spectrum of pure polystyrene showing the four characteristic absorbance bands (88).

In a later work, Howell (89) has done an extensive study on qualitative identification of polymeric materials using NIR spectroscopy. Various textile fibers and thermoplastic polymers were studied. The various textile fibers studied included polyethylene terephthalate (PET), polypropylene, cotton, acrylic, wool, rayon, and nylon. Significant differences were observed in spectra of polypropylene, PET, and acrylic. Cotton and rayon, differing only in crystalline phase morphology, show smaller but distinct spectral differences. The spectra of nylon 6 and nylon 6, 6 exhibit very subtle but observable differences in the region beyond 2000 nm. This work showed that NIR is sensitive not only to chemical changes but also to morphological changes too.

Howell, further analyzed 25 thermoplastic polymers. Although the chemical structure of PET and PBT (polybutylene terephthalate) is very similar, differing only in number of $>CH_2$ groups in polymer chain backbone, the NIR spectra obtained were sufficiently different to distinguish them from each other. Spectra of three polyolefins, i.e. high density polyethylene, polypropylene, and polymethylpentene , were also obtained. These polyolefins are also structurally similar. Differences are only in the number $>CH_2$ groups between each pendant $-CH_3$ group. The spectral differences were significant enough to distinguish between each other. Other materials analyzed included polyether sulfone, polyaryl ether ether ketone, and polyaryl ether ether ketone ether ketone.

3.3.2 Blend Composition

One way of achieving desired properties from the existing polymers is forming blends. As an example of this, blending of low density polyethylene (LDPE) and high density polyethylene (HDPE) can result in materials with properties that are intermediate between those of pure HDPE and LDPE (90). To achieve the desired properties, effective and efficient assessment of composition is required.

NIR is an effective technique to measure composition of polymer blends. Miller (91) has determined composition of HDPE and LDPE blend films. Melt-extruded films of HDPE and LDPE, at seven different blend ratios, ranging from 0% HDPE to 100 % HDPE, were analyzed using NIR spectroscopy. For each HDPE percentage, five replicate samples were used. The films were approximately 25 to 40 μm thick. The films were analyzed in transflection mode in the wavelength range of 2100 to 2500 nm. Calibrations were performed using PCR and the optimal number of factors was determined by cross validation. A total of 3 factors, giving a SEP value of 2.481% HDPE, was found to be optimum. The SEC value was 2.31% HDPE. A total of 98% spectral variation was described by the first three factors. The loadings and scores of the first three factors were analyzed to get a qualitative understanding. Factor 1 described variation between replicate samples, and factor 2 described variation between 100% HDPE samples and the rest of the samples. Factor 3 was the most relevant for determination of HDPE percentage in the samples with 0 to 50% HDPE.

In another application, Weyer (92) has used NIR to measure composition of three spectrally similar resins in a blend. The polymer resins

were linear, branched and cyclic hydrocarbons. The calibrations were performed using MLSR. The results showed high correlation (0.97). The standard errors of prediction varied between 0.06 for linear polymer and 0.4 for cyclic polymer. The NIR analysis was much faster when compared to the normal 16 hour extraction procedure for determination of one of the ingredients.

McPeters and Williams (2) have used NIR for in-line composition monitoring of polymer blends. The spectral measurements were performed at the exit port of a single screw extruder. The polymer blends were composed of styrene and acrylic polymers, with acrylic concentration varying from 0 to 45 wt%. There were distinguishable peaks in the region 1200-1650 nm. Calibrations were done using two wavelength MLR (1211 nm and 1595 nm) and PLS. MLR gave a correlation of 0.9986 and standard error of 0.79. PLS gave correlation of 0.9973 and standard error of 0.78, for three factors. The predictability of these calibration models were tested using leave-one-sample-out cross validation, as well as leave-one-group-out cross validation. The SEP values varied between 0.3 wt% and 1.13 wt%, respectively .

Hansen et. al. (16,17) have worked on a system of polystyrene (PS) and polyphenylene oxide (PPO) blends. The composition was again monitored in-line, at the exit port of a single screw extruder. The concentration of PPO was restricted to 75 wt% due to constraints on mechanical durability of NIR probes. There were significant spectral differences in the region 1600-1800 nm and 2100-2400 nm. Quantitative analysis of the spectral data was done using PLS and PCR. They were carried out by, using Unscrambler (32), a standard software by Guided Wave, Inc. (El Dorado Hills, CA), and by a self

developed approach based on SVD. Calibration models were developed using 100 samples and absorbances at 36 wavelengths (1665 nm - 1700 nm). The predictive ability of the calibration models were tested against a validation set of 50 samples. The SEP values for the four techniques namely PCR-Unscrambler, PCR-SVD, PLS-Unscrambler and PLS-SVD were 0.8567, 0.8487, 0.8115 and 0.8047, respectively.

3.3.3 Copolymer Composition

Copolymers have a long history of examination by NIR. Ethylene-Propylene copolymers have been quantified by many researchers (83, 93, 94). Combination bands at 2275, 2312 and 2466 nm were used to determine monomer ratios. These bands are less susceptible to crystallinity effects than the corresponding bands in the mid-IR. These experiments were conducted on polymers films.

Miller (9) quantified contents of ethylene propylene-diene (EPDM) copolymers. These terpolymers are mostly composed of ethylene and propylene units but also contain diene functionalities in the polymer backbone that are used to make crosslinks. EPDM is used as rubber modifier. Earlier experiments on ethylene-propylene copolymers were on films while Miller analyzed samples in bulk (pellets or thick pieces of polymer) and CCl_4 solution. Instead of using one or two wavelengths, a large number of wavelengths were chosen in combination (1950-2500 nm), first overtone (1570-1850 nm), and second overtone (1100-1550 nm) regions. CLS and PLS were used for development of calibration models. Leave one out cross validation was used to estimate the SEP values for CLS calibration. The

calibration results using absorbances in the first overtone region gave lowest SEP values. For samples in CCl_4 solution, the SEP values ranged from 2.1 to 4.1 wt%. For samples in bulk, the spectral data was corrected using MSC. The SEP values were only slightly higher for this case.

The optimal number of factors for PLS was obtained by cross validation on two user selected prediction sets. The cross validation results indicated that optimal number of factors were, three for all calibrations using solution samples and four for all calibrations using bulk samples. For most part SEP values for PLS calibrations were significantly lower than SEP values for CLS calibrations. The SEP values were drastically reduced for bulk samples. The SEP values in the first overtone region, again minimum, varied from 1.7 to 3.0 wt% for solution and 1.0 to 1.8 wt% for bulk. The spectral data for bulk samples was corrected using MSC.

Combined vinyl acetate (0-15% w/w) in vinyl chloride/vinyl acetate copolymers was measured using NIR spectroscopy (95). Spectral measurements were made on powdered samples, in the wavelength range 800 nm to 2700 nm. The spectra showed five characteristic absorbance peaks. Absorbance peaks at 1200 nm, 1750 nm and 2400 nm ,were second overtone, first overtone and combination bands, respectively of C-H stretch. The 1400 nm and 2100 nm absorbance peaks were due to third and second overtones of the ester carbonyl group. Measurements made in diffuse reflectance mode were affected by the particle size range. A poor resolution was observed for raw samples. Resolution was improved with the control of particle size range. Ratio of reflectance at 2100 nm carbonyl peak to 1750 nm C-H absorbance peak, varied linearly with the percentage vinyl acetate in the vinyl

chloride/vinyl acetate copolymer. A better correlation was observed for finer particles (≈ 0.99).

Various styrene copolymers have been subjects of NIR study. Styrene - acrylonitrile (SAN) polymers have improved heat and solvent resistance over pure polystyrene. Styrene-methyl methacrylate copolymers improve the light stability of styrene. NIR has been applied for compositional analysis of these copolymers. Styrene-acrylic copolymers were analyzed for styrene content using 2144 nm aromatic C-H combination band (96). Calibration experiments were performed on mixtures of polystyrene and methyl methacrylate dissolved in chloroform solution. Absorbance at 2144 nm was regressed against concentration to yield a calibration equation. This equation was used to predict concentration of several different copolymer solutions, with % polystyrene in copolymers ranging from 65 to 90%. The predicted values were validated using NMR data. Maximum difference of 1% between two techniques showed that NIR equally competent technique in terms of accuracy.

Miller and Willis (82) analyzed a system of butadiene/styrene copolymers. This, being a totally hydrocarbon system, is difficult to analyze with chemical methods. Heat pressed films, approximately 0.03" thick, were used in the analysis. The quantification was done using combination bands at 2200 and 2400 nm, due to aromatic and aliphatic C-H groups, respectively. The concentration ratio varied from 0 to 1.2 butadiene/styrene and the ratio of absorbances at two wavelengths (2200/2400 nm) varied linearly with it.

Monomer allyl glycidyl ether (AGE) can react through its double bond or the epoxide group, and copolymers with AGE can be analyzed effectively in

either circumstance. For example, with AGE grafted to polypropylene by reaction with the terminal double bond, the unreacted epoxide group can be measured at 2200 nm. Using this criterion, the AGE content was detected down to 0.5 wt% in copolymer plaques. Alternatively, terpolymers of epichlorohydrin, ethylene oxide, and AGE can be analyzed for AGE content using the 1630 nm absorbance peak due to terminal double bond (24).

McPeters and Williams (2) have used NIR for measurements on terpolymers samples composed of three methacrylate polymer units, with one as major component and other two being minor constituents. The spectral measurements, in the wavelength range 1200-1650 nm, were made in-line during extrusion process. Significant spectral differences, observed in the range 1200-1650 nm, were used for quantitative analysis. Compositions of major component and one minor component were calibrated using PLS. A three factor calibration model gave a correlation of 0.9946 and standard errors of 0.98 for major component. For minor component, a correlation of 0.9996 and standard errors of 0.032 were obtained. The results for minor component were better due to large spectral variations for small compositional changes.

Sohl (15) has used NIR for in-line measurements on ethylene vinyl acetate (EVA) copolymers. The spectra were obtained at the exit of a semiworks compounder (extruder) at 200-250 degrees centigrade, and 500 psi. The vinyl acetate content was varied between 12 and 15 wt% by compounding copolymers with these limiting concentrations. A calibration model built, was later used for concentration predictions. The NIR analysis performed in real-time, showed a precision well below 0.01%. These

concentration measurements in real time were used for feedback control of the compounding process. Using feedback control, it was possible to effect and hold setpoint changes in composition level.

3.3.4 Additive Content

Additives are added to prevent oxidation, discoloration or thermal degradation of polymer. UV stabilizer is a prime example of such additives. Quantitative analysis of UV stabilizer in polypropylene has been achieved using NIR. Combination bands of methylic stretches in polypropylene occur between 2000 and 2400 nm, the first overtone occurs around 1600 nm, and the second overtone occurs between 1000 and 1200 nm (25). The UV stabilizer quantified contained aromatic CH bonds. The aromatic absorptions due to UV stabilizer are shifted to shorter wavelengths and are thus distinguishable from saturated aliphatic absorptions due to polyolefins. Using this difference, quantifications have been achieved down to 100 ppm (88).

Spatafore and McDermott (97), have used NIR for quantification of polyolefin additives. Thirty three formulations of commercial polyolefin resin containing various ratios of a primary antioxidant, secondary antioxidant, and UV stabilizer were extruded to form 1 to 2 inches thick plaques. The concentration of each additive varied in the range 0 to 1%. Samples were scanned in the range 1200-2400 nm. All spectra were collected in transflectance mode. Out of 33 samples, 22 samples were used in calibration set and 11 were used in validation set to test the predictability of calibration model. Aborbances at 2032 and 1912 nm for primary antioxidant, 2129 and 1912 for secondary antioxidant, and 1546 nm for UV stabilizer, were used in

MLR calibrations. Resulting SEP values varied from 0.034 to 0.106 wt%. Calibrations were also done using PLS. The optimum calibration was found out by leave one out cross validation. The optimum number of factors was not reported. The SEP value for three additives varied between 0.032 and 0.109 wt%. The low SEP obtained using MLR and PLS demonstrated the accuracy of the method.

Plasticizer content in cellulose acetate has been measured using NIR (88). The plasticizer content ranged from 9.8 to 23%. The results showed standard error of 0.4% and correlation of 0.994. Absorbances at 1680, 1722, and 2336 nm due to aliphatic stretching, and 1982 nm due to the second overtone of >C=O, were employed in calibration.

Saturated aliphatic polyesters are plasticizers of PVC and other specialty applications. Their concentration can be estimated via hydroxyl number determination. ABS terpolymer added as modifier to PVC compounds was monitored with the aromatic CH stretch combination band at 2140 nm (98). Measurements were made on 80 mil thick plaques. %ABS ranged from 5% to 15%.

A remote non-destructive analysis of rigid PVC tiles was done for quantification of activator content (88). The activator content in PVC tiles varied from 0.08% to 0.4% and was measurable within an accurracy of 0.02%. Wavelengths used were 1268, 2150, and 2200 nm. The shift in aromatic CH was used against the straight chain CH stretch.

Dioctyl phthalate (DOP), a plasticizer in flexible PVC, was estimated using NIR (88). A calibration model was built using absorbances at 1650, 1690 and 1700 nm. The absorbance at 1690 nm is an overtone of aromatic C-

H in the phthalate ring. The absorption band for aromatic C-H is shifted to shorter wavelengths than aliphatic C-H bands. The other wavelengths were used as reference for PVC backbone. A correlation of 0.994 and SEC value of 0.2% were obtained. Epoxidized soybean oil, a processing aid, was also determined with an error of 0.1% and a correlation of 0.992.

Silicone lubricants are sprayed on textile fibers to facilitate processing. Lubricants are often referred to as finish and the amount of finish on the fiber surface is quantified as finish-on-fiber (FOF). NIR has been used for measurement of FOF on nylon 6,6 spun yarns (99). A four wavelength MLR model was built using absorbances at 1546, 1818, 2230 and 2270 nm. There was a good agreement between IR, used as a standard technique, and NIR methods, with a SEP value of 0.04%.

3.3.5 Hydroxyl Number

The most widely used polymer application of NIR is the analysis of OH functional group. The analysis of OH group is used in determination of hydroxyl number. Hydroxyl number is defined as mg of KOH equivalent to the hydroxyl content of 1g of alcohol. Jones and Brown (100) monitored hydroxyl number in polyols. Byron (101) and Turley (102) used NIR for simultaneous determination of hydroxyl number and moisture.

Hydroxyl number determination of fatty alcohols (higher aliphatic alcohols) was done based on a key wavelength of 2040 nm. Samples were analyzed in transflectance mode in a fixed pathlength temperature controlled liquid cell at 45 ^{o}C. This sampling design provided high level of accuracy (88).

The hydroxyl number ranged from 150-430. The standard error was 0.4 OH, with a correlation of 0.99999.

The NIR analysis of OH group is sensitive to temperature variations. It is desirable to account for temperature effects, when transferring NIR technology to process level. The temperature sensitivity of alcohols was examined (103). Temperature was varied from 37 to 45°C, and measurements were taken at 1°C interval. The predicted hydroxyl number decreased linearly with temperature. A 2°C change in temperature was accepted as tolerable. Larger than 2°C changes would require a correction algorithm.

Using the temperature based perturbations of hydroxyl group, Lin and Brown (104) have designed a NIR temperature sensor. Four different configurations of fiber-optic sensors were used for measurements in transmission mode. NIR spectra of water were measured in the range 5°C to 85°C, in increments of 5°C. Spectra were measured in the wavenumber range 9000 cm^{-1} to 5350 cm^{-1}; 32 scans were averaged for each spectrum. Atleast three spectra were recorded at each temperature. One spectra at each temperature was used in validation set while others were used in calibration set. Calibrations were done using linear regression (LR), MLR and PCR. PCR was done using the entire spectra while a number of different wavelengths were used for MLR and LR models. SEP values varied from 0.53 to 1.64°C for LR model, 0.22 to 0.85°C for MLR model, and 0.16 to 0.32°C for PCR model. The optimal number of factors for PCR were 7 for most of the configurations. Low standard errors, although not competent enough against the standard temperature measuring devices, are encouraging for potential applications in remote sensing and hostile chemical environments.

Unsaturated polyesters were analyzed for determination of hydroxyl number (105). Two different unsaturated polyesters, polyester 1 with hydroxyl number varying from 14 to 45 and polyester 2 with hydroxyl number varying from 15 to 70, were subjects of study. Calibration models were built using 50 and 20 samples for polyester 1 and 2, respectively. SEC values of 0.5 and 0.8 were obtained. In both cases, greater than 99.8% correlation was observed.

Commercial polyvinylbutyrate is formed from polyvinyl alcohol (PVA). The hydroxyl concentration of butyrate (expressed as % PVA) ranges from 17 to 22%. This % OH number was determined using NIR with standard error of 0.2% (88). A five wavelength calibration using 1734, 1940, 2100, 2208, and 2270 nm gave best results. Residual hydroxyl content in polymethacrylate was determined with correlation of 0.992 and standard error of 0.3 (88).

Lee et. al. (106) have used NIR for determination of hydroxyl number in polymers. Copolymer of a hydroxy functional acrylic monomer and other acrylic monomers, was the subject of study. Samples with hydroxyl numbers varying from 125 to 175 were analyzed. Samples were synthesized using a continuous reactor and two different monomer feeds. Feeds were adjusted to give the desired hydroxyl number and reactor was allowed to reach a steady state. Hydroxyl number was progressively increased from 125 to 175. Samples were pulled out at steady state and at a time period approximately half way between steady states. A total of 17 samples were used in analysis. A LR model was built using absorbance at 2044 nm due to OH stretching band. The prediction results using NIR were compared to the results from a standard chemical method. Maximum difference of 3.6 hydroxyl numbers and

minimum difference of 0.03 hydroxyl numbers was observed between results of two methods. NIR results were also compared to those obtained using mid-IR. The accuracy of NIR was comparable to that of mid-IR while mid-IR sampling was more tedious and time consuming.

3.3.6 Molecular Weight

Where the nature of the end groups of a polymer is known and absorption band characteristic of these can be found, the molecular weight of the polymer can be estimated. Molecular weight determination by endgroup analysis has been performed by measuring OH or NH absorption in the NIR range. Le Fevere et. al. (81) have used NIR for estimation of molecular weight of polyethylene glycols dissolved in benzene solution. Six polyethylene glycol samples, with molecular weights ranging between 200 and 6000, were analyzed. Spectral data was collected in the wavenumber range 6200 cm^{-1} and 8300 cm^{-1}. Absorbance peak at 7040 cm^{-1}, attributed to intermolecular hydrogen bonding through hydroxyl groups, was used in calibration. The resulting calibration equation showed a good fit to the data.

Miller and Willis (82) have made molecular weight determinations of polyethers such as polyethylene oxide and polyoxycyclobutane, in which the chain is terminated by hydroxyl groups. Molten samples were employed to eliminate any crystallinity effects. Calibrations were developed using combination band at 2100 nm. The hydroxyl content of the samples was estimated using the calibration curve so established, and the molecular weight of the materials was calculated, assuming two hydroxyl groups per

molecule. In the molecular weight range 1000-5000, a good agreement was obtained with actual values.

The NH_2 combination band at 1620 nm has been found to be very useful in determining the chain length of amine ended polysulfone oligomers (24).

3.3.7 Components of Packaging Laminates

NIR analysis of laminates with different layers of polymers is a relatively new area. Layered packaging laminates are commonly used in food industry. The relative amounts of different layers in the laminate, the microstructure of the polymers in each layer, and the concentration of additives or contaminants, greatly influences food protection qualities of a laminate. A rapid determination of laminate properties during production would be very useful for process control.

Davies et. al. (107) were probably the first one to characterize polymer laminates. The test laminates were composed of three major components i.e. cast polypropylene (CPP), linear low density polyethylene (LLDPE), and nylon (NYL), all of which were also obtained separately as films used for making laminate. Experiments were conducted using total of 12 layers of films, in which the composition was varied using different combination of films. Relative thickness (mass of the film per unit area) of different components in the samples were correlated to the spectral information. Total relative thickness of laminate samples were around 300. For all three components, single characteristic wavelength were selected that had very high correlation (>0.99) with the particular polymer. The wavelengths

selected were 1732 nm for CPP, 1716 nm for LLDPE, and 2022 nm for NYL. SEP values of 5.44, 5.43 and 6.33 were obtained for prediction of relative thickness of CPP, LLDPE, and NYL films, respectively. This demonstrated non-destructive composition determination of laminate. It was suggested that this off-line analysis could be transferred to rapid on-line analysis.

In a recent article, Miller et. al. (108) have used NIR for rapid and non-destructive analysis of food packaging laminate containing polyethylene, polyamide-6, and ethylene vinyl alcohol (EVOH). NIR spectral absorbances were obtained over the region 1100 nm to 2500 nm. Data analysis was carried out using PLC-MC and MSC for total laminate thickness, and PCR for percent polyethylene. The SEP value for thickness predictions varied between 2.36 and 4.17, while those for percent polyethylene varied from 0.74% to 1.43%. The percentage thickness of EVOH was also measured. The SEP values, for calibrations using PCR, were around 0.52%.

3.3.8 Progress of Reaction

Epoxy resins contain two or more epoxide rings per molecule. Epoxy resins react with curing agents in a ring-opening reaction to yield high performance thermosetting plastics. Determination of the state of cure advancement provides information on the nature and characteristics of polymerized material. Curing reactions of epoxy resins have been subject of extensive study using NIR (24, 88).

Several epoxy/amine reactions were studied by monitoring the disappearance of reactants and appearance of products (88). The epoxy resins used in the study were (1) a resin prepared from bisphenol A and

epichlorohydrin (Epon 828) and (2) a phenyl glycidyl ether (PGE) resin. The crosslinking agent used was hexamethylenediamine (HMDA). Reactants were combined in 1:1 and 1:2 ratios and reacted for various amounts of time. Disappearance of epoxy reactant was monitored using the 2208 nm combination band for epoxy. N-H of the primary amine in the curing agent HMDA absorbs at 1500 nm and 2000 nm. Disappearance of these peaks was also followed to record the progress in reaction.

George et. al. (109) have performed real-time monitoring of the cure reaction of epoxy resins using NIR spectroscopy. The commercial epoxy resins, consisting mostly of tetraglycidyl 4,4'-diaminodiphenyl methane (TGDDM) were cured with diaminodiphenylsulfone (DDS). The spectral measurements were made in-situ during the reaction process. Spectra were recorded in the wavenumber range 11000 cm^{-1} to 4000 cm^{-1}. The epoxy band at 8627 cm^{-1} and the primary amine bands at 6684, 6578, and 5067 cm^{-1} were found suitable for quantitative analysis. Absorbance at these wavenumbers was followed with time. Absorbance versus time plots were used to measure the cure time. The temperature dependence of the kinetics of primary amine consumption gave an activation energy of 70 kJ mol^{-1} over the range 135 to 180 ^{o}C, in agreement with the values obtained by digital scanning calorimetry (DSC).

Crandall et. al. (110) have followed the amidization and immidization process of several polyamic acid resins. The first overtone of C-H band at 1700 nm was chosen as internal standard. The 2300 nm amide band and 1950 nm amine band were compared to C-H band. The amide/C-H, amine/C-H, and amide/amine ratios can be used as a measure of degree of

polymerization and the amount of immidization. A qualitative interpretation of these ratios was used to analyze the effect of concentration and temperature.

Residual monomer content present in polymethyl methacrylate (Perspex) has been quantified using NIR (82). The residual monomer content in the polymer is normally well below 1%. At such low concentrations, the absorption band for monomer appears as a shoulder on the side of much stronger saturated C-H band. Absorbance at this shoulder band (1650 nm) varied linearly with concentration of monomer, up to 2.5% w/w concentration. Minimum detectable concentration was 0.1%.

Spectra of series of polyether polyols, with hydroxyl numbers ranging from 57 to 456, were obtained using NIR (14). The OH absorption bands at 2050 nm and 1450 nm were used to develop LR models , separately. The calibration curves showed a good fit to the data. These measurements using NIR demonstrated the possibility of monitoring the polyol production. The laboratory method for hydroxyl number determination by derivitization with acetic acid or phthalic anhydride followed by hydrolysis of the unreacted anhydride and titration of the acid formed, is slow and not suited for real time process control. The NIR measurements made with probes directly placed into the reactor allow the reaction to be followed in real time for better control of product quality.

3.3.9 Miscellaneous

Information on crystallinity and orientation of polymers has also been obtained using NIR. Basch et. al. (85) developed a new method based on NIR

for obtaining crystallinity ratios in cellulose. Absorbance peaks at 4760 cm^{-1} and 5190 cm^{-1} were selected. Intensity of the band at 4760 cm^{-1} varied directly with the crystallinity of cellulose, while the intensity of band at 5190 cm^{-1} varied inversely with the crystallinity. The crystallinity ratios were calculated using

$$\text{NIR Crystallinity Ratio} = \frac{\text{Absorbance (4760 cm}^{-1}\text{)}}{\text{Absorbance (4760 cm}^{-1}\text{) + Absorbance (5190 cm}^{-1}\text{)}}$$

The values obtained were compared to the corresponding x-ray crystallinities. A high degree of correlation, around 88%, indicated that NIR spectrum may be used to estimate crystallinity of cellulose.

Ghosh and Rodgers (111) have used NIR to measure heatset temperature of nylon yarns. Commercial nylon staple carpet yarns were used in this study. The yarns were from three fiber sources and two fiber types: Allied Anso IV (nylon 6), Du Pont Antron (nylon 66), and Monsanto Ulton (nylon 66). The sample set contained, for each fiber source, yarns heatset from 190 to 210 ^{o}C in increments of 4 ^{o}C. MLR was used for calibration of heatset temperature. Aborbances at 2250, 2130, 2180 and 1720 nm for nylon 6, and 2130, 2180 and 2100 nm for nylon 6,6, were selected for calibration. Wavelengths were selected based on previous band assignments for nylon. The results of calibrations showed more than 95% correlation and SEP values less than 2.55 ^{o}C.

Zhu and Hieftje (112) have used NIR for determination of intrinsic viscosity of polycarbonate. Six powdered samples of known intrinsic viscosities, in the range 0.49 to 0.53, were analyzed in reflectance mode.

Spectral data for eighteen wavelengths in the range 1680-2348 nm were recorded. A four wavelength calibration model gave optimum results. The optimum calibration showed a correlation of 0.98. Prediction results, shown in form of a scatter plot of predicted v/s actual intrinsic viscosity, were in good agreement with the actual values.

4. EXPERIMENTATION AND ANALYSIS

The objective of the present thesis is to demonstrate in-line composition monitoring of polymeric systems using NIR spectroscopy. The polymeric system of interest is PET filled with TiO_2. The spectroscopic measurements are to be made in-line at the exit port of a single screw extruder, on the flowing polymer stream. The following section discusses in detail the system for in-line monitoring. Subsequent sections will deal with the experimental work, and data analysis of the in-line spectral data.

4.1 EQUIPMENT

Schematic of the system for in-line monitoring is shown in Fig. 4.1. The whole assembly can be divided into three parts viz. extruder assembly, flow cell and the analyzer. A detailed description of each of these subassemblies is presented below.

4.1.1 Extruder Assembly

A single screw extruder, gear pump and a die constitute this portion of equipment. Polymer mixtures and blends are fed through a hopper to the extruder. Dry N_2 is circulated through the hopper to prevent absorption of moisture from air. The polymer is melted and homogenized in the extruder. Gear pump, located at the exit port of the extruder, takes up the emerging polymer and forces it through a die.

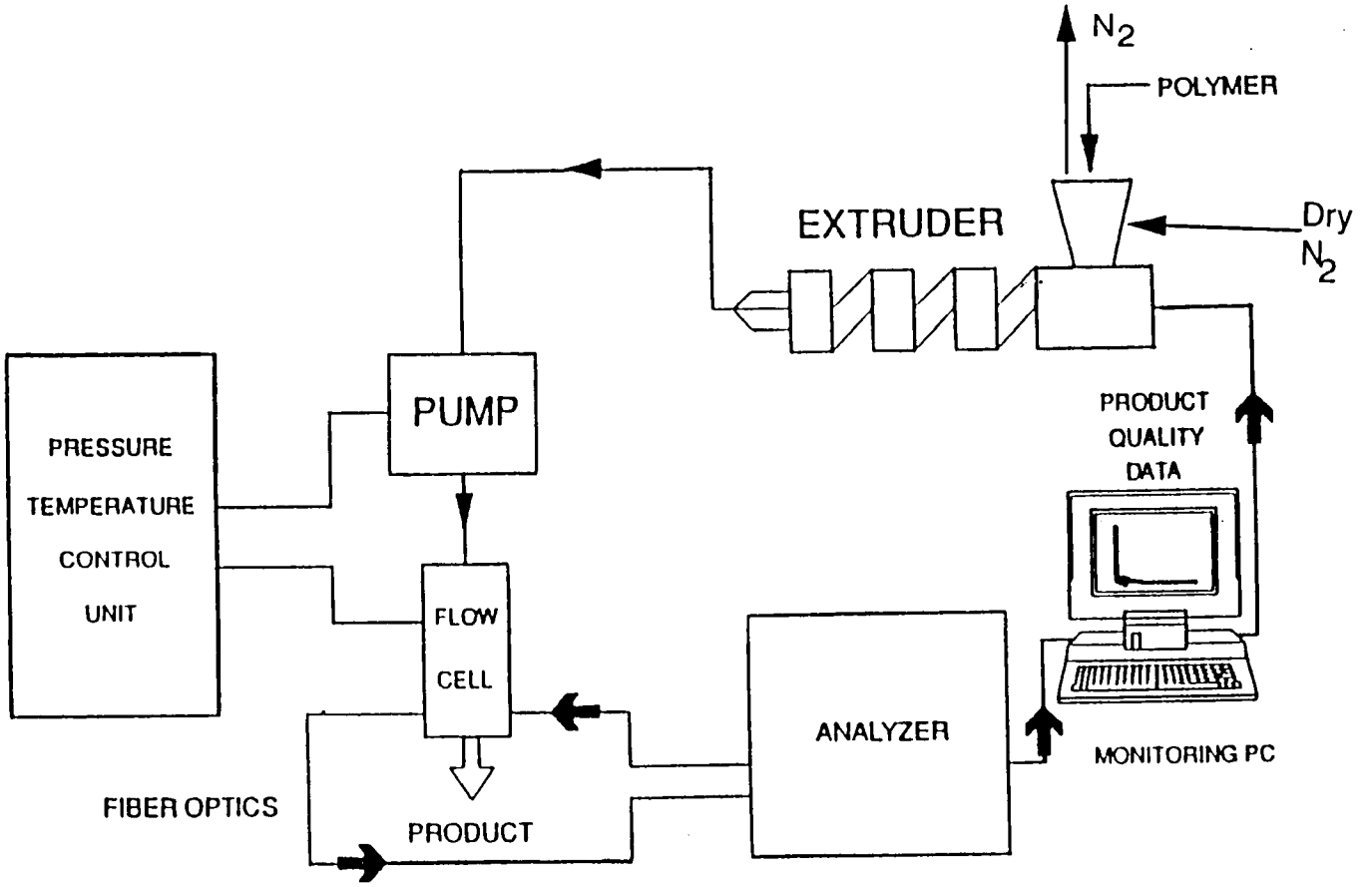


Figure 4.1 System for in-line monitoring.

C.W. Brabender Laboratory Extruder of type 2503 is used in the present setup. It has a single screw of 18.75 mm diameter (3/4") and 476.25 mm length (18.75"). The extruder is divided into four zones i.e. feed zone and heating zones 1 through 3. The temperature in the feed zone is maintained at ambient conditions using cooling water. This is necessary to prevent melting in the feed zone and thus facilitating solids conveying. The temperature in the heating zone is maintained around the melting temperature of the polymer and is increased gradually in the subsequent zones. Independent heating and cooling arrangements are provided in each of the heating zones to maintain desired temperature via external controllers. The die temperature is maintained by an independent controller.

4.1.2 Flow Cell

A modified Swagelock® 4-way fitting is used as a flow cell. This modified 4-way fitting is attached to the die. The polymer emerging from the die passes through the flow cell. The NIR fiber optic probes are mounted into the Swagelock 4-way fitting . The probes are mounted such that polymer could flow freely between the two probes. This whole assembly is shown in Fig. 4.2. This kind of probe arrangement facilitates transmission spectroscopy on the flowing polymer stream. Spectral data is obtained using the fiber optic probes as the polymer is flowing through the flow cell. A collimated beam of polychromatic NIR light emerging from one fiber optic probe, is incident on the flowing polymer sample stream. The polymer stream selectively absorbs the light depending on the composition of the polymer. The preferentially

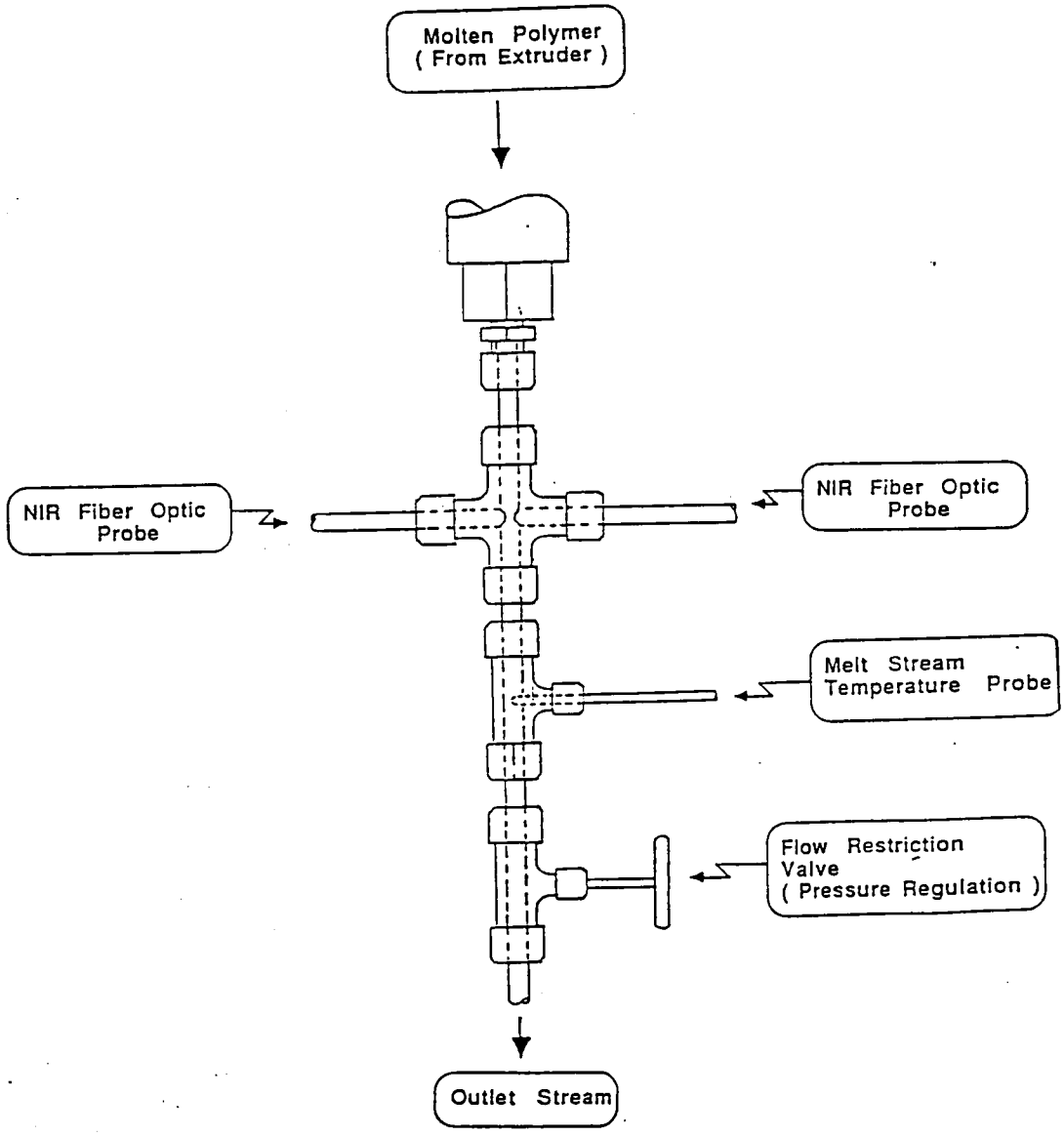


Fig. 4.2 Schematic of the flow cell.

absorbed light is received by another fiber optic probe located at the other end. The use of isotropic light eliminates any birefringence effects due to shearing of polymer chains.

4.1.3 Analyzer

The analyzer used is the Guided Wave Model 260 fiber optic spectrophotometer. It is a single beam high resolution, scanning spectrophotometer designed specifically to work with optical fibers (113). The spectrophotometer is controlled by a microcomputer, a Dell System 200 PC.

The analyzer is modular in design (113). A variety of detectors, grating, filters, slits, and accessories are available, and can be interchanged very easily to allow optimization of performance in a particular wavelength range. In the present setup a tungsten halogen lamp is used as a light source. A lead sulfide detector is used as it is optimum for the NIR range. The optimum spectral range for this particular detector is 1200 nm to 2400 nm.

The spectrophotometer is coupled to fiber optic probes in the flow cell via fiber optic cables. The length of the cables can be up to a thousand meters but for the present setup the cables are about one meter long. NIR light emerging from the analyzer is transmitted to one of the probes by a fiber optic cable. The transmitted light from the other probe is sent back to the analyzer by a similar second fiber optic cable. A comparison of the light transmitted back with a reference value gives the absorbance value at a particular wavelength. Absorbance measurements at a number of wavelengths give an absorbance spectrum. The absorbance spectrum is collected and stored on the process computer by Scanner program (113).

The function of Scanner program supplied by Guided Wave, Inc. is to provide control of the analyzer, to collect light measurement data, and to display the measurement data in useful form. The spectral data collected can be displayed and manipulated. The selection of wavelength range is also done through Scanner .

4.2 EXPERIMENTAL

4.2.1 Samples

Two commercial PET resins, one with no filler and another filled with the desired commercial requirement, representing the extremes of titanium dioxide content were chosen to make mixtures of different compositions. The exact concentration of the TiO_2 in the filled resin was not available. Thus the concentration of the filler had to be normalized between 0% and 100%. The 0% concentration represents unfilled resin and 100% represents filled resin. Intermediate concentration were obtained by mixing weighed quantities of each resin.

Both resins were dried for 24 hr's at 80 ^{o}C. The drying took place under vacuum with occasional purging with 99.99% pure nitrogen. Samples of various mixtures were obtained by dry blending the two base resins in the desired weight ratios. The samples were prepared in increments of 10% spanning the whole range of concentration from 0% to 100%. Weighed sample mixtures were then kept in closed bottles to avoid contact with atmospheric moisture. Manual shaking and tumbling of bottles were used to homogenize the mixture samples. Mixing was further enhanced in the extruder.

4.2.2 Experimental Runs

Initially pure PET at 265 ^{o}C was run through the system. The temperatures in heating zones 1, 2, and 3 were maintained at 220^{o}C, 250^{o}C, and 265^{o}C, respectively. Running time for pure PET was approximately 30 minutes to insure that the entire system was flushed and free of impurities.

The screw speed was maintained around 10 rpm. The pressure upstream of the gear pump was maintained around 2000 psi while the exit port of the flow cell was open to atmosphere. High pressure (around 2000 psi) facilitates back flow in the extruder and consequently better mixing. This kind of mixing is essential, especially for the present system of filled and unfilled PET which were available in pellet form.

Spectral data was obtained in a continuous manner after 30 minutes of flushing. The spectral data was acquired using the Scanner program. A total of 10 scans were obtained for pure PET. Using larger number of scans in the calibration will ease elimination of random noise, which in turn yields a more robust model.

After completion of scans for pure PET, the system was run until the hopper was nearly empty. PET with 10% filler concentration was introduced into the hopper at this time. Again the system was let to run for 30-35 minutes to flush out pure PET and get a stable mixture of 10% running through the system. A total of 10 scans were obtained this time also. The experiments were continued in this fashion for all the mixtures at progressively higher concentration levels. All the data was stored for later analysis.

4.3 DATA ANALYSIS

The spectral data acquired using the above methodology was stored in a microcomputer, for later analysis. Spectral information for each scan, from 1200 to 2400 nm, was stored in separate files. Approximately 10 files were stored for each blend mixture. The objective of the data analysis was application of multivariate techniques for development of calibration models.

A variety of multivariate techniques are used, as discussed in previous chapters. PLS and PCR are the most prominent ones. Being full spectrum techniques, PLS and PCR are more robust to outliers. They involve dimensionality reduction of the original data and thus can handle collinear and near collinear data. Presence of an interferent or an unknown component can also be detected. Based on all these considerations, PLS and PCR were chosen for data analysis.

Standard software, Unscrambler (Guided Wave, Inc.) (32), and self developed codes implemented in the MATLAB (114) environment on a UNIX mainframe, were available for data analysis. A PLS_Toolbox (46), with codes for PLS, PCR, and many other multivariate techniques, was also available for use in MATLAB environment. The Unscrambler software was installed on the PC, so the data could be read from the disk directly. The data files had to be imported to the mainframe UNIX for analysis using the self developed codes and PLS_Toolbox.

The Unscrambler software uses NIPALS algorithm for computation of principal components. PLS_Toolbox uses SVD based algorithm for PCR and NIPALS based algorithm for PLS. The self developed codes are based on SVD

for both PLS and PCR. Earlier comparison between results of Unscrambler PLS and SVD based PLS, showed only minor differences (18). These differences were probably due to PC roundoff error. These results were for one dependent variable, and both, NIPALS and SVD based, algorithms are exactly same for one dependent variable. This is further substantiated by the fact that results for PLS are exactly the same to the fourth decimal place using PLS_Toolbox and SVD based code (45). Results of PCR Unscrambler and PCR SVD were similar, and the small differences may be attributed to PC roundoff error.

The present system of PET and TiO_2 also had only one dependent variable in the form of TiO_2 concentration. The results from different softwares were expected to be the same within the limits of PC precision and roundoff errors. Furthermore, Unscrambler program could use only up to 200 wavelengths. In contrast, the self developed codes and PLS_Toolbox were more flexible and practically there was no limitation on the number of wavelengths that could be used in calibration. Based on the above criterion, only the analysis done using self developed codes will be discussed in the next chapter. Presentation of results using all the softwares would have been redundant. The self developed codes are shown in appendix A.

Each data file had absorbance values for 1201 wavelengths. The data files transferred to mainframe, were edited and later, moved to files with extension .mat. A .mat extension file is treated as a matrix and can be accessed in MATLAB environment directly. Subsequently, all .mat files were combined to form a larger .mat file. This .mat file formed the matrix **X**, of spectral responses. Matrix **X** was of size 85 by 1201 i.e. 85 rows and 1201

columns. The 85 rows correspond to 85 samples and 1201 columns correspond to absorbance values at 1201 wavelengths. The concentration data was stored in a matrix **Y** of size 85 by 1, 85 rows for 85 samples and 1 column for concentration of TiO_2. Both theses matrices, **X** and **Y**, were stored in a .mat file called datapet.mat.

Prior to multivariate analysis, all the variables in **X** and **Y** were mean-centered and normalized to unit variance. Mean-centering involves subtracting the mean, of measuremnts for a particular variable, from the measuremnt values. Normalization to unit variance is achieved by dividing all the measurement values for a particular variable by the standard deviation of the values. Mean-centering removes the offset and consequently, gives a better calibration fit (33). Normalization to unit variance gives every variable an equal chance to contribute to the modeling (32).

The mean centered and normalized data were then subjected to calibrations using PLS and PCR. Initially complete data set was used in building the calibration models. Calibration models were built with varying number of factors using both PLS and PCR. This was done to evaluate the contributions from various factors. The loadings and scores for different factors were computed for qualitative understanding of the data.

Later, different types of cross validations were performed on the data. Leave-one-sample-out cross validation, leave-one-group-out cross validation, and users selected groups in validation set, were used to test the predictability of various calibration models. The SEP and SEC values were computed for varying number of factors used to construct the model. The optimum number of factors was found from the predictability errors.

5. RESULTS AND DISCUSSION

5.1 SPECTRAL FEATURES OF FILLED AND UNFILLED PET

The NIR absorbance spectra of unfilled and filled PET resins are shown in Fig. 5.1. The entire spectra can be divided into three regions. The chemical structure of PET is shown in Fig. 5.2. All of the NIR absorbances are overtone and combination bands of aromatic C-H groups, methylene groups, and carbonyl groups in PET. Region I contains first overtone, and Region III has combination bands from aromatic C-H groups in the terephthalic acid (TPA) part and methylene groups in the ethylene glycol (EG) part of PET. Region II has the second overtone of carbonyl stretching band.

Specific assignments of NIR bands are difficult to determine because the absorption from each vibrational overtone and combination are overlapped extensively. Based on the tentative band assignments done for PET by Miller (9), these are summarized in Table 5.1.

Spectroscopic differences between unfilled and filled PET are essentially in the form of baseline shifts. Very few inorganic materials absorb in the NIR range and there is no known absorbance peak for TiO_2. Presence of inorganic filler causes light to scatter. This causes the baseline to move up as such, without any change in absorbance peaks.

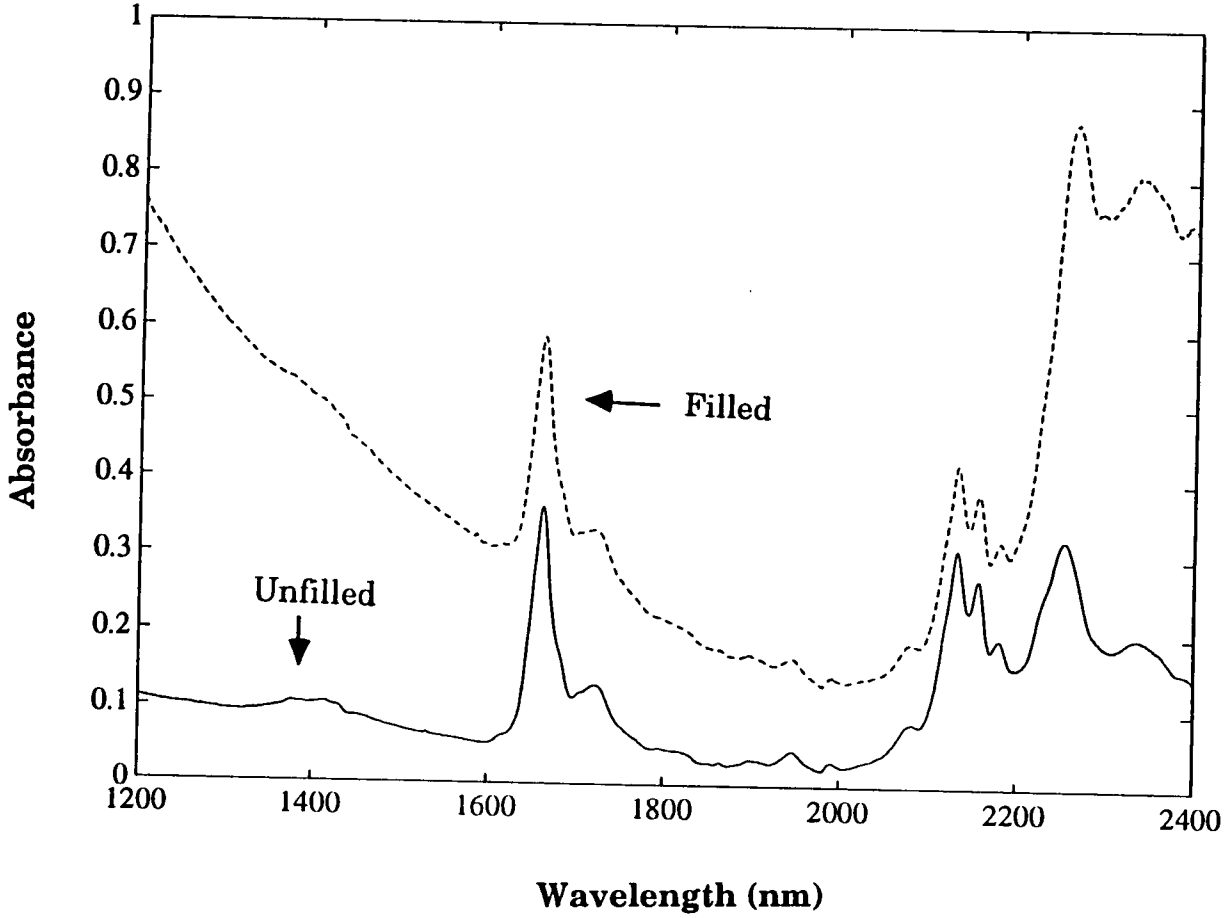


Figure 5.1 Overlaid spectra of filled and unfilled PET.

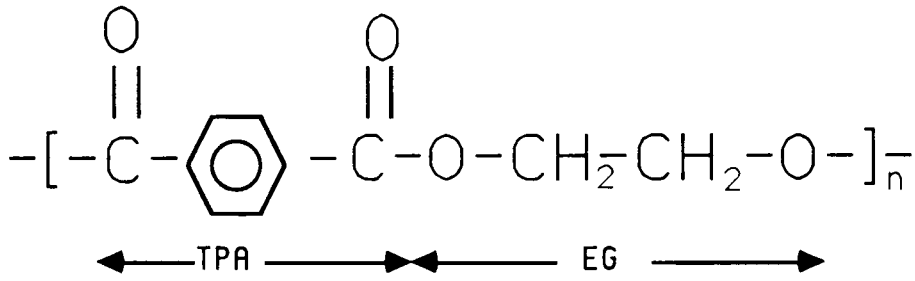


Fig. 5.2 Chemical Structure of PET.

Table 5.1 Position and assignments for peak maxima in NIR spectra of filled and unfilled PET (9) .

Spectral Region	Band Maxima (nm) Unfilled	Filled	Band Assignment
I	1661	1661	1st overtone aromatic C-H stretch overlapped with 1st overtone methylene stretch
I	1721	1720	1st overtone methylene stretch
II	1947	1947	2nd overtone C=O stretch
III	2081	2082	3rd overtone C-O stretch
III	2132	2132	combination aromatic C-H stretch and ring vibration
III	2156	2156	combination aromatic C-H stretch and ring vibration
III	2180	2181	combination aromatic C-H stretch and ring vibration
III	2253	2260	combination methylene stretch and bend
III	2334	2325	overlap of absorbances
III	2387	2392	involving methylene and aromatic C-H groups and COO^- groups

5.2 ANALYSIS OF IN-LINE DATA

NIR absorbance spectra of PET samples with different filler concentrations are shown in Fig. 5.3. A total of nine spectra are shown from the concentration range 10% to 90%, with a spectrum for each concentration level. All spectra could not be plotted on a single plot due to the limitations of printers capability. Multiple spectra at each concentration level have been plotted individually and are shown in appendix B.

The spectral data for pure resins showed random scattering of light. As an observation from the previous experiments with nylon and PET, the random scattering was assigned to degradation of polymer. This was further reinforced by the visual inspection of the extrudate. The polymer emerging from flow cell was dripping rather than the smooth flow observed for other samples. Since various mixtures did not show this sort of scattering, it was clear that degradation had occurred in extruder and not while drying. The spectral data for pure resins had to be discarded.

Analysis of Fig. 5.3 shows that there is a regular spectral change with changing filler concentration. The change in the spectra have essentially been in the form of baseline shifts. It is evident from the overlaid plots that the amount of scattering is dependent on the wavelength. This is better depicted in the plot of variance in absorbance at each wavelength, shown in Fig. 5.4. The variance in absorbance is highest at 1200 nm and thus showing that maximum scattering occurs near the left end of the spectra. The variance goes down steadily from this point to around that of 2100 nm. The spectral changes in this region are mainly from baseline shifts. Beyond this region,

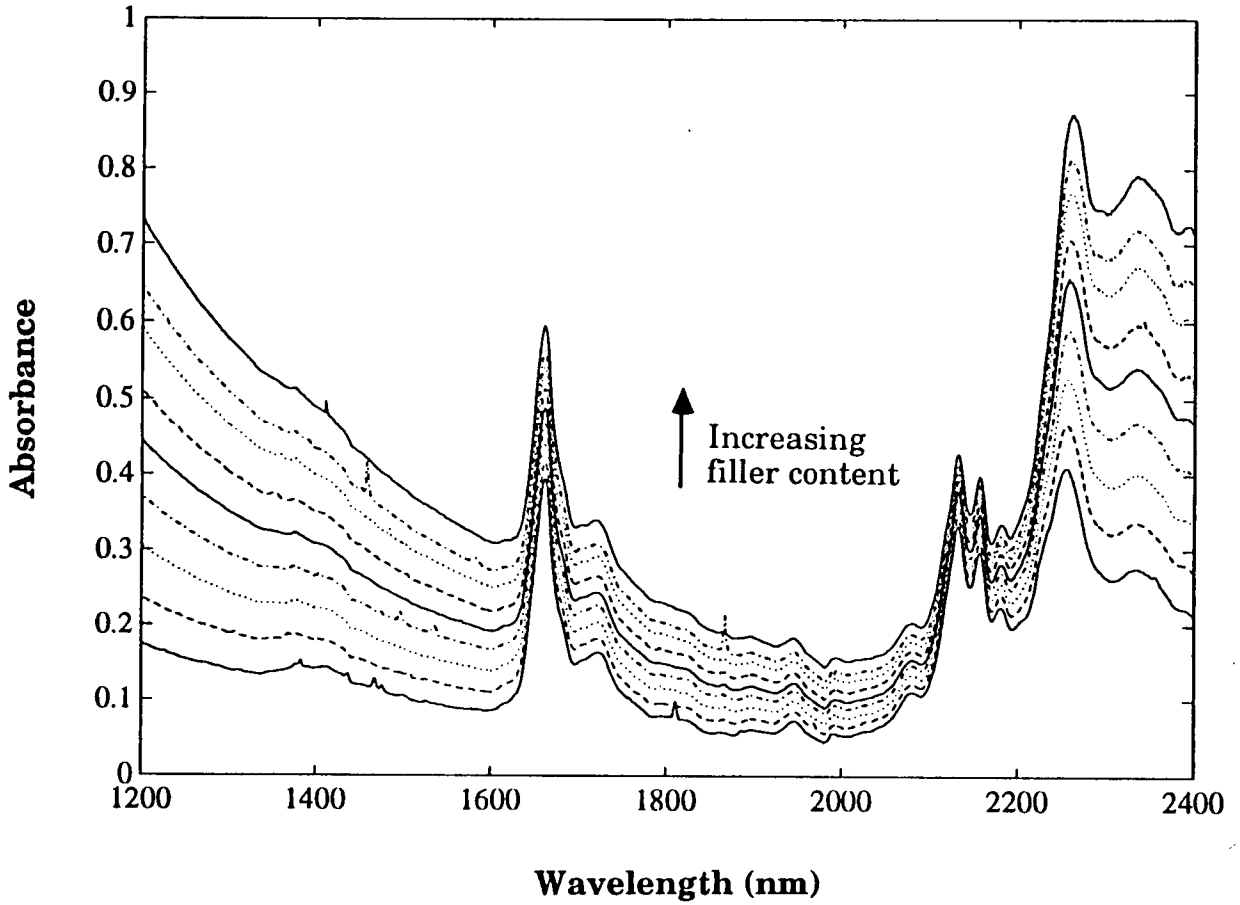


Figure 5.3 Overlaid spectra of PET with varying filler content.

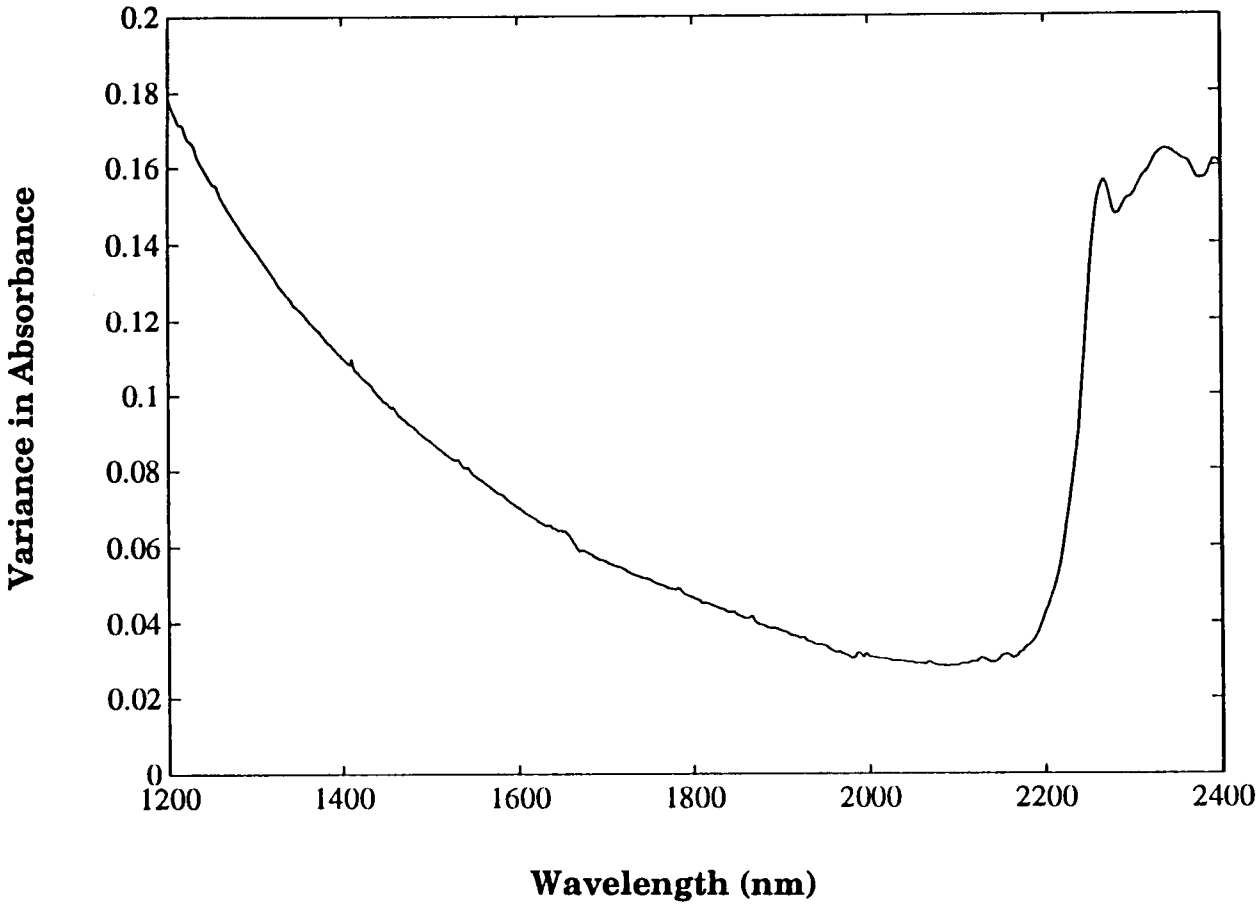


Figure 5.4 Plot of variance in absorbance versus wavelength.

there is a sudden increase in variance. The spectral changes in this region are both due to both, scattering resulting in baseline shifts, and due to absorbance from some component. The presence of absorbance peaks is very distinct.

5.2.1 Qualitative understanding of Calibrations

An important aspect of calibration is determination of optimum number of factors to be retained. This can be achieved quantitatively through cross validation. In order to be able to build a good calibration model, qualitative understanding of the contributions from different factors is essential. Sometimes it may so happen that factors with only small contributions have some unknown feature like nonlinearity, spectral interferences etc. These may even get discarded through the cross validation step. At other times, one can prevent taking into account erroneous results arising from inclusion of bad data sets in the calibration. The qualitative understanding is achieved by analyzing the loadings and scores for various factors.

Table 5.2 summarizes the results of percent variance accounted for by each factor and total percent variance up to that factor, for calibrations using PLS and PCR. In these calibrations, a total of 85 sample spectra were used. Spectral data at all 1201 wavelengths for each scan was used in the analysis. For PLS, the first factor accounts for 99.75% of the variation in X-data and 99.7% variation in the Y-data. The results for PCR are also nearly the same.

Since both PLS and PCR give nearly the same results, only scores and loadings of PLS calibrations would be discussed below.

Table 5.2 Results of percent variance captured by PLS and PCR models.

(a) PLS Model

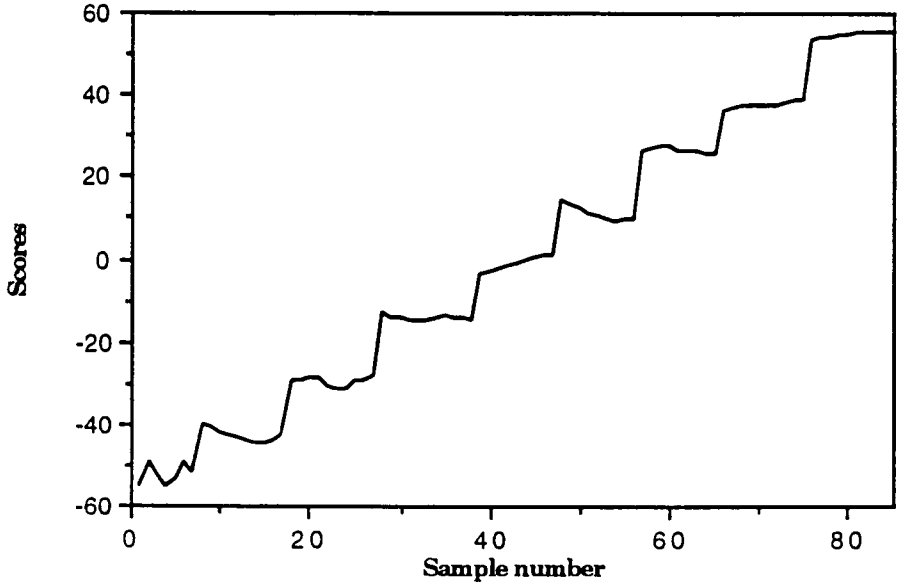
	X-DATA Percent Variance		Y-DATA Percent Variance	
Factor	This Factor	Total	This Factor	Total
1	99.7497	99.7497	99.6901	99.6901
2	0.1273	99.8771	0.1402	99.8303
3	0.0278	99.9048	0.0228	99.8531
4	0.0098	99.9146	0.0411	99.8942
5	0.0099	99.9246	0.0258	99.9200

(b) PCR Model

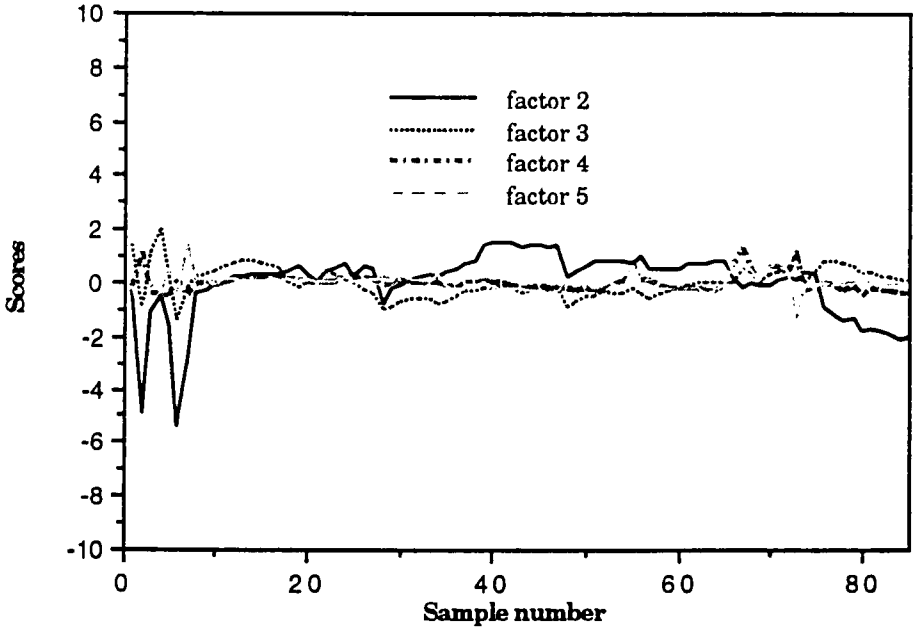
	X-DATA Percent Variance		Y-DATA Percent Variance	
Factor	This Factor	Total	This Factor	Total
1	99.7497	99.7497	99.6898	99.6898
2	0.1279	99.8776	0.1322	99.8220
3	0.0299	99.075	0.0119	99.8339
4	0.0159	99.9234	0.0018	99.8357
5	0.0126	99.9360	0.0020	99.8377

Scores

The PLS scores for the first five factors are plotted in Fig. 5.5. The scores for first factor appear in the form of step. Each step level represents a particular concentration level. Scores increase from negative to positive with increasing index number. This is in agreement with the increasing concentration level with increasing index number. Each step level is nearly horizontal with the exception of 10% concentration level. The horizontal nature means that the essential difference between different concentration levels is accounted for by the first factor. This is why there is such a large contribution from the first factor.



(a) Scores for factor one



(b) Scores for factor two through five

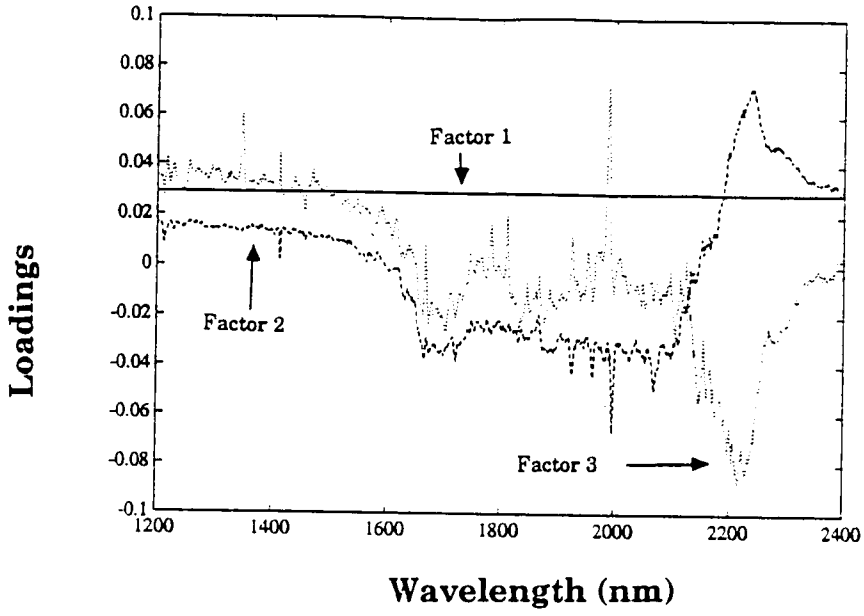
Figure 5.5 Plot of scores for first five factors v/s sample number.

The second factor scores are at least an order of magnitude lower than the first factor scores. Second factor has significant contributions only to concentration level of 10%. A large contribution to 10% concentration level implies either a nonlinear behavior or some abnormal spectral variation which is not accounted for by the first factor. The contributions from other three factors are comparatively insignificant.

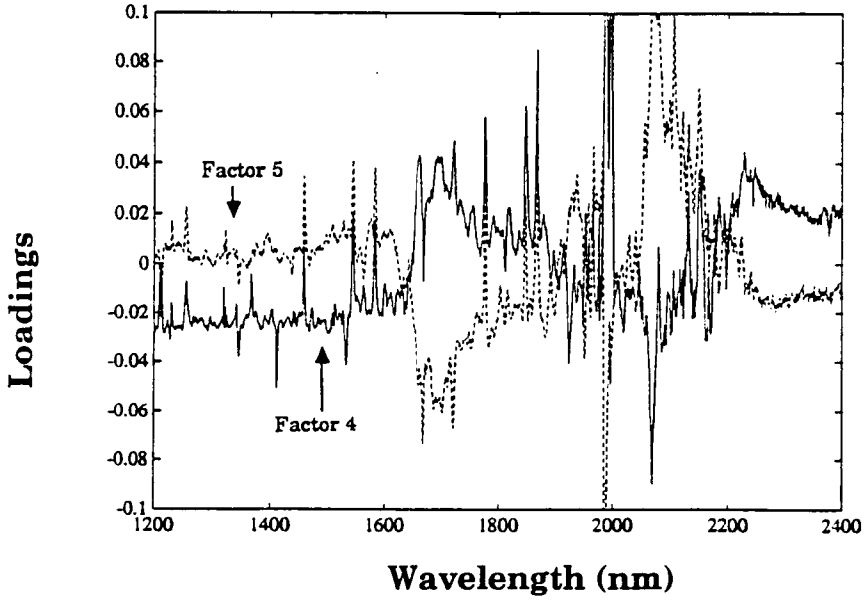
Loadings

The first five loadings are shown in Fig. 5.6. The first loading vector is almost a straight line with almost same values at all the wavelengths. This shape is in general agreement with the mean-centered and normalized spectra shown in Fig. 5.7. The general shape of straight line corresponds to baseline shifts due to scattering. The same values are result of normalization of spectra.

The second loading vector has some spectral features in the form of peaks. Thus having taken care of the majority of baseline variations through first factor, second factor accounts for the small residual baseline variations and most of changes in absorbance peaks. The region from 1200 to 1600 nm is almost of constant magnitude with positive values. The region from 1600 to 2100 nm is again of almost constant magnitude but with negative contributions. Thus these two regions are again trying to incorporate baseline shifts not accounted for by the first factor. The presence of residual variation could be due to nonlinearities or inhomogeneities in the mixture sample stream. As will be discussed later, inhomogeneity plays a dominant role in the second factor. The region of constant magnitude also has large number of



(a) Loadings for first three factors.



(b) Loadings for factor four and five.

Figure 5.6 Loadings spectra for first five factors.

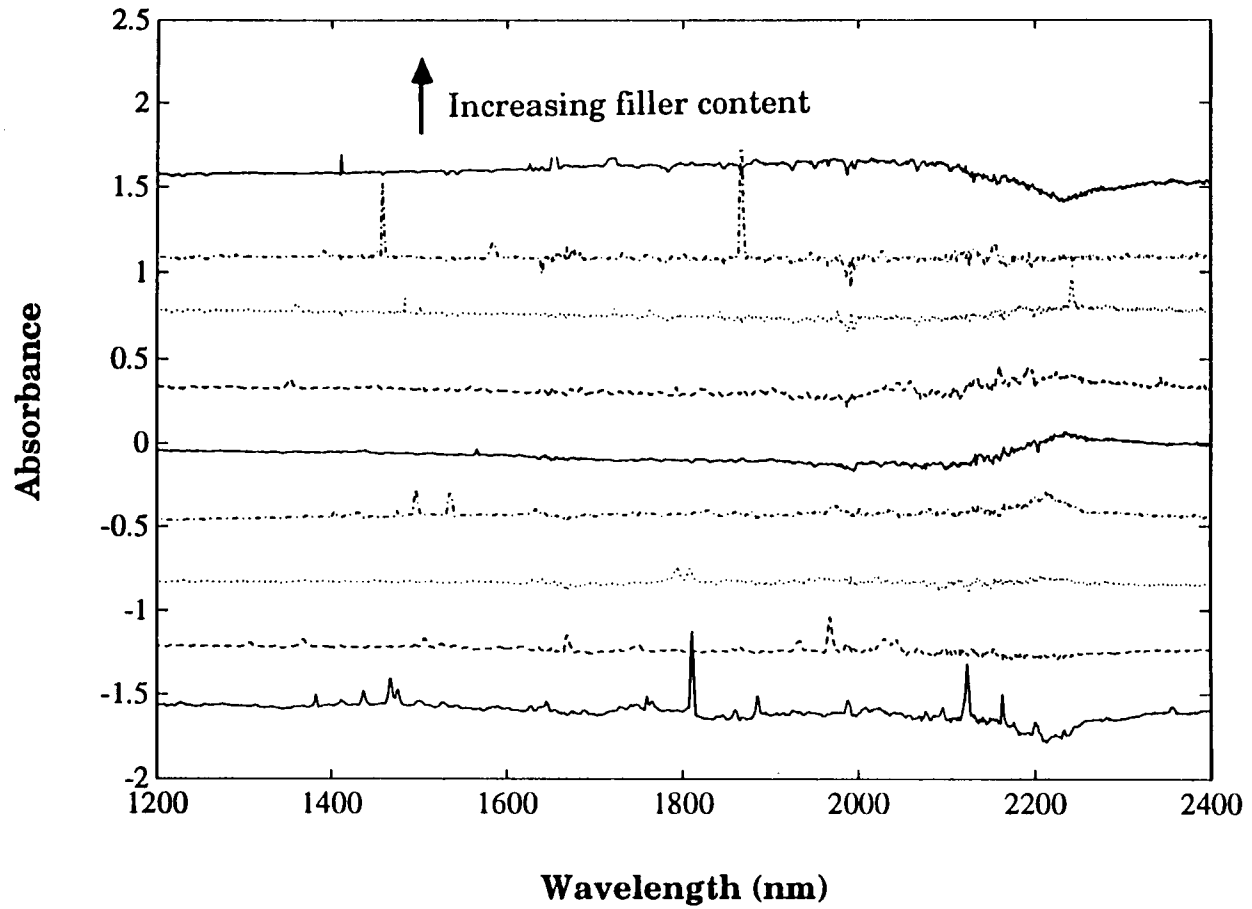


Figure 5.7 Mean-centered and normalized spectra of different concentration level.

spikes. These spikes could be due to impurities like carbon particles. It could also be due to bubbles in the sample stream. Presence of bubble causes the absorbance to go up in the form of a spike.

One cause not discussed above is the change in scattering due to changing particle size of the scattering filler. From theory, the scattering first increases with decreasing particle size, reaches a maximum as the particle size becomes equal to the wavelength, and then drops off with further size reduction (115). Since the particle sizes are distributed over a range, a variation in scattering results. This in turn leads to local variations and gives a spectra with absorbance going in zigzag form rather than sharp absorbance spectra. It is this effect which is also contributing to second loading. Since the overall contribution from second factor is not large as such, the overall effect due to particle size distribution is insignificant.

The region of interest in the second loading is from 2200 nm to 2400 nm. This exhibits an absorbance peak like shape. This implies that there is an additional component since TiO_2 does not exhibit an absorbance peak in the NIR range. TiO_2 is sometimes coated with an organic compound. This absorbance peak can be due to some kind of coating on TiO_2. Alternatively, it could be due to some organic additive. Further insight into this can be obtained by conducting experiments with PET having coated and uncoated TiO_2. The essence of discussing this peak is that it does not get fully accommodated into the first factor.

Third loading vector again has positive components in region 1200 to 1600 nm and negative components in region 1600 to 2100 nm. Both these regions are corrupted or polluted with spiked form of variation. The region

from 2100 to 2400 nm again has an absorbance peak like feature. This peak has negative contribution in contrast to the positive contributions from second loading vector. This alternating of positive and negative contributions is peculiar of nonlinear nature and thus points towards presence of nonlinearities in this region.

The fourth and fifth factors hardly contribute to the overall spectral variation and thus can be mainly discarded as noise. The local variations due to impurities etc. are more significant than any other spectral trend and thus these factors must not be included in calibration.

The above discussion gave some qualitative understanding of the contributions from different factors. This understanding is crucial in development of calibration models using cross validation. This understanding will not only be able to justify mathematical analysis but will also prevent incorporating any erroneous information.

5.2.2 CROSS VALIDATION

The optimal number of factors is obtained by cross validation. There are a number of ways of performing cross validation. One of the most common methods is leave-one-sample-out cross validation. The other commonly used cross validation procedure is leave-one-group-out. Here a group of samples for a particular concentration level are left out. Yet another process is to leave user selected groups of concentration out. All three type of cross validations were performed on the spectral data collected. The results for all these are discussed to find optimum number of factors.

Leave-one-sample-out

Leave-one-sample-out cross validation is done by leaving one sample out at a time and building calibration model from the rest of the samples. This process is repeated until all samples have been left out once. The SEP_{CV} is calculated by equation 2.27 in section 2.2.4. The SEP_{CV} obtained for the given data set are plotted against the number of factors in Fig. 5.8. There is decrease in the prediction errors as the number of factors is increased from one to two. Addition of further factors results in an increase in the errors. The lowest SEP_{CV} value is obtained for two factors. Thus the optimal number of factors suggested by leave-one-sample-out calibration is two.

Leave-one-group-out

Leave-one-group-out cross validation is performed by leaving out a group of samples at one concentration level. The SEC and SEP values are computed as given by equations 2.24 and 2.25, respectively. The procedure is repeated until all the samples have been left out once. The results are then analyzed to obtain the optimal number of factors.

In all there are 9 concentration levels in present data set. The results for this cross validation are summarized in Table 5.3 and 5.4. Maximum of four factors were employed for determination of SEP and SEC values.

The SEC values decrease with increasing number of factors. This is because the SEC values are computed from the predictions of samples used in building the calibration model. Increasing the number of factors makes the calibration model to fit the given data in a better way. This may even amount to taking some noisy information which may not be true of data in general.

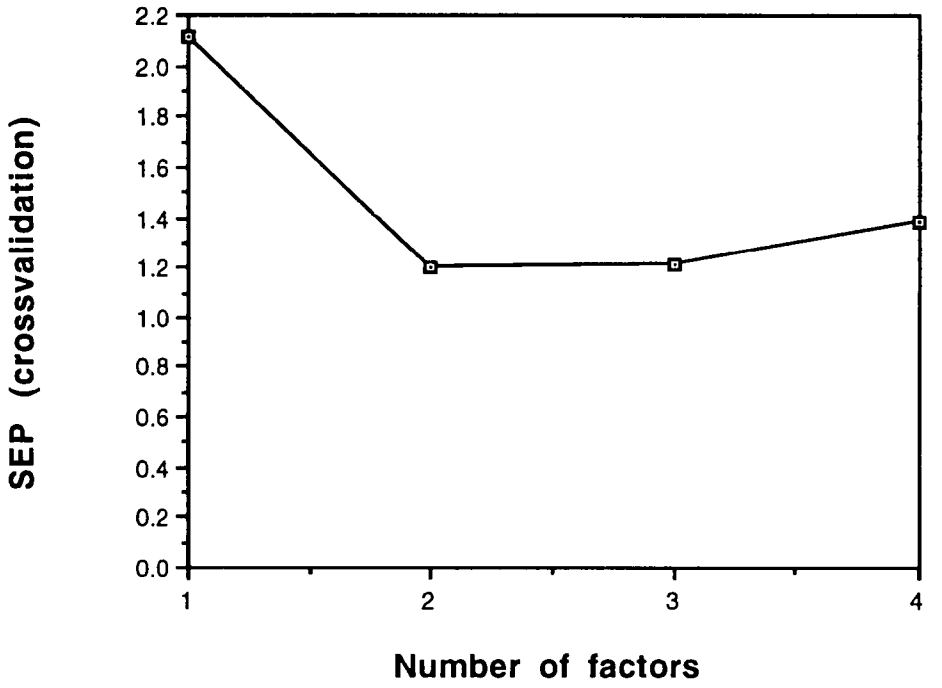


Fig. 5.8 Plot of SEP_{CV} versus the number of factors for cross validation using PLS.

Table 5.3 The results for leave-one-group-out cross validation using PLS

(a) SEC values

No.	Concentration level	Number of Factors in the Model			
		1	2	3	4
1	10	1.1311	1.0266	0.8969	0.7315
2	20	1.4313	1.0395	0.9592	0.8162
3	30	1.4289	1.0514	0.9730	0.8152
4	40	1.5051	1.0948	1.0089	0.8570
5	50	1.4485	0.9333	0.8540	0.7368
6	60	1.3971	1.0261	0.9360	0.7530
7	70	1.4861	1.0543	0.9812	0.8495
8	80	1.3989	0.9694	0.9131	0.7884
9	90	1.3715	1.0903	1.0067	0.8210

(b) SEP values

No.	Concentration level	Number of Factors in the Model			
		1	2	3	4
1	10	1.6701	0.8026	0.9778	1.1271
2	20	1.0641	0.9077	0.8124	0.7961
3	30	0.8007	0.7305	0.6516	0.6851
4	40	0.4046	0.3368	0.3747	0.3572
5	50	1.1632	1.1068	1.0916	0.9987
6	60	1.2622	1.1213	1.0699	1.1027
7	70	0.4959	0.4040	0.3817	0.3494
8	80	0.5503	0.6461	0.7753	1.1945
9	90	0.5290	0.2388	0.1681	0.3440

Table 5.4 The results for leave-one-group-out cross validation using PCR.

(a) SEC values

No.	Concentration level	Number of Factors in the Model			
		1	2	3	4
1	10	1.1312	1.0829	1.0264	1.0220
2	20	1.4324	1.0542	1.0401	1.0391
3	30	1.4298	1.0780	1.0406	1.0359
4	40	1.5060	1.1120	1.0955	1.0891
5	50	1.4494	0.9636	0.9323	0.9124
6	60	1.3978	1.0568	1.0126	1.0045
7	70	1.4871	1.0804	1.0444	1.0348
8	80	1.3999	0.9942	0.9490	0.9428
9	90	1.3721	1.1180	1.0920	1.0850

(b) SEP values

No.	Concentration level	Number of Factors in the Model			
		1	2	3	4
1	10	1.6705	1.2409	0.6033	0.6045
2	20	1.0644	0.9196	0.8903	0.8717
3	30	0.8008	0.7477	0.6911	0.6736
4	40	0.4049	0.3433	0.3433	0.3647
5	50	1.1633	1.1103	1.1200	1.1125
6	60	1.2624	1.1362	1.1055	1.0851
7	70	0.4960	0.4142	0.3959	0.4007
8	80	0.5502	0.6182	0.6999	0.7178
9	90	0.5293	0.2723	0.2352	0.1995

The SEP values are obtained for data set which is not included in the calibration model and thus is unknown to the model. It is predictability for unknown sample set which determines the optimum number of factors.

The analysis of SEP values does not show any regular trend. There is a distinct decrease in SEP values for 10% concentration with inclusion of second factor. The SEP values for other concentrations also show a decrease with the exception of 80% concentration level.

As an observation, the second factor for PLS is able to model better than the second factor for PCR. While the SEP values for 1 factor are almost same for both PLS and PCR, the results are distinctly better for 2 factor PLS in comparison to 2 factor PCR.

The unduly large SEP values for 10% concentration level is still a matter of concern. To understand the contributions from the first two factors, scores of the first factor are plotted against scores for the second factor in Fig. 5.9. An anomalous behavior is clearly visible for three samples having high scores for factor 2. The analysis of plot shows that while the first factor essentially differentiates between different concentration levels, the second factor accounts for differences between samples at same concentration level.

To explain this abnormal behavior for three samples, the spectra of these samples were examined more closely and compared with other spectra with 10% concentration. Fig. 5.10 compares these three spectra to a good spectrum of 10% concentration level. The good spectrum is selected on the basis of similarity with all the other spectra of same concentration level. The good spectrum, of sample 1, is plotted using a solid line. The three bad spectra are plotted using dotted lines. The abnormalities in these spectra are

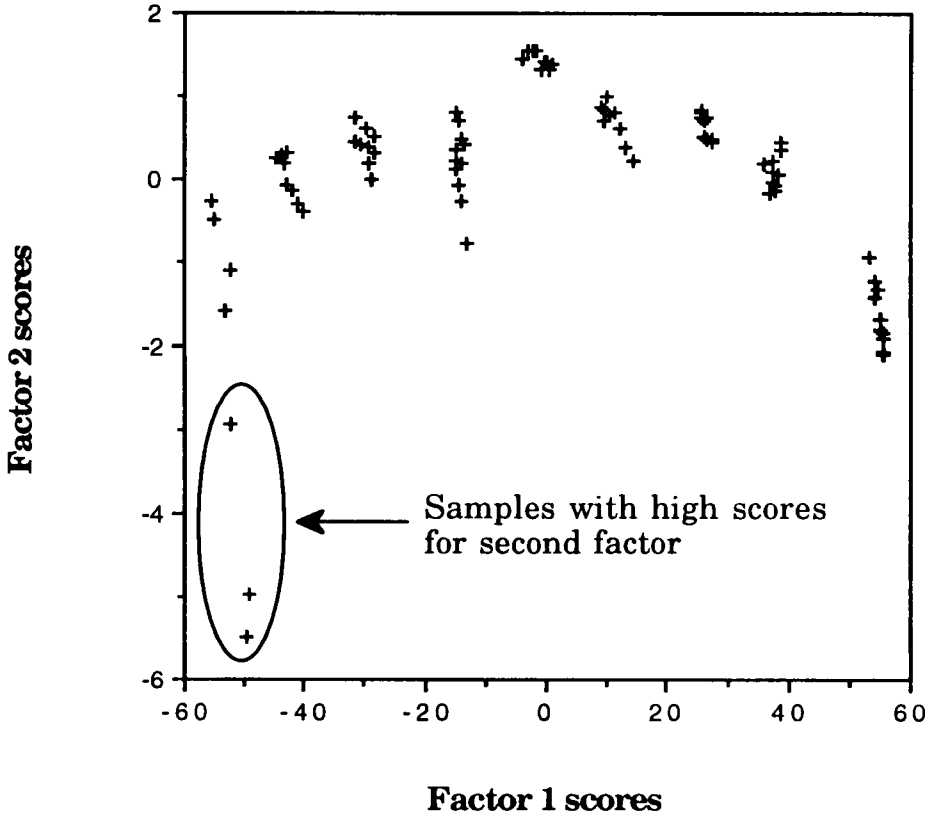
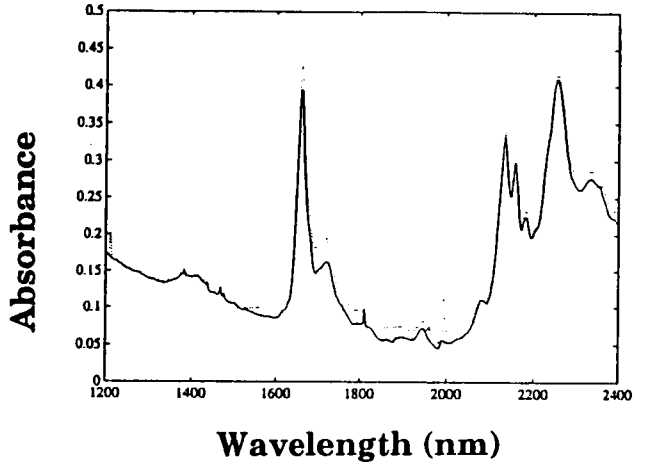
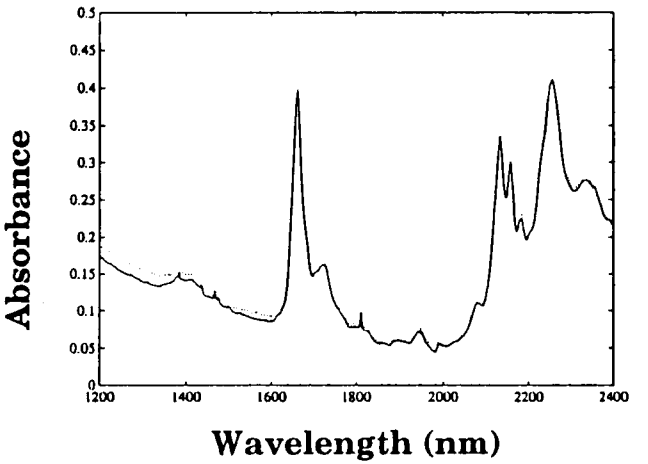


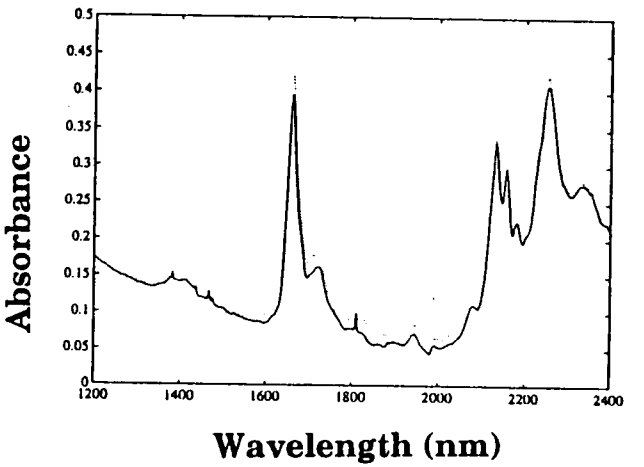
Figure 5.9 Plot of the second factor scores versus the first factor scores.



(a) Overlaid plots of sample 1 (–) and 2 (··)



(b) Overlaid plots of sample 1 (–) and sample 3 (··)



(c) Overlaid plots of sample 1 (–) and 6 (··)

Figure 5.10 Comparison of three bad spectra to one good spectrum of 10% concentration level.

clearly evident from the plots. In the Fig. 5.10(a), as the spectrum for sample 2 is being scanned, there is a sudden increase in the absorbance level around 1500 nm. This change continues into the spectrum of sample 3, as shown in Fig. 5.10(b) . This change is due to the inhomogeneities in the sample. It was assumed that concentration of mixtures was 10% and remained constant throughout the scan time. This is definitely not the case here.

The mixture inhomogeneities or change in concentration were also evident at other concentration levels. This is justified by the thick band of overlaid spectra at each concentration level rather than an overlapping feature, clearly evident in plots in appendix B. Nevertheless, variations at other concentration levels were not as severe as those at the 10% level.

The cross validation was redone leaving out these erroneous samples. The results for SEP and SEC values are summarized in Table. 5.5 and 5.6. There is clear improvement in results for 10% concentration level. The maximum change comes in results for 1 factor. Errors have been reduced nearly by 50%. The results are in general better for other concentration levels too.

These results were used to determine the optimum number of factors. Examining the SEP values, predictability improves with the addition of second factor. With the addition of third factor, results are better for some concentrations and poorer for others. Thus the optimum number of factors is two.

Using the two factors, predictions of concentrations were obtained in cross validation form. The prediction samples were unknown to model. The

Table 5.5 The improved results for leave-one-group-out cross validation using PLS.

(a) SEC values

No.	Concentration level	Number of Factors in the Model			
		1	2	3	4
1	10	1.1311	1.0266	0.8969	0.7315
2	20	1.2052	1.0314	0.9139	0.7539
3	30	1.2086	1.0385	0.9319	0.7480
4	40	1.2389	1.0674	0.9350	0.7575
5	50	1.1950	0.9255	0.8197	0.6372
6	60	1.1422	0.9895	0.8717	0.6624
7	70	1.2454	1.0441	0.9442	0.7656
8	80	1.1090	0.9375	0.8732	0.7012
9	90	1.1397	1.0220	0.9382	0.7570

(b) SEP values

No.	Concentration level	Number of Factors in the Model			
		1	2	3	4
1	10	0.9662	0.3146	0.7743	0.2002
2	20	1.0504	0.9218	0.7357	0.8140
3	30	0.7923	0.7429	0.6334	0.7195
4	40	0.3996	0.3235	0.3769	0.2868
5	50	1.1527	1.0997	1.0847	0.9978
6	60	1.2508	1.1405	1.0525	1.1306
7	70	0.4911	0.4213	0.3763	0.4332
8	80	0.5453	0.6051	0.7464	1.2549
9	90	0.5219	0.2497	0.2695	0.4348

Table 5.6 The improved results for leave-one-group-out cross validation using PCR.

(a) SEC values

No.	Concentration level	Number of Factors in the Model			
		1	2	3	4
1	10	1.1312	1.0829	1.0264	1.0220
2	20	1.2055	1.0574	1.0382	1.0309
3	30	1.2089	1.0805	1.0314	1.0249
4	40	1.2392	1.0926	1.0713	1.0647
5	50	1.1953	1.0003	0.9052	0.9031
6	60	1.1424	1.0400	0.9816	0.9744
7	70	1.2457	1.0920	1.0288	1.0242
8	80	1.1093	0.9720	0.9146	0.9134
9	90	1.1398	1.1069	1.0547	1.0523

(b) SEP values

No.	Concentration level	Number of Factors in the Model			
		1	2	3	4
1	10	0.9666	0.7203	0.3275	0.3025
2	20	1.0506	0.9544	0.8652	0.8614
3	30	0.7923	0.7718	0.6804	0.6859
4	40	0.3997	0.3277	0.3410	0.3407
5	50	1.1528	1.1121	1.1094	1.1088
6	60	1.2509	1.1809	1.1017	1.0845
7	70	0.4911	0.4472	0.4123	0.4083
8	80	0.5452	0.5655	0.6907	0.6894
9	90	0.5221	0.4049	0.2635	0.2674

prediction results for PLS are compared to the actual values in Fig. 5.11. None of the predicted values show substantial deviation from actual values. Thus a good calibration fit is obtained using 2 factors.

User Selected Groups

In this cross validation, 40% and 60% concentration levels were left out. The calibration model was built using rest of the samples. The results for SEP and SEC values obtained using PLS are shown in Fig. 5.12. As expected, SEC values show a regular decrease with increasing number of factors. The SEP value decreses as the number of factors is increased from one to two. There is not much change with addition of third factor but further increase in the number of factors results in a sharp increase in SEP values. The optimum number of factors is again 2, since it gives the lowest SEP value.

5.2.3 Proposed Calibration Model

The results all three cross validation suggest use of 2 factors in calibration models. Results for PLS and PCR are nearly same, with PLS giving marginally better results. Thus, a PLS model using 2 factors is proposed. The calibration model is developed using all the data except for three bad samples. Predictions results are presented in form of a scatter plot in Fig. 5.13. There is good agreement between the predicted and actual values. The predicted concentration values are within 2 wt% of actual values. Spectral data regenerated using 2 factors is shown in Fig. 5.14. A comparison with Fig. 5.3 shows that random variations in form of absorbance spikes have

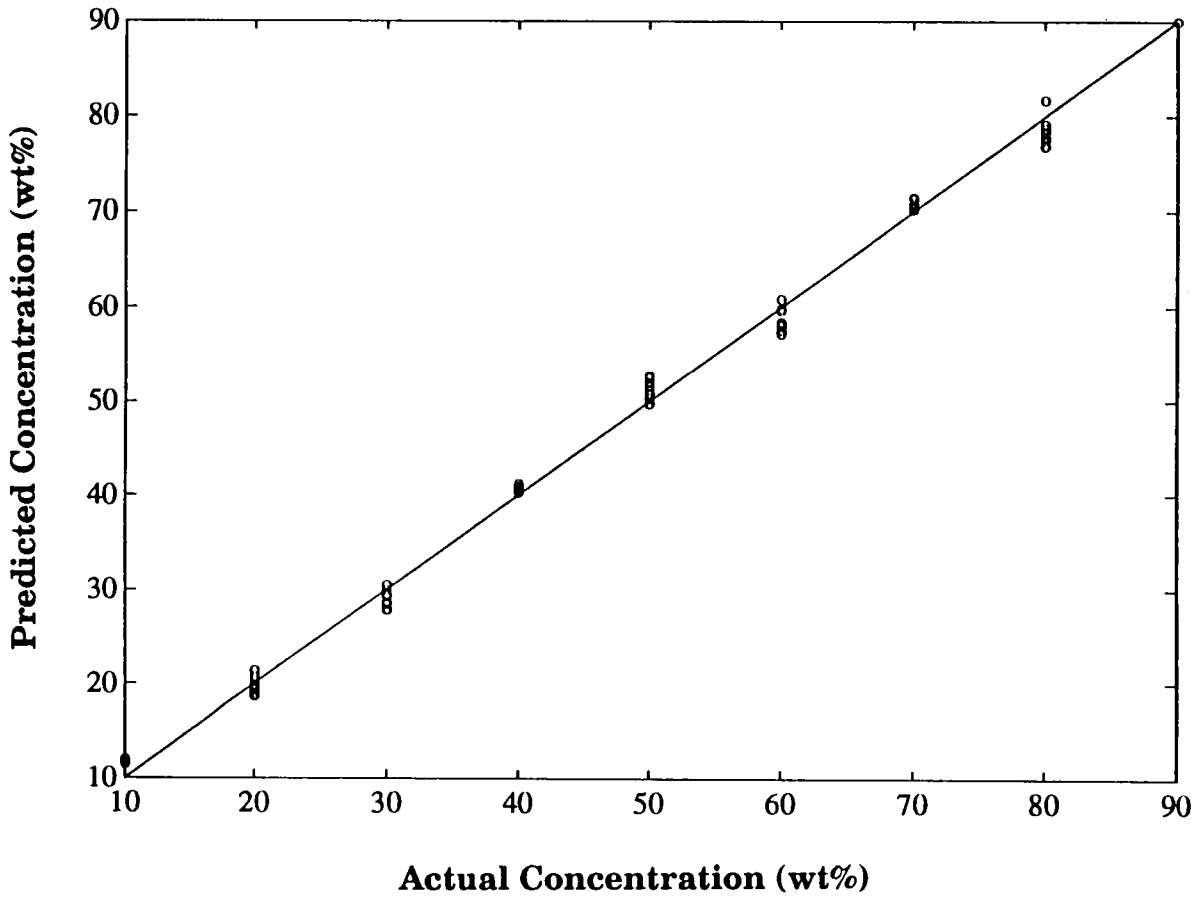


Figure 5.11 Scatter plot for predictions in the leave-one-group-out cross validation.

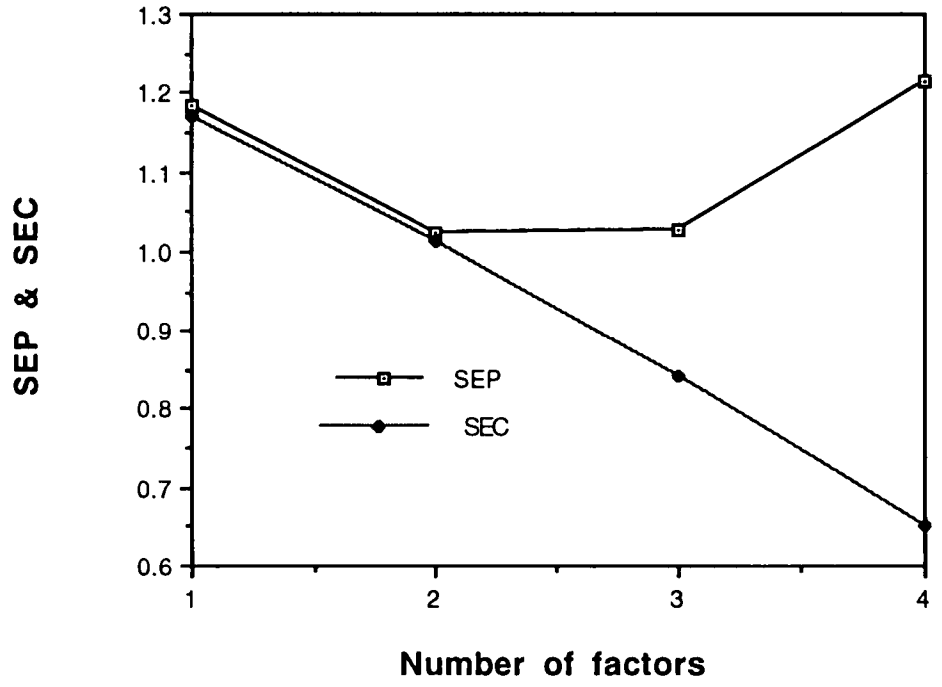


Fig. 5.12 Plot of SEP and SEC versus the number of factors for cross validation using PLS, with user selected groups in the validation set.

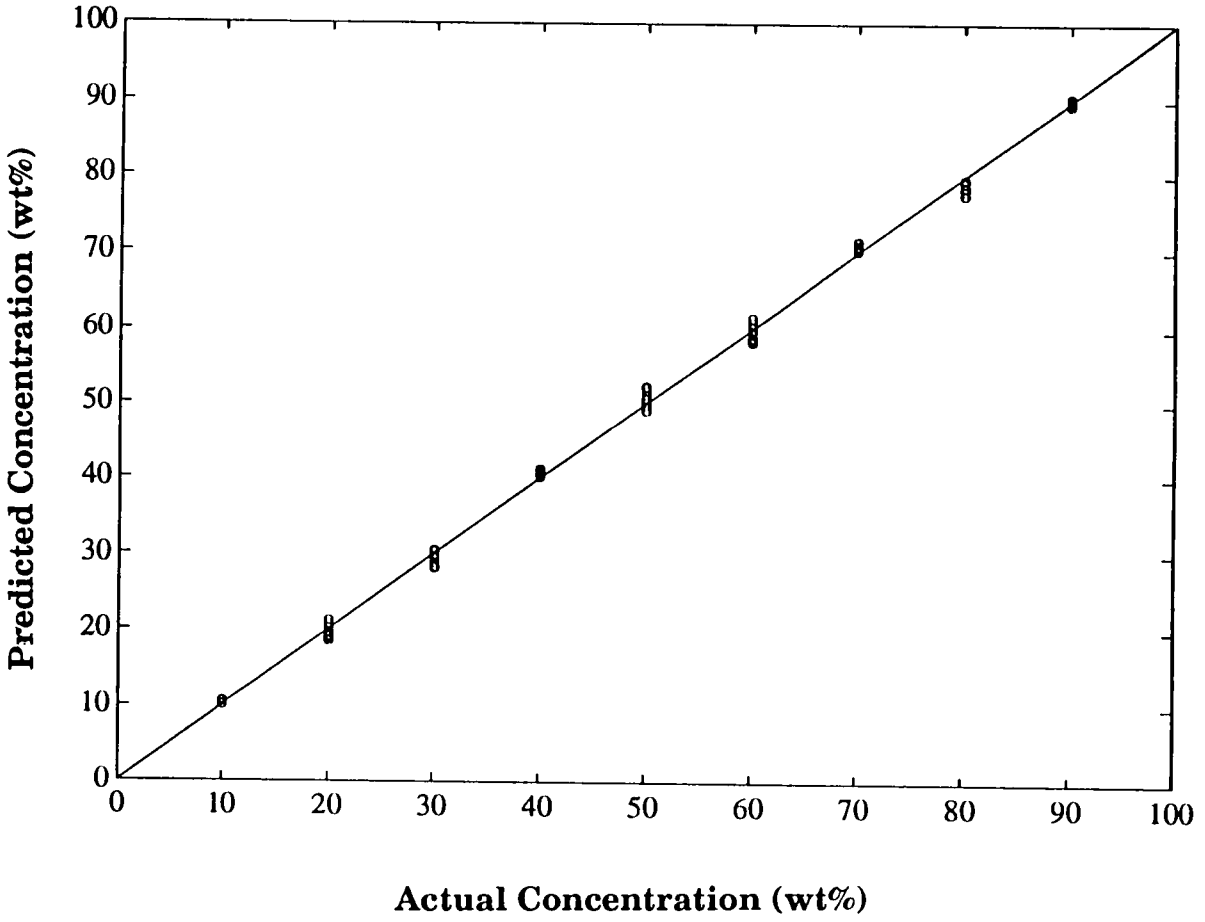


Figure 5.13 Scatter plot for predictions on the calibration samples in the proposed calibration model using two factor PLS.

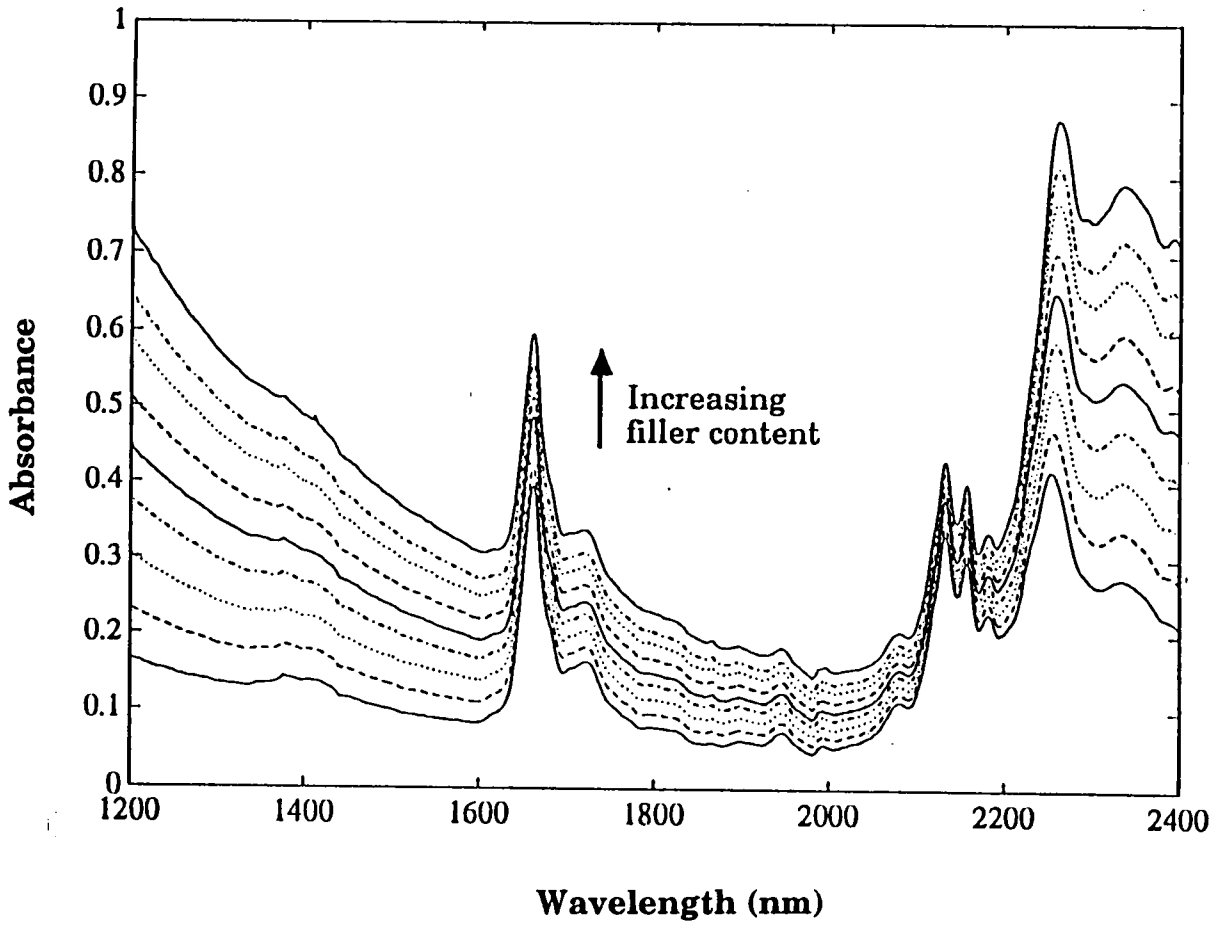


Figure 5.14 Overlaid spectra of PET with varying filler content, regenerated using two factor PLS model.

been eliminated. Thus the overall effect, in using lower dimensional data, is elimination of random variations.

5.2.4 Summary of Results for Data Analysis

Spectral data, obtained in-line, was analyzed using the multivariate techniques of PLS and PCR. Initially, contributions from various factors were analyzed to get a qualitative understanding of calibrations. Analysis of percent variance contribution from various factors showed significant contribution from the first factor only. The results for PLS and PCR were not much different, with PLS giving marginally better results. Scores and loadings were also analyzed.

Various types of cross validations were done to obtain the optimum number of factors. Results of leave-one-sample-out cross validation showed that two factors were optimum. Leave-a-group-out cross validation also suggested use of two factors in the calibration model. Cross validation using users selected groups in the validation set further reinforced that two factors were optimal. In all the cases, SEP values of around 1% were obtained. Such low SEP values demonstrated the soundness of various calibration models.

Utilizing the results from the above analysis, a calibration model was proposed. The proposed calibration model was built using PLS. Two factors were used in the development of the proposed calibration.

6. CONCLUSIONS

Several options for process analysis were discussed. Remote in-line monitoring stands out as the most promising option. Measurements made directly in the process stream cause minimum time delay between process changes and their detection through monitoring system. Remote measurements provide substantial saving on maintenance and labor costs. A single instrument can be used in multiplex mode for several measurement points.

Near infrared offers specific advantages for in-line monitoring. The low absorbances, due to overtones, facilitate use of higher pathlengths. Higher pathlengths, in turn, permit measurements to be made in-line in the process stream. The complexity of absorbance spectrum in NIR range has been turned into an advantage by development of state-of-the-art multivariate techniques.

A review of the applications showed diversity and depth of the work done using NIR spectroscopy. NIR applications for agricultural products are already in an advanced stage. The process monitoring and control systems using NIR spectroscopy are well understood in this area. The NIR applications in the areas of petrochemicals and polymers have been mainly for benchtop applications. Only a recent trend has pushed the need for NIR based process monitoring and control systems in these areas.

The objective of the experimental work done here was to demonstrate feasibility of using NIR spectroscopy for in-line monitoring of polymeric

processes. More specifically a system of PET filled with TiO_2 was analyzed. Spectral measurements were made in-line at the exit port of a single screw extruder. The spectral information was later correlated to the concentration data.

Analysis of the spectral data showed that the main spectral variation was due to baseline shifts. Presence of an inorganic filler caused the incident NIR light to scatter. This scattering doesn't result in a change in the absorbance peaks of the base polymeric material. Instead scattering causes the whole spectrum to move up and consequently show up as baseline shift. The magnitude of scattering or baseline shift was dependent on the concentration of the filler.

Experiments with different concentrations of filler showed that change in baseline absorbance, at a particular wavelength, varied directly with the concentration. Even the naked eye could detect an almost linear relationship between baseline and concentration variations. These baseline shifts were then correlated to the concentration, to yield a calibration model. The results for PLS and PCR were not much different and the optimum number of factors in both cases was two. The low SEP values emphasized the sound predictability of the calibration models.

Despite PET and TiO_2 being the only known components of the polymeric system, the quantitative analysis required an additional factor. The additional factor could be due to nonlinearity, samples inhomogenities, or presence of an additional unknown material.

The qualitative understanding of loadings and scores brought an insight into contributions from various factors. Analysis of loadings pointed

towards presence of an unknown component. Analysis of scores plot clearly showed the abnormal variations in 3 samples. The scores plot can be used in statistical process control to define the limits of scores and thus ensure better product quality by maintaining the process within limits. Any erroneous data will show up outside these limits and can be detected easily.

Finally, the successful measurements made in-line demonstrated the viability of using NIR for process monitoring and control. The low errors in prediction have shown the reliability of this technique.

7. FUTURE WORK

There is great deal of work which can be followed up on this novel method of monitoring inorganic filler using NIR transmission spectroscopy. The filler content of the filled PET resin was not known. Dealing with known concentrations of filler can be an important aspect of future work. The inorganic filler content can be determined using atomic absorption spectroscopy . Alternatively, mixtures of varying filler content could be custom made by mixing TiO_2 and unfilled PET resin. In this case one has to be careful about mixing. An efficient method of mixing TiO_2 and PET has to be worked out since the filler concentration is conjectured to be of the order of 1-2 wt%.

In the present work, the spectral data was collected and stored at the time of experiments and later analyzed to get the calibration model. An extension of this work would be to use this calibration model to predict concentrations using the Monitor program available through Guided Wave Inc. Monitor provides control of the Analyzer in a continuous real time mode using previously developed calibration models. The predicted values of concentration etc. would be output to the video screen, process computer or other output device. This would demonstrate real-time process monitoring. Further, one can develop control methodology to use such information obtained in real time. In cases where faster measurements are required, the number of wavelengths in a spectral scan could be reduced. Efficient control of such bledning processes would lead to reduced waste

and consequently, reduced manufacturing costs.

LIST OF REFERENCES

LIST OF REFERENCES

1. Z. Tadmor and C.G. Gogos, *Principles of Polymer Processing*, John Wiley and Sons, New York (1979).

2. H. L. McPeters and S.O. Williams, *In-line Monitoring of Polymeric Processes by Near Infrared Spectroscopy,* A private communication from Lee McPeters, Rohm and Haas Company, Spring House, PA. May (1992).

3. M.G. Hansen, *Conference Proceedings (ANTEC) SPE Inc., Technical Papers*, **37**, 840 (1991).

4. P.J. Cooper, *Cereal Foods World*, **28** (4), 241 (1991).

5. R. Mackison, S.J. Brinkworth, R.M. Belchamber, R.E. Aries, D.J. Cutler, C. Deeley, H.M. Mould, *Appl. Spectosc.*, **46** (6), 1020 (1992).

6. I.M. Ward, *Advances in Polymer Science*, Springer-Verlag, Berlin (1985).

7. W.W. Wendladt, *Thermal Analysis*, Wiley, New York (1986).

8. W.W. Yau, *Gel Permeation Chromatography*, Wiley-Interscience, New York (1979).

9. C.E. Miller, *Ph.D. Dissertation*, University of Washington (1989).

10. H.G. Fritz and S. Ultsch, *Kunststoffe*, German Plastics, **9** (1989).

11. R. Stengler and G. Weis, *Kunststoffe*, German Plastics, **10** (1989).

12. H.L. McPeters, *Anal. Chim. Acta.*, **83**, 238 (1990).

13. J. Curry, P. Anderson, A.V. Veen, *Conference Proceedings*, Annual Meeting of the Society of Polymer Processing , Spring (1991).

14. R.E. Schirmer, *ISA Transactions*, **28** (2), 65 (1989).

15. C.H. Sohl, *Conference Proceedings (ANTEC) SPE Inc., Technical Papers*, **37**, 846 (1991).

16. A. Khettry, J. Batra, D.A. Stewart, and M.G. Hansen,*Conference Proceedings (ANTEC) SPE Inc., Technical Papers*, **38**, 2674 (1992).

17. M.G. Hansen,A. Khettry, J. Batra, and D.A. Stewart,*Conference Proceedings (ANTEC) SPE Inc., Technical Papers*, (1993).

18. G.W. Davis and J.R. Talbot, in *Encyclopedia of Polymer Science and Engineering*, eds H.F. Mark, N.M. Bikales, C.G. Overberger, and G. Menges, John Wiley & Sons, New York, **12**, 127 (1985).

19. D.A. Burns and M. Margoshes, in *Handbook of Near-Infrared Analysis*, eds Burns and Ciurczak, Marcell Dekker, New York, 1 (1992).

20. K.B. Whestel, *Appl. Spec. Rev.*, **2** (1), 1 (1968).

21. A.M.C. Davies, *European Spec. News*, 1 (1987).

22. H.J. Goldner, *R&D Magazine*, May, 56 (1991).

23. E.H. Baughman and D. Mayes, *Am. Lab.*, Oct., 54 (1989).

24. L.G. Weyer, *Appl. Spec. Rev.*, **21** (1&2), 1 (1985).

25. R.F. Goddu, *Adv. Anal. Chem. Instrum.*, **1**, 347 (1960).

26. D.E. Honigs, *Anal. Instrument.*, **14**, 1 (1985).

27. E. Stark, K. Luchter and M. Margoshes, *Appl. Spec. Rev.*, **22** (4), 335 (1986).

28. D.A. Burns and E.W. Ciurczak, *Handbook of Near Infrared Analysis*, Marcell Dekker, New York, 1992.

29. J.L. Ilari, H. Marteens and T. Isaksson, *Appl. Spectrosc.*, **42**, 722 (1988).

30. C.E. Miller and T. Naes, *Appl. Spectrosc.*, **44**, 895 (1990).

31. P. Kubelka and I. Munk, *Z. Tech Phys.*, **12**, 593 (1931).

32. H. Marteens and T. Naes, *Multivariate Calibration*, Wiley, New York, 1989.

33. P. Green, *Mathematical Tools for Applied Multivariate Analysis*, Academic Press, San Diego, 1978.

34. B.R. Kowalski and M.B. Seasholtz, *J. Chemometrics*, **5**, 129 (1991).

35. P.M. Lang and J.H. Kalivas, *J. Chemometrics*, **7**, 1 (1993).

36. D.M. Halland and E.V. Thomas, *Anal. Chem.*, **60**, 1193 (1988).

37. K.A. Kosanovich and M.J. Piovoso, Int. J. of Control, Oct. (1992).

38. Wold H., in Multivariate Analysis, ed P.R. Krishnaiah, Academic Press, New York, 391 (1966).

39. J. Mandel, *The Amer. Statistician*, **36**, 15 (1982).

40. I.S. Helland, *Commun. Statist-Simul.*, **17** (2), 581 (1986).

41. P. Geladi and B.R. Kowalski, *Analytica. Chim. Acta.*, **185**, 1 (1986).

43. A. Hoskuldsson, *J. Chemometrics*, **2**, 211 (1988).

44. A. Lorber, L.E. Wangen, and B.R. Kowalski, *J. Chemometrics*, **1**, 19 (1987).

45. T.W. Wang, M. Berry, J. Batra, A. Khettry, P. Sarma, and M. Hansen, paper 373, 44th Pittsburgh Conference, Atlanta, Georgia, Mar. (1993).

46. B.M Wise, *PLS_Toolbox for use with MATLAB,* Version 1.2 , A public domain software available through Barry M. Wise, 1415 Wright Avenue, Richland, WA 99352.

47. D.M. Halland and E.V. Thomas, *Anal. Chem.*, **60**, 1202 (1988).

48. I. Ben-Gera and K.H. Norris, *Isr. J. Agr. Res.*, **18**, 125 (1968).

49. I. Ben-Gera and K.H. Norris, *J. Food Sci.*, **33**, 64 (1968).

50. P.C. Williams, *paper no. 347, Canadian Grain Commission,* Manitoba, Canada 1975.

51. C.A. Watson, *Anal. Chem.*, **49** (9), 835A (1977).

52. B.G. Osborne, *Anal. Proc.*, **20**, 80 (1983).

53. Polesello and Giancummo, CRC Crit. Rev. Food Sci. Nutr., **18** (3), 203 (1983).

54. K.H. Norris and Hart, *Proceedings of the International Symposium on Humidity and Moisture, Principles and Methods of Measuring Moisture in Liquids and Solids*, Reinhold, New York, **4**, 19 (1965).

55. K.H. Norris, *Sixth Intl. Cereal and Broad Congress*, AACC, May (1978).

56. P.C. Williams, *Cereal Chem.*, **56** (3), 169 (1979).

57. P. Williams, B. Thompson, D. Wetzel, G. McLang, and D Loewen, Cereal Foods World, **26**, 234 (1981).

58. B.G. Osborne, *Proceedings of the 7th Intl. Symp. on NIRA*, Technicon, Tarrytown, New York (1984).

59. D. Baker, *Cereal Chem.*, **60**, 217 (1983).

60. D. Baker and K.H. Norris, *Appl. Spec.*, **39**, 618 (1985).

61. D. Baker, *Cereal Chem.*, **60**, 217 (1983).

62. E. Lanza, *J. Food Sci.*, **48** (2), 471 (1983).

63. W. Ahmed and M. Goldstein, *Lab. Pract.*, **25**, 385 (1976).

64. W. Kruggel, R. Field, M. Riley, H. Radloff, and K. Horton, *J. Assoc. of Anal. Chem.*, **64**, 692 (1982).

65. T. Isaksson, C.E. Miller, and T. Naes, *Appl. Spec.*, **46** (11), 1685 (1992).

66. *The Atlas of Near Infrared Spectra*, Sadtler Research Laboratories, Philadelphia, 1981.

67. S.C. Lo and C.W. Brown, *Appl. Spec.*, **46** (5), 790 (1992).

68. F.W. Rose, *Bur. Stand. J. Res.*, **20**, 129 (1938).

69. R.R. Hibbard and A.P. Cleaves, *Anal. Chem.*, **21**, 486 (1949).

70. C. Tosi and A. Pinto, Spectochim. Acta., **28A**, 585 (1972).

71. B. Buchanan, in *Handbook of Near-Infrared Analysis*, eds Burns and Ciurczak, Marcell Dekker, New York, 643 (1992).

72. D.E. Honigs, T.B. Hirschfeld, and G.M. Hieftje, *Anal. Chem.*, **57**, 443 (1985).

73. J.J. Kelly, C.H. Barlow, T.M. Jingiji, and J.B. Callis, *Anal. Chem.*, **61** (4), 313 (1989).

74. S.J. Swarin and C.A. Drumm, *Spectroscopy*, **7** (7), 42 (1992).

75. K.R. Carduner, *SAE Spec. Publication 903, Sensors and Actuators,* Detroit, Feb. (1992).

76. K. Chan, H. Iho, and H. Inaba, *Appl. Phys. Letter*, **43**, 634 (1983).

77. K. Chan, H. Iho, and H. Inaba, *Appl. Optics*, **22**, 3802 (1983).

78. K. Chan, H. Iho, and H. Inaba, *Appl. Phys. Letter*, **45**, 220 (1984).

79. S.M. Donahue, C.W. Brown, B. Caputo, and M.D. Modell, *Anal. Chem.*, **60** (18), 1873 (1988).

80. L. Glatt and J.W. Ellis, *J. Chem. Phys.*, **19** (4), 449 (1951).

81. R.J.W. Le Fevre, G.M. Parkins, and R. Roper, *Aust. J. Chem.*, **13**, 169 (1960).

82. R.G.J. Miller and H.A. Willis, *J. Appl. Chem.*, **6**, 385 (1956).

83. C. Tosi, *Makromol. Chem.*, **112**, 303 (1968).

84. H. Danneburgh, *SPE Tans.*, Jan, 78 (1963).

85. A. Basch, T. Wasserman, and M. Lewin, *J. Polym. Sci., Polym. Chem. ed.*, **12**, 1143 (1974).

86. E.W. Crandall and A.N. Jagtap, *J. Appl. Polym. Sci.*, 21, 449 (1977).

87. C.N. Foster, S.B. Row and R.G. Griskey, Ibid., **8**, 1357 (1964).

88. C. Kradjel and L. McDermott, in *Handbook of Near Infrared Analysis*, eds Burns and Ciurczak, Marcell Dekker, New York, 565 (1992).

89. H. Howell, *Qualiative Identification of Polymeric Materials using NIR Spectroscopy*, A private communication from Huston Howell, BASF Corporation, Fibers Division R&D, Enka, NC, Oct. (1991).

90. J. Martinez-Salazer, M. Sanchez-Cuesta, and J. Plais, *Polymer*, **32**, 2984 (1993).

91. C.E. Miller, *Appl. Spec.*, **47** (2), 222 (1993).

92. L.G. Weyer, *J, Appl. Poly. Sci.*, **31**, 2417 (1986).

93. R.M. Bly, P.E. Kiener, and B.A. Fries, *Anal. Chem.*, **38** (2), 217 (1966).

94. T. Takeuchi, S. Tsuge, and Y. Sugimura, *Ibid.*, **41** (1), 184 (1969).

95. G.F. Kirkbright and K.R. Menon, *Anal. Chim. Acta.*, **136**, 373 (1982).

96. A. Giammarise, *Anal. Letts.*, **2** (3), 117 (1969).

97. R. Spartafore and L. McDermott, *Conference Proceedings (ANTEC) SPE Inc., Technical Papers*, **37**, 1942 (1991).

98. W.H. Greive and D.D. Doepken, *Polym. Eng. Sci.*, Jan., 19 (1968).

99. S. Ghosh and J. Rodgers, in *Handbook of Near Infrared Analysis*, Marcell Dekker, New York, 495 (1992).

100. C. Jones and J.A. Brown, *J. Adv. Inst.*, **38** (1), 429 (1983).

101. T. Byron, *Proc. 2nd Annual NIRA Symp.*, Technicon, Tarrytown, New York, 1982.

102. P. Turley and A. Pietrantonio, *J. Cell. Plastics*, July-August, 274 (1984).

103. J. Lin and C.W. Brown, *Appl. Spec.*, **47** (1), 62 (1992).

104. J. Lin and C.W. Brown, *Appl. Spec.*, **47** (12), 1809 (1992).

105. R.B. Roy and C. Kradjel, *J. Polym. Sci., Polym. Chem.*, 26A, 1773 (1988).

106. K.A.B. Lee, R.W. Chylla, and T.E. Janota, *Appl. Spec.*, **47** (1), 94 (1993).

107. A.M.C. Davies, A. Grant, M. Gavrel, and R.V. Steeper, *Analyst*, **110** (6), 643 (1985).

108. C.E. Miller, S.A. Svendsen, and T. Naes, *Appl. Spec.*, **47** (3), 346 (1993).

109. G.A. Goerge, P. Cole-Clark, N. St. John, and G. Friend, *J. Appl. Polym. Sci.*, **42**, 643 (1991).

110. E.W. Crandall, E.L. Johnson, and C.H. Smith, *Ibid.*, **19**, 897 (1975).

111. S. Ghosh and I. Rodgers, *Text. Chem. Color*, **18** (2), 25 (1986).

112 C. Zhu, and G.M. Hieftje, *Appl. Spec.*, **46** (1), 69 (1992).

113. Guided Wave Model 260 Users Manual (1989).

114. PRO-MATLAB, The Mathworks, Inc., Natick, MA.

115. K.B. Whestel, D.E. Honigs, and G.J. Kemeny, *Applied Near Infrared Spectroscopy,* Notes of a Short Course conducted by Society of Applied Spectroscpy at Pittsburgh Confrence, New Orleans, LA, March (1992).

APPENDICES

A. PROGRAM CODES FOR PLS AND PCR

A.1 CODE FOR PLS

```
%*******************MAIN PROGRAM FOR PLS **********************

% This is the main program for carrying out PLS on the spectroscopic data
% collected. A SVD based routine is used for carrying out PLS.

% Clears any variable in temporary memory of MATLAB work enviroment
      clear;
% Clears graphic window
      clg;
% Loads "x" and "y" data in to temporary memory of MATLAB work
% enviroment using the file datapet.mat
      load datapet;
% The following loop performs the leave-one-group-out cross validation.
% Here a group samples with same concentration is left out and calibration
% is done on the rest of samples. The left out group is used as a validation
% set.Since there were nine different concentration levels or groups, the
% loop is repeated nine times.

for j = 1:9,

% Finds all the samples of same concentration level.
     conc = 10*j
     in = find(y == conc);
% All the spectra are included in calibration matrix xc.
     xc = x(:,1:1201);
% Selected group is eliminated from xc.
     xc(in,:) = [];
% Selected group is included in validation set matrix xp.
     xp = x(in,1:1201);
%Evaluation of size of xc and xp
      mxc = min(size(xc));
      mxp = min(size(xp));
% Selection of concentrations in calibration and validation set
     yc = y;
     yc(in,:) = [];

     yp = y(in,1);

% Mean-centering and normalization of x and y using a m-file auto.m
% mx and my are mean of x and y respectively.
% stdx and stdy are the corresponding variances
```

```
% xcc and ycc are the scaled matrices

        [xcc,mx,stdx] = auto(xc);
        [ycc,my,stdy] = auto(yc);

% Scaling of the validation set spectra
        xpc = scale(xp,mx,stdx);


% Building a PLS calibration model using 4 factors.
lv=4;
% The PLS calibration is carried out using a m-file "spls.m"
% "spls.m" uses SVD for compuation of principal components.

[P,Q,W,T,U,b,ssqdif]=spls(xcc,ycc,lv);

% This loop is used to compute SEC and SEP values for varying number of
% factors

for k =1:4,
lv = k;
% Concentration predictions of the samples in calibration set
ypc  = plspred(xcc,b,P,Q,W,lv);
sypc = rescale(ypc,my,stdy);

% Concentration predictions of the samples in validation set
ypred = plspred(xpc,b,P,Q,W,lv);
sypred = rescale(ypred,my,stdy);

% Computation of SEC and SEP values

sec(j,k) = sqrt(sum((sypc - yc) .^2)/(mxc-1));
sep(j,k) = sqrt(sum((sypred - yp).^2)/mxp);
end
end

-------------------------------------------------------------------------------------------------------
% ******************FUNCTION FILE SPLS.M************************


function [P,Q,W,T,U,b,ssqdif] = spls(x,y,lv)
%  This PLS program calculates the P, Q, W, T, and U matrices
%  for the given x and y blocks and the number of latent
%  variables specified.  It also outputs the fraction of
%  variance used in the x and y matrices.
%  Input format is as follows:
%  function [P,Q,W,T,U,b,ssqdif] = spls(x,y,lv);
```

```
% Copyright @J. Batra, P. Sarma, A. Khettry and T.W. Wang
% 1993

% This step computes the dimesions of x any y blocks.
[mx,nx] = size(x);
[my,ny] = size(y);

% The number of latent variable can not exceed the number of variables in x
if nx < lv
  error('No. of LVs must be <= no. of x-block variables')
end
% Initiallization of P, Q, W, T, U, b matrices
P = zeros(nx,lv);
Q = zeros(ny,lv);
W = zeros(nx,lv);
T = zeros(mx,lv);
U = zeros(my,lv);
b = zeros(1,lv);

% ssq is the matrix used to store variance in x and y, accounted
% for by each factor
ssq = zeros(lv,2);

% total variance in x
ssqx = 0;
for i = 1:nx
  ssqx = ssqx + sum(x(:,i).^2);
end
% total variance in y
ssqy = sum(sum(y.^2)');
X = x;
Y = y;

for i = 1:lv
% Compute the loadings and scores of x and y,  one factor  at a time
% Uses the routine plssvd.m
  [p,q,w,t,u] = plssvd(x,y);
% Regression between scores of x and y.
  b(1,i) = u'*t/(t'*t);
% Computation of residual x and y , subtracting the contribution from
% present factor
  x = x - t*p';
  y = y - b(1,i)*t*q';
% Computation of percent contribution up to this factor
  ssq(i,1) = (sum(sum(x.^2)'))*100/ssqx;
  ssq(i,2) = (sum(sum(y.^2)'))*100/ssqy;
```

```
 T(:,i) = t(:,1);
 U(:,i) = u(:,1);
 P(:,i) = p(:,1);
 W(:,i) = w(:,1);
 Q(:,i) = q(:,1);
end

% Contribution from this factor
ssqdif = zeros(lv,2);
ssqdif(1,1) = 100 - ssq(1,1);
ssqdif(1,2) = 100 - ssq(1,2);
for i = 2:lv
 for j = 1:2
   ssqdif(i,j) = -ssq(i,j) + ssq(i-1,j);
 end
end
% Display contribution from different factors.
disp(' ')
disp('       Percent Variance Captured by PLS Model')
disp(' ')
disp('           ----X-Block------  ----Y-Block------')
disp('    LV#   This LV   Total   This LV   Total ')
disp([(1:lv)' ssqdif(:,1) cumsum(ssqdif(:,1)) ssqdif(:,2) cumsum(ssqdif(:,2))])


-------------------------------------------------------------------------------------------------------
% **********************FUNCTION FILE PLSSVD.M*****************

function [p,q,w,t,u] = plssvd(x,y);
% This program executes the SVD  based algorithm for
% PLS. This runs as a subprogram of a bigger program as
% it calculates only one latent variable or factor. The
% format to invoke in the main program is:
% [p,q,w,t,u] = plssvd(x,y)
       R = x;
       Y = y;
% Determination of most aligned space between x and y
       RY = R'*Y;
       [my,ny] = size(Y);
% If number of variables in y is one, the most aligned space is obtained
% directly from R'*Y. For this case both NIPALS and SVD based PLS
% are same.
       if ny == 1
              w = RY/norm(RY);
              t = R*w;
              q = 1;
       end
```

```
% If number of of variables in y is greater than one, the NIPALS methods
% uses an iterative algorithm for computation of most aligned vector.
% The present approach uses SVD of RY and the first principal component
% is the most aligned vector between X and Y.
      if ny ~= 1,
            [UR,SR,VR] = svd(RY,0);
            w = UR(:,1);
            t = R*w;
            q = (t'*Y)';
            q = (q'/norm(q'))';
      end
            p = (t'*R/(t'*t))';
            p_norm = norm(p);
            t = t*p_norm;
            w = w*p_norm;
            p = p/p_norm;
            u = Y*q;
```

A.2 CODE FOR PCR

```
%*****************MAIN PROGRAM FOR PCR************************

% This programs uses the spectral data stored in x and the concentration
% data in y for principal component regressoion.

% Clear is used to clear any variables in temporary memory of MATLAB
     clear;
% Clears the graphic window
      clg;
% Inputs the matrix x and y using file datapet.mat
      load datapet;
% Crossvalidation routine
for j = 1:9,
      conc = 10*j
      in = find(y == conc);
      xc = x(:,1:1201);
      xc(in,:) = [];
    xp = x(in,1:1201);
      mxc = min(size(xc));
      mxp = min(size(xp));
    yc = y;
      yc(in,:) = [];

    yp = y(in,1);
```

```
[xcc,mx,stdx] = auto(xc);

xpc = scale(xp,mx,stdx);

[ycc,my,stdy] = auto(yc);

% Computation of loadings and scores using the m-file PCR.m
lv = 4;
[T,P,b]= pcr(xcc,ycc,lv);

for k = 1:4,
ypc  = xcc*b(k,:)';
sypc = rescale(ypc,my,stdy);

ypred = xpc*b(k,:)';
sypred = rescale(ypred,my,stdy);

% SEC and SEP value computation.

sec(j,k) = sqrt(sum((sypc - yc) .^2)/(mxc-1));
sep(j,k) = sqrt(sum((sypred - yp) /mxp);
end
end
```

```
%********************* FUNCTION FILE PCR.M************************

function [T,P,b] = pcr(xblock,yblock,maxlv)
% This function uses the principal components regression
% method to build a correlation between two blocks of data.
% For this routine the dependant block must be a vector.
% The I/O format is: [T,P,b] = pcr1(xblock,yblock,maxlv);
% where the inputs are the independant variables xblock,
% the dependant variables yblock, and the maximum number
% of latent variables to consider in the model, maxlv.  The
% outputs are the xblock scores T, the xblock loadings P and
% the regression coefficients for each latent variable b.


[mx,nx] = size(xblock);
[my,ny] = size(yblock);

% Reduced SVD of xblock to obtain principal components corresponding to
% nonzero singular values.

[u,s,v] = svd(xblock,0);
```

```
% Computation of scores and loadings

T = u(:,1:maxlv)*s(1:maxlv,1:maxlv);
P = v(:,1:maxlv);
b = zeros(maxlv,nx);
ssqty = zeros(maxlv,1);
ssqy = yblock'*yblock;

for i = 1:maxlv

 r = T(:,1:i)\yblock;
% Computation of regression coefficients beta matrix

 b(i,:) = (P(:,1:i)*r)';
 dif = yblock - T(:,1:i)*r;
 ssqty(i,1) =  ((ssqy - dif'*dif)/ssqy)*100;
end

% Percent variance in x and y, accounted for upto this factor.
temp = diag(s)*100/(sum(diag(s)));
temp = temp(1:maxlv);
ssqy = zeros(maxlv,1);
ssqy(1,1) = ssqty(1,1);
for i = 1:maxlv-1
 ssqy(i+1,1) = ssqty(i+1,1)-ssqty(i,1);
end

% Display of variance

disp(' ')
disp('       Percent Variance Captured by PCR Model')
disp(' ')
disp('           ----X-Block------  ----Y-Block------')
disp('    LV#   This LV   Total   This LV   Total ')
ssq = [(1:maxlv)' temp cumsum(temp) ssqy ssqty];
disp(ssq)
```

B. COMPLETE SPECTRAL DATA

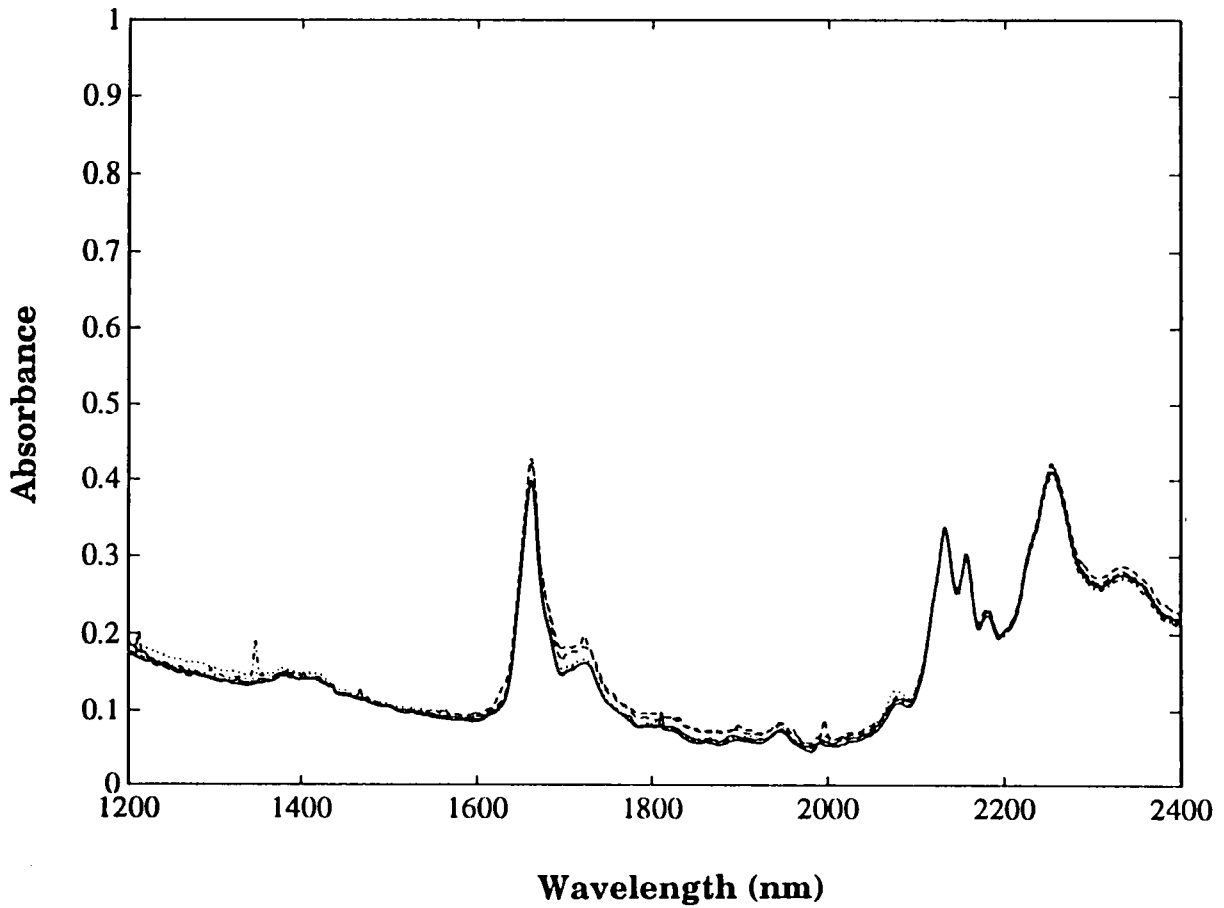


Figure B.1 Overlaid spectra of all the samples of 10% concentration level.

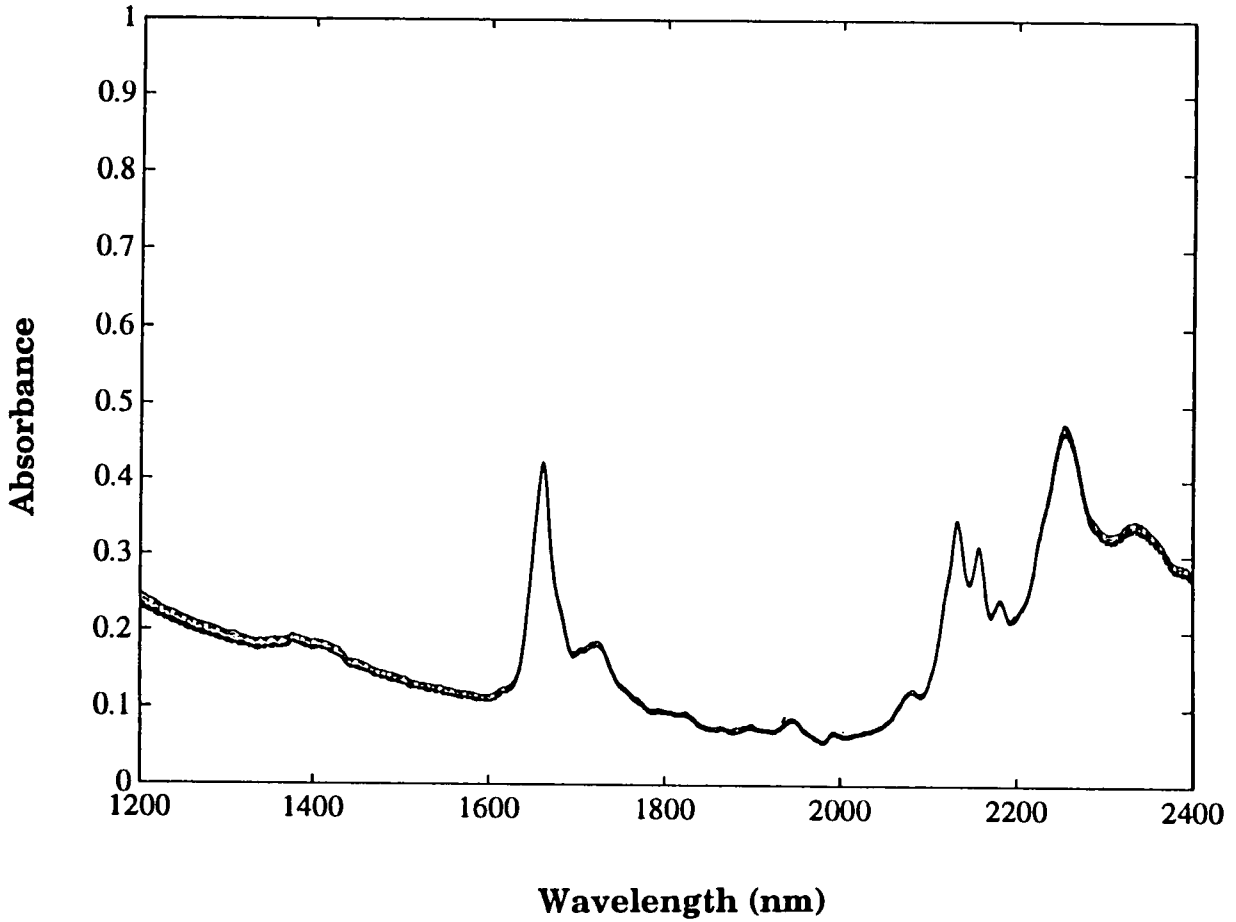


Figure B.2 Overlaid spectra of all the samples of 20% concentration level.

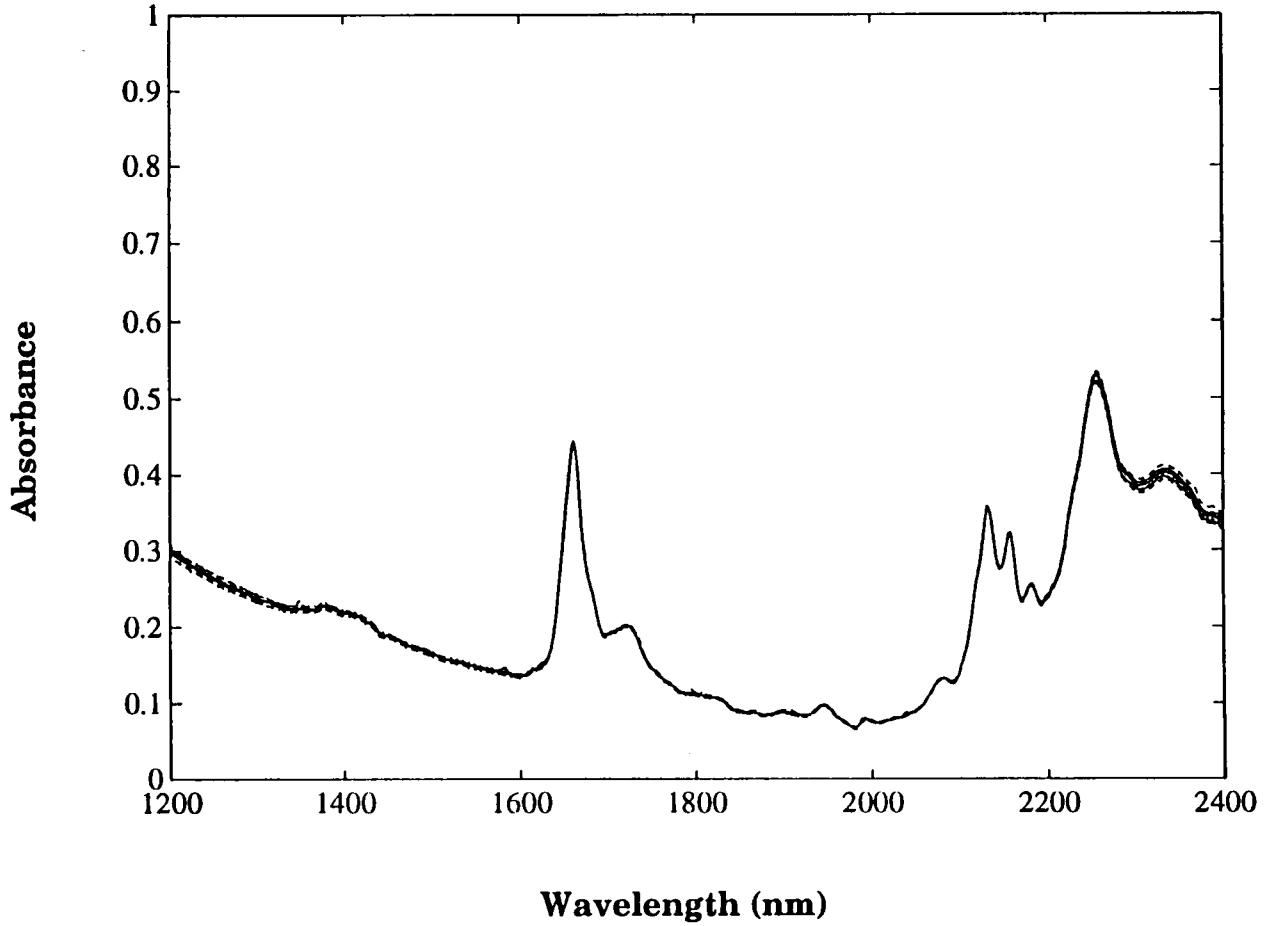


Figure B.3 Overlaid spectra of all the samples of 30% concentration level.

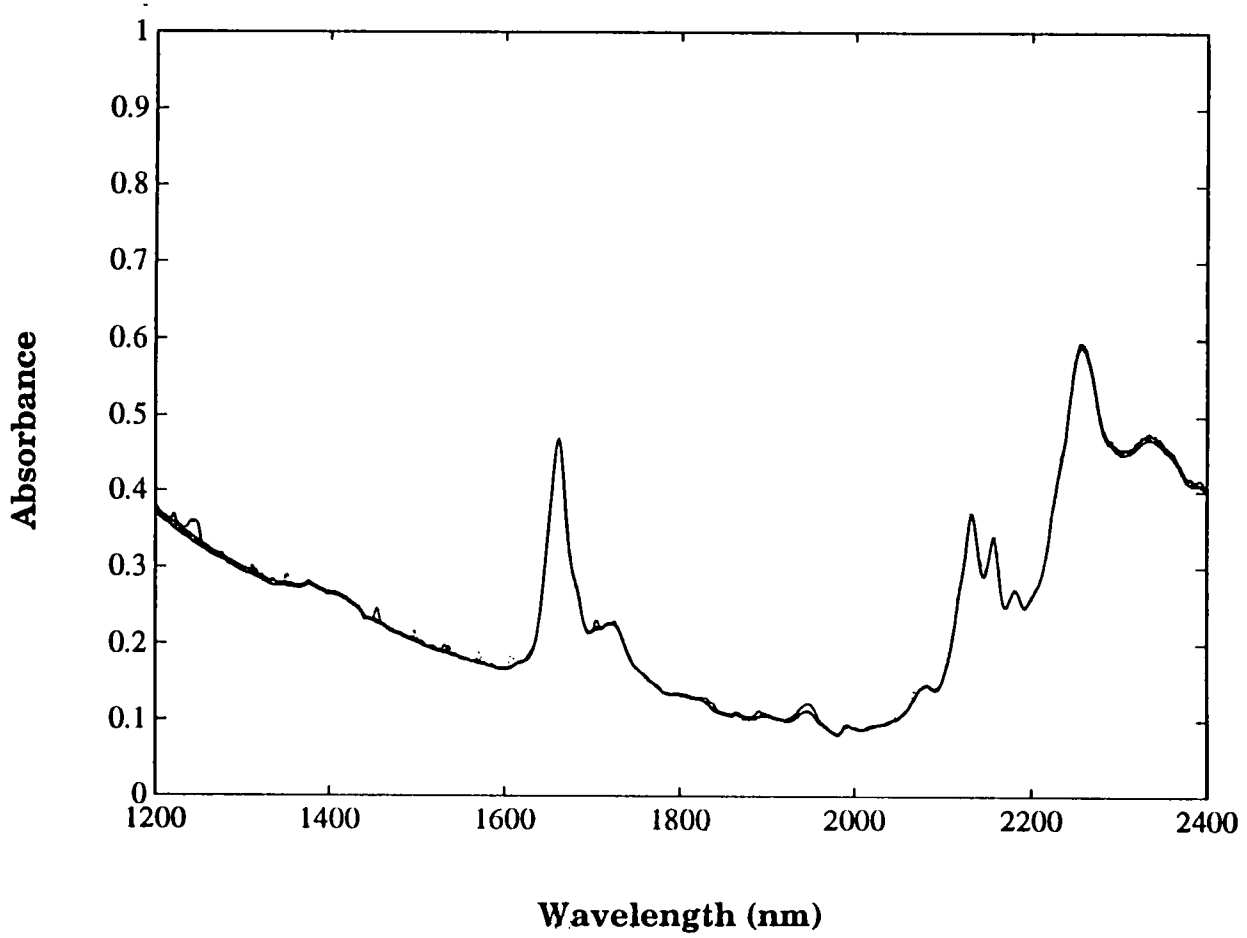


Figure B.4 Overlaid spectra of all the samples of 40% concentration level.

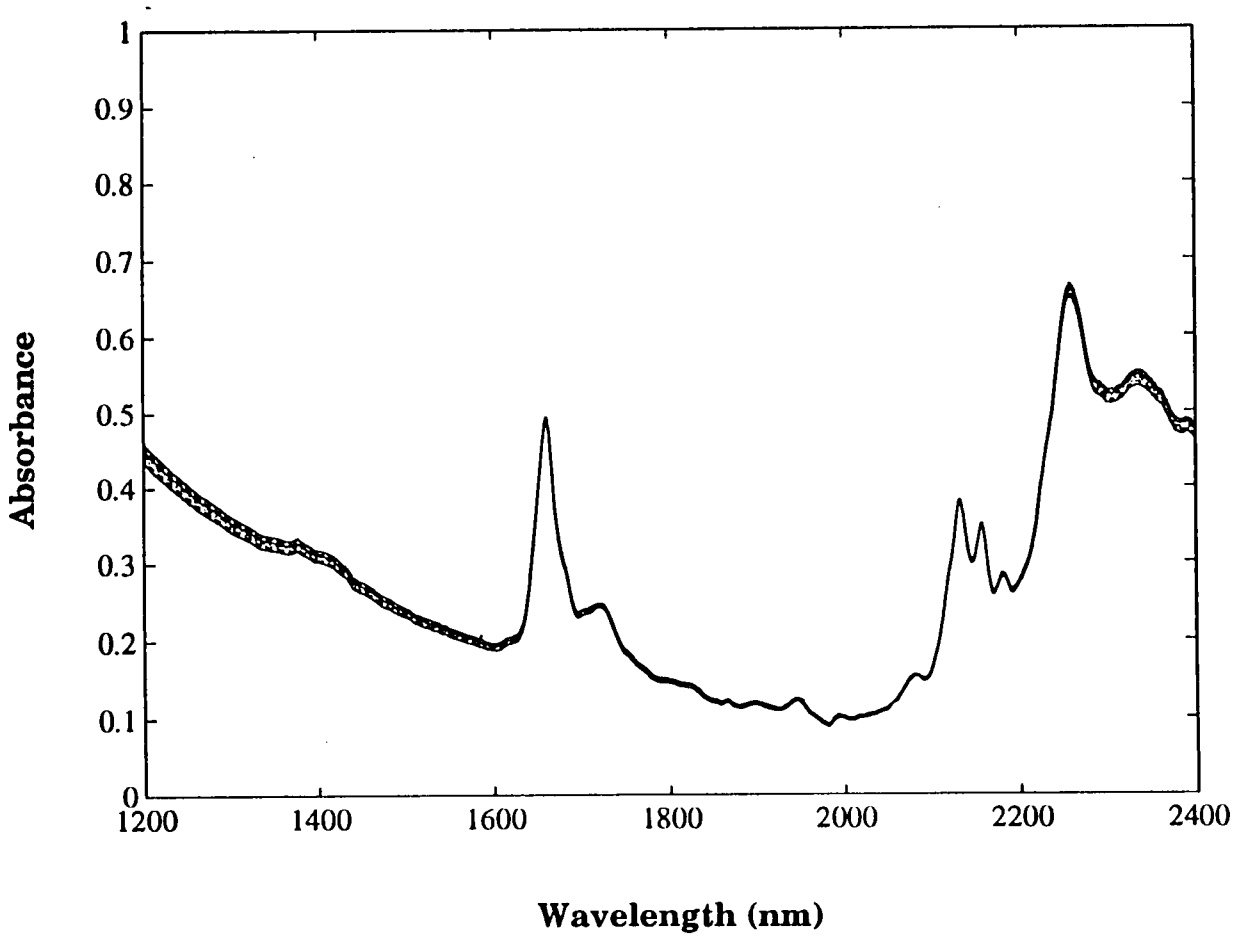


Figure B.5 Overlaid spectra of all the samples of 50% concentration level.

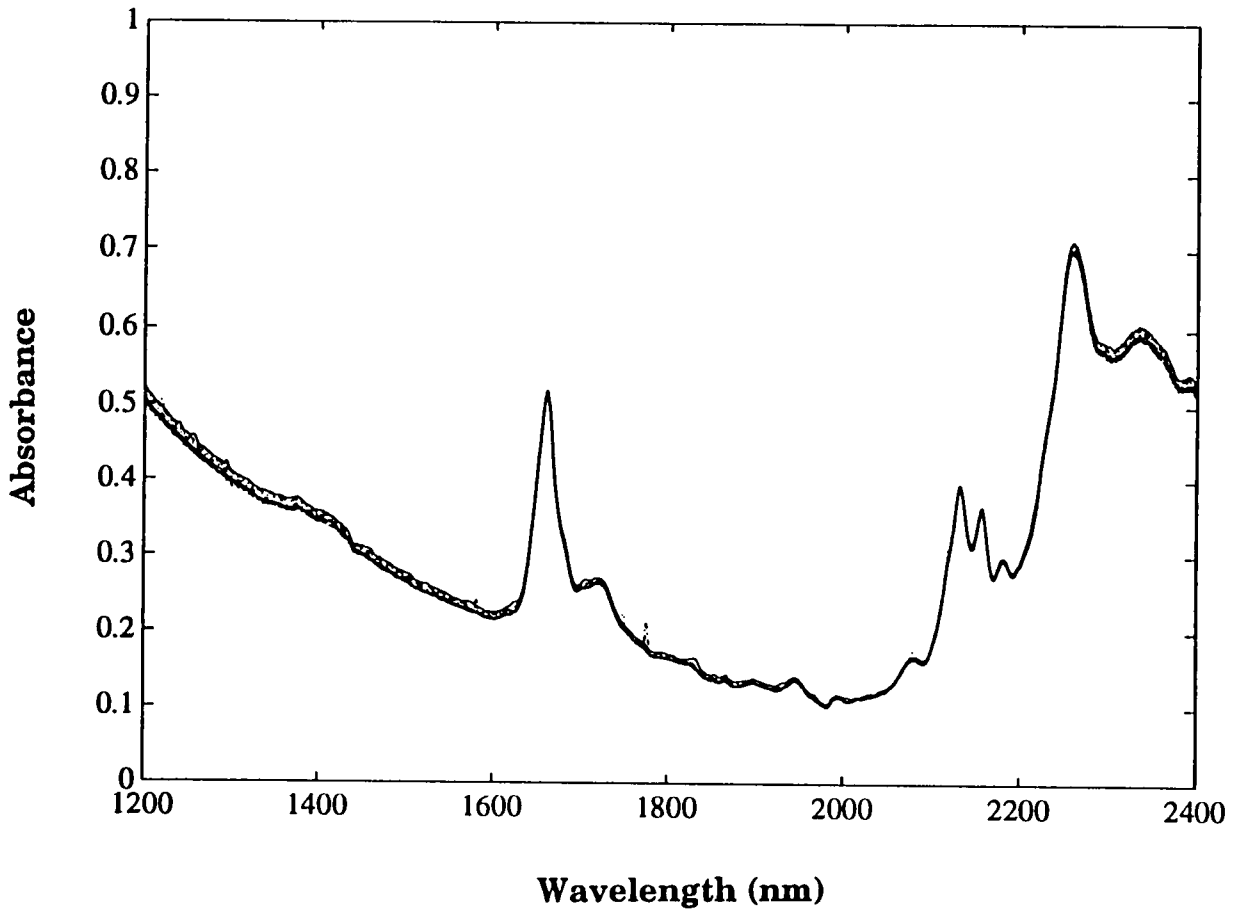


Figure B.6 Overlaid spectra of all the samples of 60% concentration level.

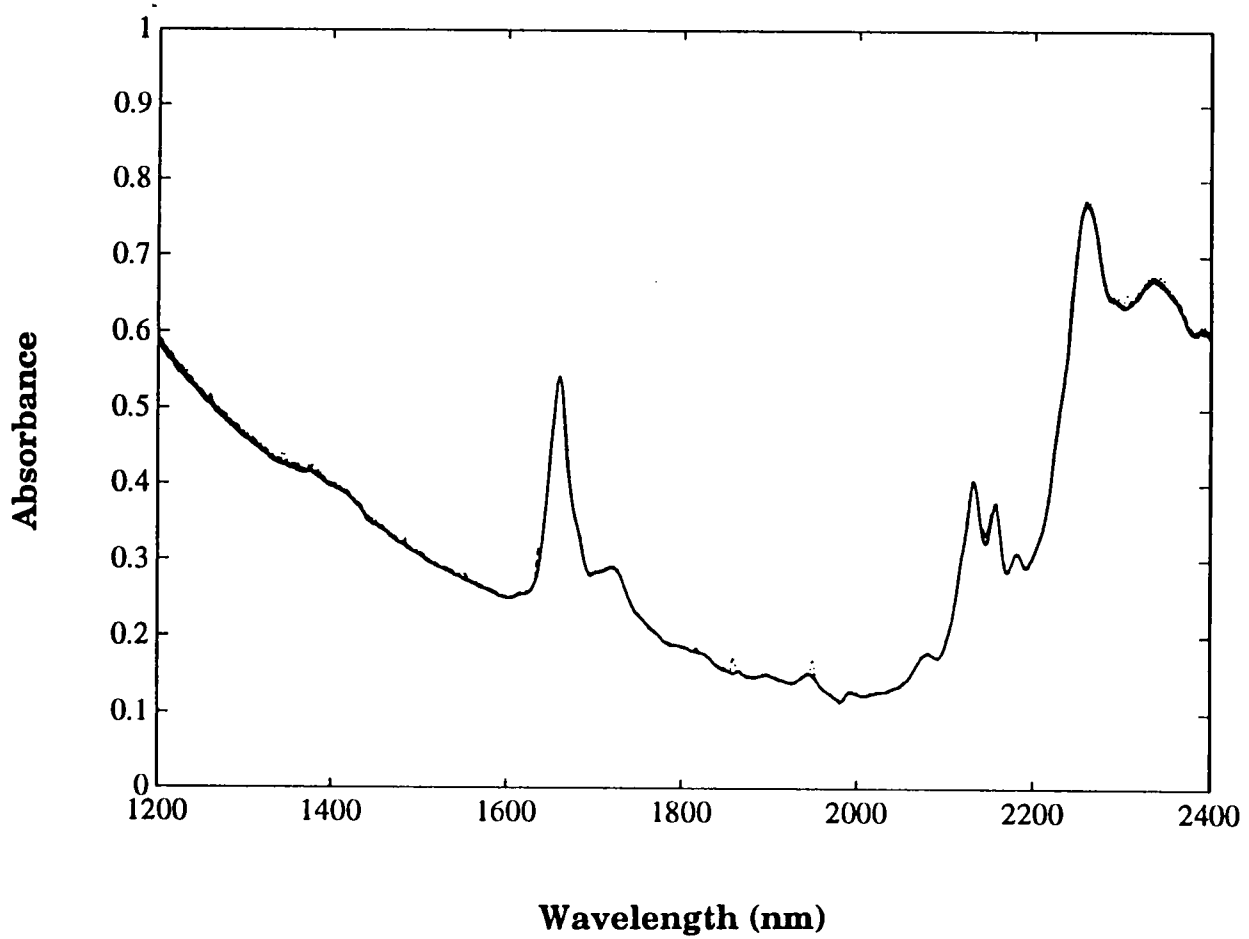


Figure B.7 Overlaid spectra of all the samples of 70% concentration level.

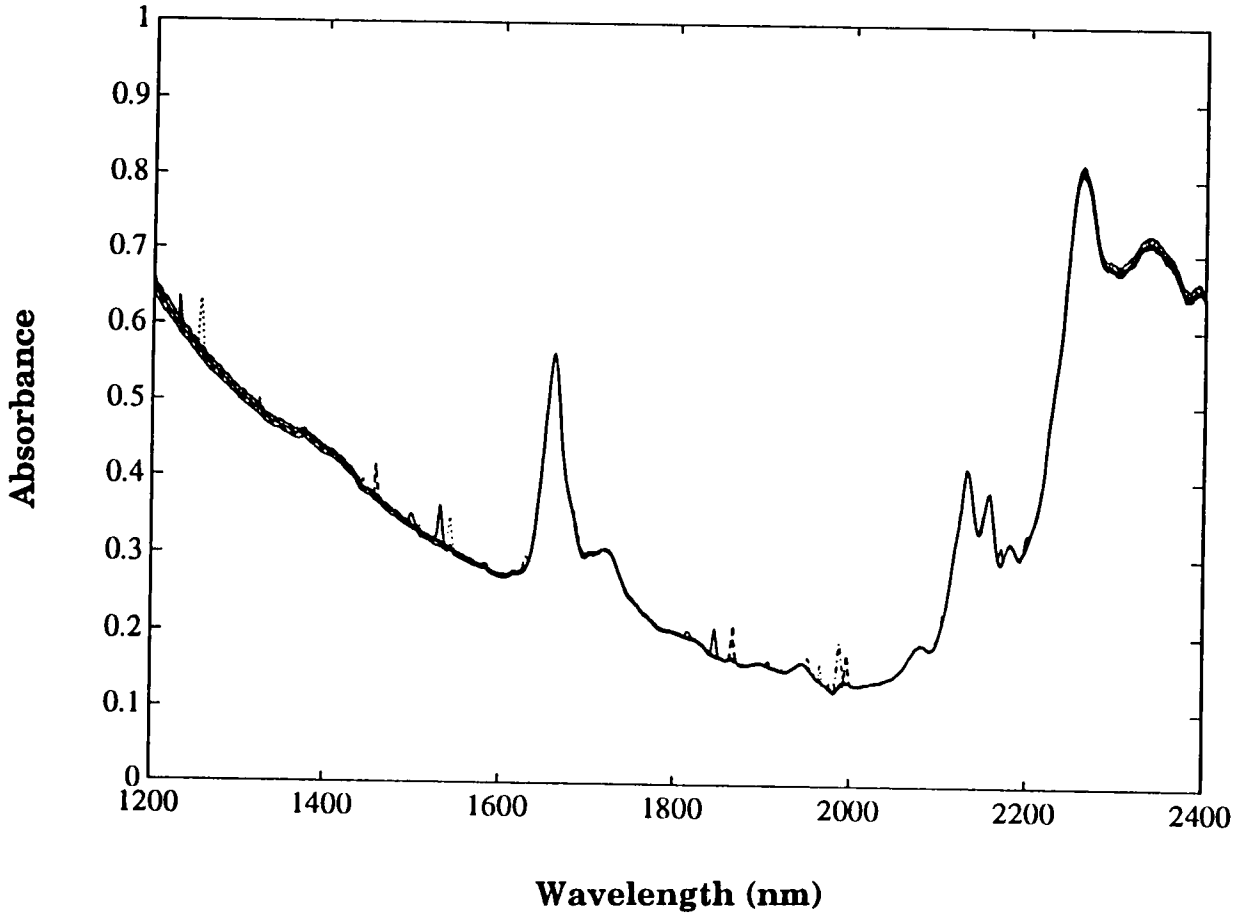


Figure B.8 Overlaid spectra of all the samples of 80% concentration level.

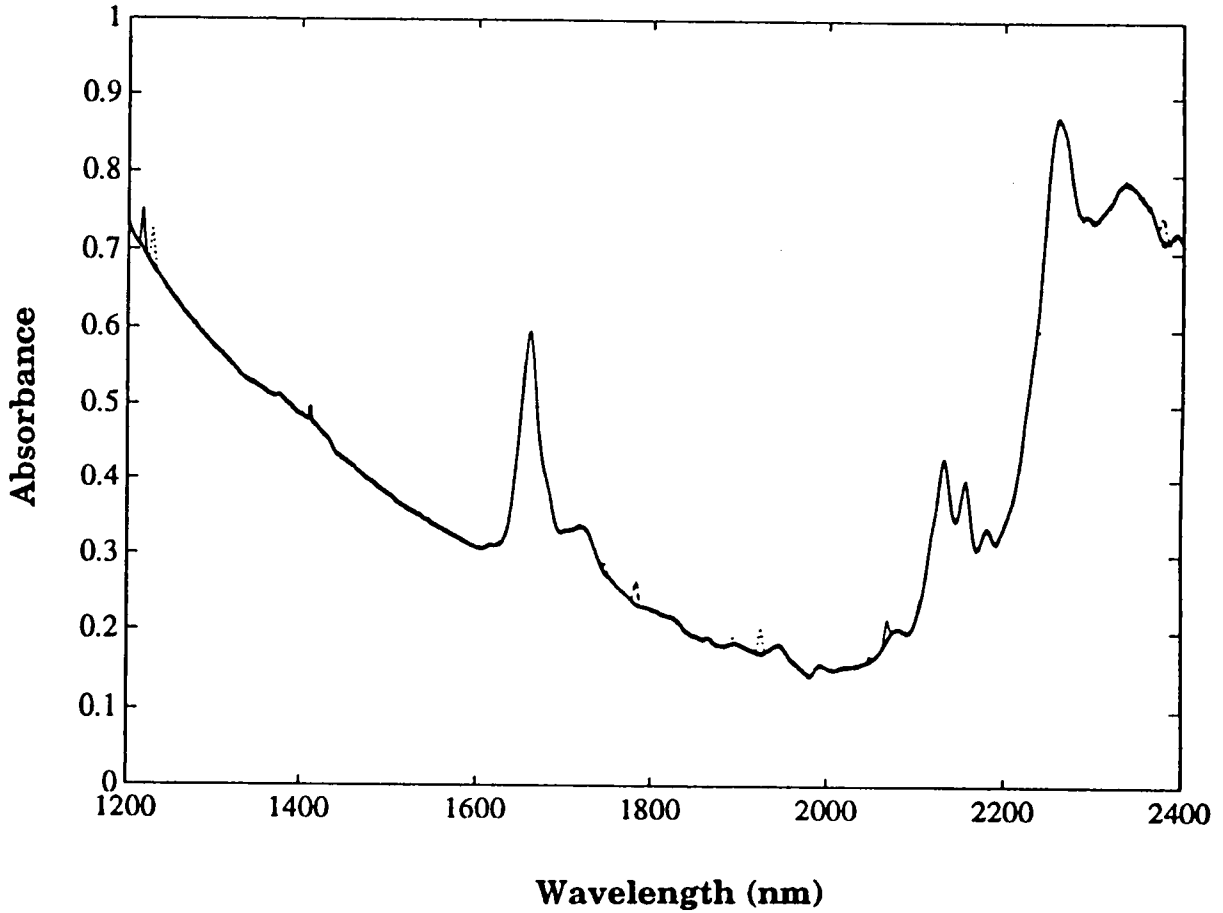


Figure B.9 Overlaid spectra of all the samples of 90% concentration level.

C. PROGRAM OUTPUT

The following section diaplays the program output for leave-one-group-out cross validation using PLS. This cross validation is executed using file cpet.m. "conc" displays the concentration left out. The subsequent output displays the percent variance in X and Y captured by the calibration models using varying number of factors or latent variables (LV).

All the variables involved in execution of the main program are stored in the temporary memory of MATLAB environment. These variables can be displayed by using the command "who". The values for a particular variable can be output to the screen by typing the variable name. The ouputs for SEC and SEP values displayed so are shown towards end.

****

```
>> cpet

conc =

    10
```

Percent Variance Captured by PLS Model

	----X-Block------		----Y-Block------	
LV#	This LV	Total	This LV	Total
1.0000	99.8306	99.8306	99.7651	99.7651
2.0000	0.0662	99.8968	0.0414	99.8065
3.0000	0.0196	99.9165	0.0458	99.8523
4.0000	0.0068	99.9233	0.0494	99.9018

conc =

20

Percent Variance Captured by PLS Model

	----X-Block------		----Y-Block------	
LV#	This LV	Total	This LV	Total
1.0000	99.7612	99.7612	99.7252	99.7252
2.0000	0.1096	99.8708	0.0735	99.7987
3.0000	0.0210	99.8918	0.0433	99.8420
4.0000	0.0116	99.9033	0.0505	99.8925

conc =

30

Percent Variance Captured by PLS Model

	----X-Block------		----Y-Block------	
LV#	This LV	Total	This LV	Total
1.0000	99.7888	99.7888	99.7631	99.7631
2.0000	0.0956	99.8844	0.0620	99.8251
3.0000	0.0248	99.9092	0.0340	99.8591
4.0000	0.0083	99.9175	0.0501	99.9093

conc =

40

Percent Variance Captured by PLS Model

	----X-Block------		----Y-Block------	
LV#	This LV	Total	This LV	Total
1.0000	99.8211	99.8211	99.7740	99.7740
2.0000	0.0869	99.9080	0.0582	99.8323
3.0000	0.0142	99.9222	0.0390	99.8713
4.0000	0.0074	99.9296	0.0442	99.9155

conc =

50

Percent Variance Captured by PLS Model

	----X-Block------		----Y-Block------	
LV#	This LV	Total	This LV	Total
1.0000	99.8315	99.8315	99.7921	99.7921
2.0000	0.0657	99.8971	0.0832	99.8753
3.0000	0.0233	99.9204	0.0269	99.9022
4.0000	0.0059	99.9263	0.0387	99.9409

conc =

60

Percent Variance Captured by PLS Model

	----X-Block------		----Y-Block------	
LV#	This LV	Total	This LV	Total
1.0000	99.8243	99.8243	99.8080	99.8080
2.0000	0.0786	99.9028	0.0479	99.8559
3.0000	0.0220	99.9249	0.0323	99.8882
4.0000	0.0068	99.9317	0.0473	99.9354

conc =

70

Percent Variance Captured by PLS Model

	----X-Block------		----Y-Block------	
LV#	This LV	Total	This LV	Total
1.0000	99.8108	99.8108	99.7593	99.7593
2.0000	0.0854	99.8962	0.0715	99.8308
3.0000	0.0239	99.9201	0.0308	99.8616
4.0000	0.0068	99.9269	0.0474	99.9090

```
conc =

    80


        Percent Variance Captured by PLS Model

              ----X-Block------    ----Y-Block------
      LV#     This LV    Total     This LV    Total
    1.0000    99.8156   99.8156    99.7863   99.7863
    2.0000     0.1004   99.9161     0.0610   99.8473
    3.0000     0.0277   99.9438     0.0202   99.8675
    4.0000     0.0040   99.9478     0.0471   99.9146


conc =

    90


        Percent Variance Captured by PLS Model

              ----X-Block------    ----Y-Block------
      LV#     This LV    Total     This LV    Total
    1.0000    99.8066   99.8066    99.7243   99.7243
    2.0000     0.0513   99.8579     0.0540   99.7782
    3.0000     0.0349   99.8927     0.0349   99.8132
    4.0000     0.0113   99.9040     0.0652   99.8784


>> sec

sec =

    1.1311    1.0266    0.8969    0.7315
    1.2052    1.0314    0.9139    0.7539
    1.2086    1.0385    0.9319    0.7480
    1.2389    1.0674    0.9350    0.7575
    1.1950    0.9255    0.8197    0.6372
    1.1422    0.9895    0.8717    0.6624
    1.2454    1.0441    0.9442    0.7656
    1.1090    0.9375    0.8732    0.7012
    1.1397    1.0220    0.9382    0.7570
```

```
>> sep

sep =

    0.9662    0.3146    0.7743    0.2002
    1.0504    0.9218    0.7357    0.8140
    0.7923    0.7429    0.6334    0.7195
    0.3996    0.3235    0.3769    0.2868
    1.1527    1.0997    1.0847    0.9978
    1.2508    1.1405    1.0525    1.1306
    0.4911    0.4213    0.3763    0.4332
    0.5453    0.6051    0.7464    1.2549
    0.5219    0.2497    0.2695    0.4348

>> diary off
```

VITA

Jitender Batra was born in Rudrapur, Nainital (India) on June 15, 1969. He graduated from Campus School, Pantnagar, Nainital (India) in June 1987. The following July he entered Indian Institute of Technology, Bombay (India) and in July, 1991 received a degree of Bachelor of Technology in Chemical Engineering. In August, 1991 he joined The University of Tennessee, Knoxville and in December, 1993 received a Master of Science in Chemical Engineering.